

ISTANBUL TECHNICAL UNIVERSITY ★ INFORMATICS INSTITUTE

**ANTENNA and MEASUREMENT SYSTEM for MICROWAVE IMAGING of
BREAST TUMORS**

Ph.D. THESIS

Mehmet ABBAK

Department of Communication Systems

Satellite Communication and Remote Sensing Programme

MAY 2015

ISTANBUL TECHNICAL UNIVERSITY ★ INFORMATICS INSTITUTE

**ANTENNA and MEASUREMENT SYSTEM for MICROWAVE IMAGING of
BREAST TUMORS**

Ph.D. THESIS

**Mehmet ABBAK
(705092006)**

Department of Communication Systems

Satellite Communication and Remote Sensing Programme

Thesis Advisor: Prof. Dr. Ibrahim AKDUMAN

MAY 2015

İSTANBUL TEKNİK ÜNİVERSİTESİ ★ BİLİŞİM ENSTİTÜSÜ

**MEME TÜMÖRÜNÜN MİKRODALGA ile GÖRÜNTÜLENEBİLMESİ İÇİN
ANTEN ve ÖLÇÜM SİSTEMİ**

DOKTORA TEZİ

**Mehmet ABBAK
(705092006)**

İletişim Sistemleri Anabilim Dalı

Uydu Haberleşmesi ve Uzaktan Algılama Programı

Tez Danışmanı: Prof. Dr. İbrahim AKDUMAN

MAYIS 2015

To Beliz and Eylül,

FOREWORD

First of all, I wish to offer my sincere thanks to my advisor Prof. Ibrahim Akduman for his guidance, advice and full support at every stage of this study. I am grateful to him for giving me the opportunity to work in an excellent scientific atmosphere with sparkling people during the past six years.

I would like to sincerely thank Prof. Ali Yapar, and Prof. İřşadi Aksun, for their valuable time and for serving on my committee.

I would like to genuinely thank to Assist. Prof. Mehmet ayren, Assoc. Prof. Serkan ŐimŐek, Mehmet Nuri Akıncı and all the former and current members of the Electromagnetics Research Group, in particular, directly or indirectly contributed to this work; I deeply thank them all.

I absolutely thank my parents Cemil and Nurlu, also my sister Firuze and rest of my family for their continuous encouragement and faith in me. Finally and most importantly, I am grateful to my wife Beliz for everything. The fundamental elements that made this thesis possible are her infinite patience and unconditional support.

May 2015

Mehmet Abbak
(M. Sc. Eng.)

TABLE OF CONTENTS

FOREWORD	vii
TABLE OF CONTENTS	ix
ABBREVIATIONS	xii
LIST OF TABLES	xii
LIST OF FIGURES	xv
SUMMARY	xvii
ÖZET	xix
1. INTRODUCTION	1
1.1 Microwave Imaging	2
1.1.1 Benefits, advantages, and difficulties	5
1.1.2 Applications of microwave imaging	8
1.2 Purpose of the Thesis	10
1.3 Organization of the Thesis	11
2. MICROWAVE IMAGING ANTENNAS	13
2.1 Biomedical Microwave Imaging Antennas.....	13
2.2 Wideband Imaging Antennas	15
2.3 Antennas Design criteria’s specifically for LSM and Contrast Source Algorithms	16
3. MICROWAVE BREAST PHANTOM MEASUREMENTS with a CAVITY- BACKED VIVALDI ANTENNA	19
3.1 Introduction	19
3.2 Microwave Breast Measurement Systems	19
3.3 Antenna Design and Performance.....	21
3.4 Breast Phantom Measurements	25
3.5 Conclusion	34
4. CORRUGATED VIVALDI ANTENNA for MICROWAVE IMAGING	35
4.1 Introduction	35
4.2 Corrugated Vivaldi Antenna	38
4.3 Microwave Tomography System and Experimental Verification	44
4.3.1 Brief introduction to S-LSM	44
4.3.2 Experimental results and performance assessment of vivaldi antennas....	47
4.4 Conclusion	62
5. CONCLUSION	65
REFERENCES	63
CURRICULUM VITAE	72

ABBREVIATIONS

MWI	: Microwave Imaging
MRI	: Magnetic Resonance Imaging
CT	: Computer Tomography
PET	: Positron Emission Tomography
CSI	: Contrast Source Inversion
GPR	: Ground Penetrating Radar
LSM	: Linear Sampling Method
SLSM	: S-Parameter Linear Sampling Method
FEM	: Finite Element Method
FM	: Factorization Method
VA	: Vivaldi Antenna
CBVA	: Cavity Backed Vivaldi Antenna
CVA	: Corrugated Vivaldi Antenna
VNA	: Vector Network Analyser
SNR	: Signal to Noise Ratio

LIST OF TABLES

	<u>Page</u>
Table 1.1: Imaging methods and detected tissue properties.....	2
Table 4.1: Lengths of the slots	39
Table 4.2: Localization and shape errors	61

LIST OF FIGURES

	<u>Page</u>
Figure 1.1: Geometry of the problem.....	4
Figure 2.1: Most widely preferred antenna elements in microwave imaging. (a) Monopole antenna formed from coaxial cable in which outer conductor is stripped 3.5cm from the top [27](b) Dipole antenna using with a balun reducing the additional radiation caused by undesirable currents on the outer shield of the cable [44](c)Antenna array consisting of 32 monopole antennas [47].....	14
Figure 2.2 : Pyramidal ridged horn [41].	15
Figure 2.3: Horn antenna profile.....	15
Figure 3.1: Front view of the designed Vivaldi antenna: Feed section is detailed ...	22
Figure 3.2: Cavity-backed Vivaldi type antenna (CBVA).....	22
Figure 3.3: The reflection coefficient of the antennas (S_{11})	23
Figure 3.4: Measured radiation patterns at 4GHz, 6GHz, and 8GHz	24
Figure 3.5: Maximum gain on broadside direction.....	25
Figure 3.6: Homogenous breast and tumour phantoms (a) Semi-spherical breast phantom (b) The tumour phantom is inserted inside breast phantom	27
Figure 3.7: Relative dielectric permittivities ϵ_r and conductivities σ of breast and tumour phantoms.....	28
Figure 3.8: Measurement configurations (a) Two antennas are positioned opposite to each other and the breast phantom is in between (b) Antennas positioned side by side and directed towards the breast phantom.....	29
Figure 3.9: Comparison of S_{21} between the measured and the simulation	30
Figure 3.10: Amplitude and phase of measured $S_{21}^{brs\phi}$ values for the configurations (I) and (II) at 4 GHz.....	31
Figure 3.11: Amplitude and phase of $S_{21}^{sct\phi}$ for the tumour and the metallic object at 4 GHz in configuration (II).....	32
Figure 3.12: Amplitude and phase of $S_{21}^{sct\phi}$ for the tumour and the metallic object at 8 GHz in configuration (I).....	33
Figure 3.13: The comparison of measured $S_{21}^{sct\phi}$ for the standalone antenna and CVBA in configuration (I). The measurements are performed for horizontal polarization at 8 GHz.	33
Figure 4.1: Top view of the proposed CVA (Darker gray part is the back view.)....	38
Figure 4.2: Measured reflection coefficient (S_{11}) response for both antennas	40
Figure 4.3: Measured principal plane radiation patterns of the VA and the CVA ...	42
Figure 4.4: Measured gain characteristics of the proposed antenna and the VA.....	43
Figure 4.5: Experimental setups for (a) dielectric scatterer (b) single metallic scatterer (c) double metallic scatterer.....	46
Figure 4.6: Indicator function for the dielectric scatterers obtained with following antenna: (a) Wn ; with CVA (b) Wb ; with CVA (c) Wn ; with VA (d) Wb ; with VA (Exact borders of the scatterers are marked with red dashed lines, threshold for normalized gradient is selected as $Q = 0.7$)	48

Figure 4.7: Indicator function for the dielectric scatterers obtained with following antenna: (a) Wn ; with CVA (b) Wb ; with CVA (c) Wn ; with VA (d) Wb ; with VA (Exact borders of the scatterers are marked with red dashed lines, threshold for normalized gradient is selected as $Q = 0.7$)	51
Figure 4.8: Indicator function for the dielectric scatterers obtained with following antenna: (a) Wn ; with CVA (b) Wb ; with CVA (c) Wn ; with VA (d) Wb ; with VA (Exact borders of the scatterers are marked with red dashed lines, threshold for normalized gradient is selected as $Q = 0.7$)	54
Figure 4.9: Indicator function for the single conductor scatterer obtained with following antenna: (a) Wn ; with CVA (b) Wb ; with CVA (c) Wn ; with VA (d) Wb ; with VA (Exact borders of the scatterers are marked with red dashed lines, threshold for normalized gradient is selected as $Q = 0.9$)	58
Figure 4.10: Indicator function for the double conductor scatterers obtained with following antenna: (a) Wn ; with CVA (b) Wb ; with CVA (c) Wn ; with VA (d) Wb ; with VA (Exact borders of the scatterers are marked with red dashed lines, threshold for normalized gradient is selected as $Q = 0.9$)	59

ANTENNA and MEASUREMENT SYSTEM for MICROWAVE IMAGING of BREAST TUMORS

SUMMARY

With the increasing demand for better medical imaging technologies, different medical screening procedures become a research topic for scientific community. One of the important challenges in today's medical imaging is surely the early detection of breast cancer. The breast cancer is one of the very dangerous health threat for women. This disastrous illness is observed approximately one in eight women by the age of ninety years old. The likelihood of successful treatment increases with early detection of breast cancer increases. Up to now, X-ray tomography is the golden standard for characterizing and detecting the breast cancer. In contrast to this fact, X-ray mammography has significant disadvantages. These disadvantages trigger a search for different imaging modalities, which can be integrated with currently available imaging technologies. Microwave imaging is one of those newly emerging solutions. The use microwaves in the early detection of breast cancer is motivated by several reasons. First of all, it is shown that the electrical properties of the malignant and normal tissues are substantially different, which can be easily revealed by microwave imaging. Moreover, microwaves can easily penetrate into breast tissue at a few GHz ranges. Considering that the dimensions of the breast is comparable with the wavelength at those frequencies, the malignancies can be detected from the scattered field by means of nonlinear inverse scattering algorithms.

Nowadays, there are many different studies to design microwave imaging systems for the early detection of the breast cancer. An inevitable part of these systems is the nonlinear imaging methods. With the recent developments in computer technology and the newly introduced efficient algorithms, these methods are now employed in any microwave imaging system. However, the quality of reconstructed images produced by these methods is closely connected with the scattered field data that is acquired by the microwave antennas. Hence, one of the most important parts of the microwave imaging systems is the transceiving antennas. It is shown that, regardless of the method in the hand, the resolution of the produced images increases with the increasing signal-to-noise ratio (SNR) and with the increasing sampling density of the field. To increase SNR, the designed antenna must have higher gain levels together with a lower back-to front ratio level; whereas the sampling density of the field increases when the dimensions of the antenna gets smaller. Furthermore, the microwave imaging methods require certain preprocessing steps, which accept only a single polarization of the incident field as input. Thus, the designed antennas must be highly linearly polarized. Finally, the microwave imaging of the malignancies is a highly ill-posed inverse problem. Thus, the frequency diversity in the scattered field data must be as high as

possible. Consequently, today's microwave breast cancer imaging systems require high gain, linearly polarized, wide-band and compact antennas as their scattered field sensors.

In this context, the first contribution of this thesis is the design of a cavity-backed Vivaldi antenna (CBVA) for microwave breast measurements. The design criteria for the antenna is shaped by the requirements of the free-space measurement scenario where the receiving and the transmitting antennas are rotated by a mechanical scanner. Later, various breast phantom measurements is conducted with the CBVA to reveal its feasibility for microwave tomography.

As the second contribution, a novel Corrugated Vivaldi antenna (CVA) is proposed. The main idea is opening corrugations on the edge of the antenna to decrease the induced currents, which can degrade the performance. Doing so a design with better properties such as higher gain, smaller beam width, lower back-to-front ratio is obtained. The characteristics of the obtained CVA is measured in a detailed manner. Furthermore, the imaging performance of the introduced design is compared with a generic Vivaldi antenna (VA) of the same size. For this purpose, several experimental configurations are prepared in an anechoic environment and scattering parameter (S-parameter) measurements are obtained for those setups by means of the both antennas. Acquired S-parameters are then employed in a recently proposed qualitative imaging method, the S-parameter based Linear Sampling Method (S-LSM), which is a more suitable form of Linear Sampling Method (LSM) for real world applications. Experimental results show that the proposed design performs better than VA in such real world microwave imaging problems.

MEME TÜMÖRÜNÜN MİKRODALGA ile GÖRÜNTÜLENEBİLMESİ İÇİN ANTEN ve ÖLÇÜM SİSTEMİ

ÖZET

Yeni görüntüleme teknolojilerine artan ihtiyaçla birlikte, çeşitli medikal görüntüleme metotları günümüz bilim camiası için aktif bir araştırma konusu ve etkin bir geliştirme alanı olmaya başladı. Günümüz medikal görüntülemesinde en önemli zorluk ve problemlerden biri de kesinlikle meme kanserinin erken tespiti için memedeki tümörlü dokunun tespit ve teşhis edilmesidir.

Meme kanseri kadınlar açısından en kritik ve en tehlikeli hastalıklardan birisidir. İstatistiklere göre günümüzün en korkunç hastalıklarından biri olan meme kanseri sekiz kadından birinde doksan yaşına kadar gözükmektedir. Bu hastalığın bilinen en iyi tedavi yöntemi de memedeki tümörlü dokunun erken yaşlarda tespit ve teşhis edilmesidir. Erken teşhis edilen meme kanserlerinde tedavideki başarı oranında yüksek olduğu tespit edilmiştir.

Şimdiye kadar, meme kanserinde malignan dokunun görüntülemesinde kullanılan en etkili teknik X-ray görüntüleme yöntemleridir. X-ray görüntüleme tekniğinin bu yaygın kullanımına ve meme kanserini teşhis ve tedavideki büyük önemine karşın, X-ray tomografinin pek çok zararı olduğu bilimsel olarak ortaya konulmuş bir gerçektir. Özel olarak açıklamak gerekirse, X-ray tomografinin en önemli dezavantajı dokuda iyonlaşmaya sebep olmasıdır. X-ray'in bu iyonlaştırma etkisi sebebiyle bu görüntüleme tekniği belli bir yaşın altındaki hastalara uygulanmakta olup gerekli olduğu durumlarda dahi uygulanacak kişi açısından risk taşıdığı çok açıktır. Bununla birlikte, X-ray mamografi yüksek bir false-pozitif oranına sahiptir. İstatistiklere göre mamografinin call-back (Normal olan bir dokunun mamografide kanserli gibi gözüküp ikinci bir testi gerektirmesi durumu) oranı %11. Ayrıca X-ray mamografinin false negatif oranı da yapılan çalışmalarda %4 ve %34 arasında bulunmuştur ki bu değerler hiç de azımsanacak ölçüde değildir. (False negatif oranındaki bu değişiklik false negatif tabirinin değişik tanımlarından kaynaklanmaktadır.) X-ray mammografinin diğer bir dezavantajı da memedeki radyolojik olarak yoğun olan fibroglandular dokunun artışı ile hassasiyetin azalmasıdır. Burada dikkat edilmesi gereken önemli bir nokta da genç bayanlarda fibroglandular doku miktarının daha fazla olduğu gerçeğidir. Bunlardan başka, X-ray mammografinin yapılabilmesi için memenin bastırılması gerekmektedir. Bu tekniğin uygulanacağı kadınlarda rahatsızlık ve acı verici bir hissiyata yol açmaktadır. Son olarak, X-ray mammografi sonunda elde edilen görüntüler radyolojistler tarafından değişik şekillerde yorumlanabilmektedir. Açık ki bu da yukarıda bahsedilen false pozitif ve false negatif oranlarının belirtildiği gibi yüksek olmasına neden olmaktadır. Bu yukarıda bahsettiğimiz farklı dezavantajlar ve kusurlarında ötürü, bilim camiası meme kanserinin erken teşhisi için X-ray

görüntüleme tekniğinden farklı çeşitli teknik ve metotlar aramakta ve bunların X-ray mammografi ile entegre edilmesine çalışmaktadır.

Üretilen yeni çözümlerden birisi de özel olarak mikrodalga frekanslarındaki elektromanyetik dalgaların meme kanserinin erken tanı ve teşhisinde kullanılması fikridir. Mikrodalga frekanslarındaki elektromanyetik dalgaların meme kanserinin erken tanı ve teşhisinde kullanılmasının çeşitli bazı sebepleri vardır. Her şeyden evvel, mikrodalga frekanslarında memedeki normal ve kanserli dokunun elektriksel özellikleri (görelî dielektrik sabiti, elektriksel iletkenlik) önemli ölçüde farklılık arz eder. Bundan dolayıdır ki mikrodalga frekanslarında bu dokuları saçtıkları alanların farkından ayırt etmenin mümkünatı olduğu çeşitli çalışmalarda gösterilmiştir. Ayrıca mikrodalga frekansındaki elektromanyetik dalgaların, özellikle de bir kaç GHz civarında, meme dokusu içinde kolaylıkla ilerleyebilecekleri değişik makalelerde gösterilmiştir. Bu frekans bandında ortalama meme boyutlarının bir – bir kaç dalga boyu olacağı da göz önüne alınırsa meme içinde bulunması olası malignan dokulardan saçılan alanların kolayca ölçülebileceği ve bu saçılan alanlardan lineer olmayan ters saçılma algoritmaları ile tümörlü dokunun tespit edilebileceği anlaşılmaktadır.

Günümüzde, meme kanserinin erken teşhisi için değişik mikrodalga görüntüleme sistemleri geliştirilmektedir. Bu sistemlerin vazgeçilmez bir parçası da hiç şüphesiz ki doğrusal olmayan görüntüleme yöntemleridir. Bilgisayar teknolojisindeki son gelişmeler ve geliştirilen efektif algoritmalar sayesinde bu doğrusal olmayan metotlar artık tüm mikrodalga meme kanseri tanı ve teşhis sistemlerinde kullanılmaktadır. Doğrusal olmayan görüntüleme algoritmalarının çalışmasını etkileyen en önemli faktör antenler tarafından örneklenen saçılan alanlardır. Bu yüzden mikrodalga meme kanseri tanı ve teşhis sistemlerinin en hayati parçalarından biride alıcı/verici antenlerdir. Yapılan çalışmalar göstermiştir ki, herhangi bir mikrodalga görüntüleme algoritmasının ürettiği sonucun çözünürlüğü saçılan alan bilgisinin sinyal-gürültü oranı (signal-to-noise ratio) ile doğrudan bağlantılıdır. Ayrıca yine bu resimlerin çözünürlüğünü etkileyen önemli bir diğer faktör de saçılan alanın örneklenme yoğunluğudur. Örneklenme yoğunluğunun bu etkisini anlamak için ters saçılma problemine sezgisel açıdan yaklaşmak gerekir. Şöyle ki, tespit edilmek istenen nesne ne kadar küçükse saçılan alan da o derece zayıf olacaktır. Ayrıca bu nesneyi tespit etmek için kullanılması gereken frekans da yüksek olacaktır. Yüksek frekansların kullanılması durumunda saçılan alanın band genişliği artacak ve Nyquist ilkesi gereğince sinyali tam olarak tanımlamak için almamız gereken örnek sayısı da yükselecektir.

Yukarıdaki sebeplerden ötürü meme kanseri tanı ve teşhis sistemlerinin gerektirdiği antenler özel olarak tasarlanmalıdır. İlk olarak, tasarlanan antenin olabildiğince yüksek bir kazançla sahip olması gerekmektedir. Bu yüksek kazanç sayesinde antenin arka lob güç seviyesi-önlob güç seviyesi oranı (back to front ratio) düşük olacak ve antenin radyasyon hüzmesinin 3dB genişliği (3dB beamwidth) azalacaktır. Düşük arka lob güç seviyesi-önlob güç seviyesi ve küçük bir 3dB radyasyon hüzme genişliği, mikrodalga meme kanseri tanı ve teşhis sistemlerinde kullanılacak bu antenlerin yüksek bir sinyal-gürültü oranına sahip olmasına sebep olacaktır. Anten tasarımında ikinci bir kıstas ise antenin boyutlarının olabildiğince küçük tasarlanmasıdır. Bu sıkı tasarımı ile mikrodalga meme görüntülemesinde kullanılacak bu antenlerin saçılan alanı

örnekleme oranının olabildiğince yüksek olması hedeflenmektedir. Ayrıca, mikrodalga görüntüleme yöntemlerinin tamamı belirli bir ön işlem aşaması gerektirir. Çünkü mikrodalga görüntüleme yöntemlerinin giriş olarak kabul ettiği enformasyon saçılan elektrik alanıdır, lakin mikrodalga görüntüleme sistemlerinde kullanılan vektörel devre analizörleri (vector network analyzer) saçılma parametreleri (scattering parameter) ölçebilmektedir. Saçılma parametrelerinin elektrik alanına çevrilmesi ise belirli kalibrasyon yöntemleri ile olur. Bu kalibrasyon yöntemlerinin ekseriyeti ise tek polarizasyonlu bir gelen alan için tasarlanmıştır. Bundan dolayıdır ki, mikrodalga meme kanseri tanı ve teşhis sistemlerinde kullanılacak antenlerin olabildiğince doğrusal polarizasyonlu olması hedeflenir. Son olarak ve en önemli şart olarak, mikrodalga meme kanseri tanı ve teşhis sistemlerinde kullanılacak antenlerin giriş empedansı band genişliğinin mümkün olduğunca yüksek olması istenir. Bu antenlerin böyle tasarlanmasının arkasında yatan sebep ise ters saçılma problemlerinin hemen hemen hepsinin kötü koşullanmış (ill posed) olması ve bu kötü koşullanmayı aşmanın tek yolunun ise enformasyon miktarının artırılması olmasıdır. Şu açık bir gerçektir ki herhangi bir görüntüleme sisteminde toplanan veriyi arttırmanın en kolay yolu saçılan alanı daha çok frekansta örnekleme yapmaktır. Sonuç olarak, günümüzde kullanılan mikrodalga meme kanseri tanı ve teşhis sistemlerinde kullanılacak antenlerin olabildiğince yüksek kazançlı, mümkün olduğunca doğrusal polarize, geniş bantlı olması ve sıkı bir tasarıma sahip olması beklenmektedir.

Bu bağlamda, bu tezin ilk katkısı, metal bir kavite ile arkalanmış bir Vivaldi antenin (Cavity backed Vivaldi antenna) mikrodalga meme ölçümleri için tasarlanmış olmasıdır. Antenin tasarımı için gereken parametrelerinin tamamı dış ortamın hava olduğu durum için tasarlanmıştır. Çünkü bu antenlerin mekanik bir tarayıcı içinde (boş uzayda) kullanılması hedeflenmektedir. Tasarlanan kavite ile arkalanmış Vivaldi antenin yararlılığını gösterebilmek amacıyla çeşitli meme fantomları ile saçılan alan ölçümü yapılmıştır.

Bu tezin ikinci katkısı ise, eni bir oluklu Vivaldi anten (Corrugated Vivaldi antenna) yapısının sunuluyor olmasıdır. Antenin kenarında açılan olukların Vivaldi tipi antenlerin verimini azaltan kenar akımlarını azalttığı gözlenmiştir. Açılan bu oluklar sayesinde elde edilen oluklu Vivaldi antenin yukarıda bahsettiğimiz yüksek kazanç, küçük 3dB radyasyon hüzmeleri genişliği, düşük arka lob güç seviyesi-ön lob güç seviyesi oranına sahip olduğu benzetimlerde gözlenmiştir. Bu gözlemlerin doğrulaması için tasarlanan oluklu Vivaldi antenin tüm parametreleri ayrıntılı bir biçimde ölçümlerle verilmiştir. Üstüne üstlük, tasarlanan oluklu Vivaldi anten ile aynı boyutlardaki jenerik bir Vivaldi antenin mikrodalga görüntüleme performansları deneysel olarak karşılaştırılmıştır. Bu amaçla İstanbul Teknik Üniversitesi Elektrik-Elektronik Fak. Yansız odasında çeşitli düzenekler kurulup bu düzeneklerin her biri için mikrodalga alan ölçümleri hem jenerik Vivaldi hem de oluklu Vivaldi ile yapılmıştır. Yapılmış olan bu ölçümler, yeni önerilen bir nitel mikrodalga görüntüleme algoritması olan saçılma parametresi bazlı doğrusal örnekleme yönteminde kullanılmıştır. Elde edilen deneysel sonuçlar göstermiştir ki önerilen anten tasarımı mikrodalga görüntüleme jenerik bir Vivaldi antene göre çok daha etkilidir.

1. INTRODUCTION

With the momentum in the evolution of the computers, solutions of the extensive and complex problems started to be appear, which is not possible to solve analytically, by bringing theory and experiments together by the coupler impact of the computational facilities. Medical imaging is one of the most positively influenced technology from these developments many new imaging methods like magnetic resonance imaging (MRI), computer tomography (CT), positron emission tomography (PET), etc. have been emerged, which are intensively used in the healthcare. Actually, every new method in biomedical engineering reveals endless unknown features of the human body, and used in diagnosing disorders, as a part of the treatment [1], which becomes very critical power in the hands of radiologist by providing observation and awareness on the human body and human diseases. Some of the research indicates that medical imaging is one of the most influential and most significant technology for over thousands of years in throughout the medical advancements [2]. Approximately, with the beginning of the 20th century internal image of the human body has been obtained by the development of the x-ray technology. From that time extensive researches for improving x-ray modality, creating new applications of it like mammography, or inventing additional techniques on x-ray like as CT. In addition, new imaging methods based on different physical properties of the human tissue, are also invented like as MRI and ultrasound. However, accomplishments obtained until today are enable facilitate fascinating applications, there are still a long road on improving biomedical imaging exist due to many deficiencies for diagnostic and treatment purposes.

Though, there are still many highly developed applications competing on the market, because of that a new modality should obtain some properties like as, to cause low radiation and being healthy, having high sensitivity, being specific in terms of showing different physical properties of the tissues, being non-invasive, low-cost system, comfortable usage by the patient that is not causing any pain, lastly but not least delivering steady, not subjective, can be easily depicted results.

In broad terms, all of the imaging technologies are form on illumination of the body area by a penetrating wave, receiving the scattered fields, which interacted with human body tissues, by a sensor or antenna. Besides properties of the signals with the contact of the signal to the biological tissue, it will be affected in some sense. An algorithm can process this effect and image of the domain can be reconstructed, by this way any effect that is changing scattered field can be converted to a significant data, which can be analysed and interpreted, by a radiologist. Based on the modality, sensor or antenna, diverse properties of the tissue linked with its physical biological or electrical attributes, can be accessed as shown in Table 1.1. Because of the fact that every method brings additional information, sometimes usage of multiple methods can expose the internal structure of the biological tissue. This is why many research progress on developing new sensors and medical imaging methods extensively.

Table 1.1 : Imaging methods and detected tissue properties.

Physical	<ul style="list-style-type: none"> • Photon Attenuation • Temperature 	<ul style="list-style-type: none"> • MRI • X-ray • Pet
Electrical	<ul style="list-style-type: none"> • Permittivity • Conductivity • Impedance 	<ul style="list-style-type: none"> • Microwave Imaging
Mechanical	<ul style="list-style-type: none"> • Elasticity • Architecture 	<ul style="list-style-type: none"> • Ultrasounds
Biological	<ul style="list-style-type: none"> • Perfusion • Protein Function 	<ul style="list-style-type: none"> • MRI • Pet

1.1 Microwave Imaging

Although there are many imaging methods available at the moment, there are many drawbacks and limitations of these imaging methods, which are commonly used. For this reason, many ongoing researches to lessen the current drawbacks of medical imaging and exploit the additional properties of the biological tissues. One of the most decisive recent technique, which is under development, is microwave imaging for medical applications.

Microwave imaging which is technically a development of classical wave-based diffraction methods of imaging to microwave frequencies. To describe the microwave imaging with the aid of X-rays, which is the glorious and prominent standard of the medical imaging, is straightforward by creating analogy with it. Mainly in the active microwave imaging, object under test is illuminated with an incident wave, like as in X-ray methods. By measuring the total signal, which is composed of incident signal and scattered signal from the object, with an appropriate sensor or antenna, variations of the features of the object, which is interacted with the incident wave, can be reconstructed as an image. In the conventional X-ray method, total signal is obtained by photographic film, which is used as a sensor. However, in the microwave imaging as a sensor microwave antennas are used. In addition, antennas should be present at the vicinity of the object under test, by use of mechanically rotating scanner systems or fixed antenna systems.

In general both methods are very similar, from many perspective, however main difference lies in the frequency spectrum, and so the waves that are applied on the biological tissues. As it is depicted in Table 1.1, in the X-ray frequencies photonic attenuation can be measured, and with this information physical property of the tissues, like as density, can be detected, however, microwaves can give information about the electrical properties, like as conductivity, σ , and permittivity, ϵ , of the tissues. Every tissue has different and unique electrical properties. The divergence between electrical properties of the tissue and neighbouring tissues is called as contrast. Contrast is actually the one of the main motivation in the research of microwave imaging for biomedical applications, which can help to figure out the variation in the tissues in related to electrical properties. Electrical properties can give information about status of the tissue like as healthiness, cancerous, etc.

If it is compared in the respect of the wavelength, X-rays has much smaller regarding to the microwaves. In the case of X-rays, wavelength is also smaller than the organs and just passes human body in the linear path. However, in the microwaves, wavelength is similar to the size of the organs, and when microwaves penetrate to the human body multiple interruptive effects occur, which is causing multiple scattering. Scattering appears when the electromagnetic wave come across the variation in the dielectric medium. Due to the inhomogeneous structure of biological tissues electromagnetic waves is subject to high amount of scattering with different directions,

because of that, scattered microwave fields should be detected in as much as possible directions around the human body. However, it is enough for X-ray to detect in the one-way direction, regarding to the source.

In addition, one more difference between microwaves and X-ray methodology is the dimensions of the reconstructed image. X-ray image presents kind of a projection of the three-dimensional (3D) properties of the human body on the two-dimensional (2D) image. However, in the microwave imaging multi-layered images can be obtained. To have separate image for each level can prevent not to see a small part, which is behind a bulky part, due to possible shadowing effects.

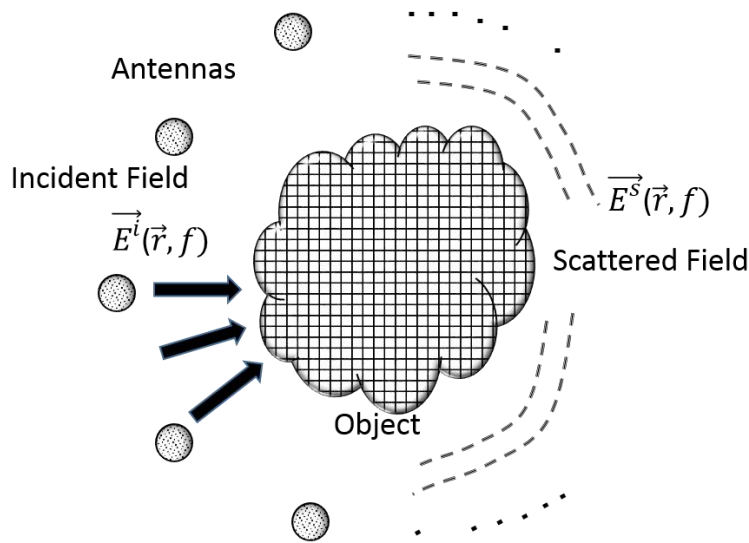


Figure 1.1: Geometry of the problem.

It can be concluded that, microwave-imaging method can provide electrical properties of the object by detecting the scattered fields from inhomogeneous tissues, around the imaging domain with help of the antennas. Typical microwave imaging setup can be summarized as in Figure 1.1. Illuminating antennas surrounding the object are placed to detect the scattered field. Number of the different positions of the antennas or the number of the antennas directly determine the extent of the data. It would be better to get data as much as possible around the object to have high-resolution image. If it is going to be static system with a fixed antenna system, number of the antennas, that is to be placed around the object, are related to the dimensions of the antennas, distance from the acquisition surface to the center of the object, and the mutual coupling between each other. However, with a rotating system much more measurement points can be handled with under less effect of the mutual coupling between the antennas. Nevertheless, with a rotating antenna system total measurement acquisition time is

going to be longer. To obtain the scattered field firstly a measurement of the system without any object should be completed, which can be named incident field. After that total field, representing the object and the system, is measured by placing the object in the system, and scattered field corresponds to the difference between the total field and incident field. After the measurements, to reconstruct the image an ill-posed inverse scattering problem is posed, because of the non-linear dependency between the scattered field and dielectric distribution of the object.

1.1.1 Benefits, advantages, and difficulties

1.1.1.1 Benefits and advantages

Microwave imaging has achieved high popularity in the academic community due to its probable potential as a biomedical imaging methodology. One of the essential reasons of that, microwave imaging can supply the outline of the electrical properties distribution of the tissues accurately [3]. It has been known that with knowledge of the dielectric properties, provide perception of changes in the pathological or physiological situations of the biological tissues [4][5][6][7][8]. It has been shown that when healthy cells become cancerous their electrical properties change straight. Not just the malignant tumours also, tissue changes caused by blood supply, like ischemia and infarction can directly change the electrical properties [9]. Also, electrical properties of bone at the microwave frequencies, are related to the some mechanical properties of it. With an inspection of dielectric properties health of bone can be monitored [10].

Also, if we compare the microwave imaging in terms of the safety issues to the other methods, it is seen that microwave imaging is one of the safeties. One of the reasons is that microwave imaging can be utilized non-invasively, and does not require any uncomfortable compression. In addition, microwave imaging utilizes non-ionizing radiation with very low level of power, which results a harmless and comfortable assessment. Moreover, with the developments in the wireless communications technologies, microwave components can be obtained much more cheaply, and microwave imaging systems can be composed with very reasonable costs, especially compared to other expensive imaging systems like CT and MRI. So that, due to the benefits of being harmless and cost effective, microwave imaging can be easily adopted for mass screening programs.

1.1.1.2 Difficulties

Besides many advantages of the microwave imaging, there are also some essential obstacles, which arise inherently from the interaction of the microwaves with biological tissues, to implement the technology in commercial basis. However, with the design and implementation of new measurement systems, antennas, and imaging algorithms these obstacles can be resolved. One of the challenging issue in the general medical imaging is the resolution of the system, which is also a key parameter for microwave imaging. Resolution can be defined as the smallest feature that can be accurately identified, or the least possible distance between two different features, and when these features are closer than the resolution of the system they will appear in one piece. Resolution is directly related with the highest frequency in the incident fields' frequency band of the microwave imaging system. Hypothetically, the resolution of the tomography imaging ways depend on the far-field measurements is a function of the wavelength (λ) of radiation in the medium, for example, the spatial resolution of diffraction tomography is limited by [11]

$$\delta \geq \frac{\lambda}{2}, \quad (1)$$

Consequently, microwave tomography cannot compete with X-ray tomography in terms of the resolution, in the far field. Nevertheless, for near-field imaging, it has been approximated that image reconstruction is fundamentally unlimited by wavelength and is restricted by signal-to-noise ratio [12]. With use of first-rate microwave measurement equipment, objects with diameter of down to $\lambda/7$ - $\lambda/10$ has been reconstructed in [13] [14], also recently resolution of as far as $\lambda/30$ has been demonstrated in near-field microwave imaging [15]. This phenomenon, which is called super-resolution, is first experimentally exhibited in [16], and it has been suggested that the major reason for superior resolution is counting on the multiply scattered effects, and gathering evanescent field data which cuts the relation between the resolution and the diffraction limit. So, due to the limitations on the measurement systems, it is still important to include higher frequency into the operating bandwidth for increasing the resolution of the reconstructed image. Another factor that increases the resolution beyond the diffraction limit is the reconstruction procedures form on non-linear optimization.

However, at this moment another issue with related to medical imaging that should be mentioned is the penetration depth, because which is also directly related with the frequency range, and it is inversely proportional to the frequency. Depth of penetration, which describe the range after which the field intensity is $1 / e$ of its incident value, for low-loss dielectric medium can be given as,

$$\text{depth of penetration} = \frac{c\sqrt{2}}{w\sqrt{\mu_r\epsilon_r[\sqrt{1+\tan^2\delta_c}-1]^{1/2}}} \quad (2)$$

Conductivity of almost many tissues is at certain level, which signifies that depth of penetration is biological tissues is going to be limited. For example, at 10 GHz it has been measured that even in a few centimetres electromagnetic wave attenuates 80 dB [17]. Also, at the 8 GHz it has detected that penetration depth of 2 cm at fatty tissue and 4mm in the muscle is obtained [8]. To summarize, in the microwave imaging of biological tissues trade-off between these three parameters, which are directly related to each other, exists, and should be carefully examined. In one of the previous study, optimum frequency range has been investigated for microwave imaging of biological tissues, and it is stated between 2 to 8 GHz [18].

1.1.2 Applications of Microwave Imaging

Before the medical applications of microwave imaging, first prototypes has been appeared for different purposes. A prototype using modulated scattered technique is developed at the University of Genoa [19], [20]. One of the first microwave imaging array composed of monopole antennas has been implemented at Illinois University [21]. A prototype system of microwave subsurface thermal imaging is applied by Miyakawa [22]. Millimetre wavelength imaging system using focal plane arrays is realized by Goldsmith et al. [23]. Resonant dielectric sensor for detection of dielectric contrast has been designed at the Bristol University [24], [25]. For passive radiometric imaging focal plane arrays has been developed working at 94 and 185 GHz in University of California [26]. With the developments on the inverse scattering algorithms and the computational power of the systems, first medical application prototypes of the microwave imaging systems are appeared. One of the first applications are aimed to be used in the medical, where clinical trials performed at the Dartmouth College. The proposed system has circularly arranged 32 monopole antennas which are working between 300 - 1000MHz. Also area between the antennas and imaging region is filled with coupling medium to decrease the reflection from the skin layer, and decreasing mutual coupling between the antennas [70]. Also microwave imaging system prototypes based on radar techniques is implemented. One of them is realized at the University of Bristol, in which system operates in the much higher wideband frequency range between 4.5 – 10 GHz [71]. Similarly, prototypes of microwave imaging systems for brain stroke detection have been appeared [27], and, in Chalmers University, for the same purpose a helmet composed of 10 antenna array of triangular patches is presented [28].

1.1.2.1 Breast Cancer

After realization of the fact that microwaves can be used in the imaging of the biological tissues theoretically and practically, breast cancer detection is become needed as one of the most essential application of this technology. Main reason of breast cancer detection gained prominence over the other applications of microwave imaging is that it is one of the dominant sources of deaths between the women. Presently, one of the major health worry for societies is cancer since one of a three men and one of a four woman is facing with cancer at the overall of the life. It is one of the ultimate critical present-day disease with a high mortality rate, and it is the second preeminent source of death after the cardiovascular disorder in the world [29]. In a late work, it is approximated that 1.3 million of people is going to die in a next year [33]. Furthermore, breast cancer is one of the prevailing type of cancer that is detected, as well as most detected cause of cancer deaths. All over the world above a million of women is diagnosed with breast cancer in each year; it has been found out that rate of diagnosing a woman is with breast cancer in United States very three minutes, and every 2.5 minutes in European Union [32]. Corresponding to the late studies, one of the eight women in America is going to experience breast cancer during entire of her life [31].

So, immediate detection and adequate treatment is awfully critical yet. Early detection is the leading way of protecting from breast detection. And, for early detection microwaves can provide noteworthy and steady contrast between malignant and other breast tissues [34]. For early detection of the breast cancer mass screening is going to be needed. As a consequence, to apply the mass screening all over the world, costs of the imaging or detecting devices should have more reasonable expense. However at the moment, most generally applied clinical diagnostic devices for breast cancer are X-Ray (Mammography), MRI, and Ultras-Sound [30]. And with these imaging systems, it is going to be hard to employ a mass screening. Microwaves are also a good candidate for the treatment of breast cancer with mass screening. With the rapid development of the wireless communication technologies, circuit costs at these frequencies are much more reasonable, compared to the other modalities.

1.2 Purpose of the Thesis

In last decade microwave imaging has highly progressed due to the high computational power of the computers and with the development of the nonlinear inverse scattering algorithms. On the other side, in the medical area need for a new imaging modality is increasing day after day. Some of the current imaging technologies has some health problems due to their ionizing radiation, also many of them cost too expensive which limits the mass screening. On the other hand, breast cancer becomes women's vital health issue, being epidemic, and becoming diagnosed even in younger people. Microwave imaging is very promising technology for early detection of breast tumor. It is non-ionizing and it can be easily applied on younger people, and it is possible to use in mass screening to detect the cancer in very early stage, which is very critical and known best method in the treatment of the cancer. However to implement the microwave imaging technology to the medical imaging of the breast tumor, an electromagnetic measurement system is needed. The most critical part of a electromagnetic measurement system is the antenna. In the first applications of the microwave imaging, like ground penetrating radar and through wall imaging, developing antennas are much easier due to non-existent space limitations. Besides space limitation, it is also known that the designed antennas must satisfy a minimum gain criterion to obtain sufficient signal to noise ratio levels, which is directly related to the spatial resolution. Other than that to further increase the spatial resolution the size of the antenna profile, polarization and the operating bandwidth of frequency must be specified carefully. For this reason, despite to the antennas which has been used in earlier applications of microwave imaging, like as ground penetrating radar, medical imaging requires more compact, wideband, linearly polarized, and high gain antennas. In this thesis, two novel types of Vivaldi antennas are presented to overcome these problems. Characteristic parameters of these antennas are measured and compared with a generic Vivaldi antenna. Additionally, these antennas have been tested with breast and tumor mimicking phantoms. It is shown that sensitivity of the system to the tumor response is increased with these antennas. Also, in another work, a nonlinear inverse scattering algorithm is used to test the imaging performance of the antenna. From the comparison of the reconstructions, which are obtained by classical Vivaldi

antenna and corrugated Vivaldi antenna, it is shown that the proposed novel antenna performs better in terms of the quality of the reconstructed images.

1.3 Organization of the Thesis

The work to accomplish towards to the purpose of thesis, is summarized in five chapters including this introduction one. In chapter 2, general type of microwave imaging antennas in the literature are referred. Also, requirements of the medical microwave imaging systems that differs from the general microwave imaging applications are indicated. In chapter 3, a novel cavity backed Vivaldi type antenna is introduced. After antenna is simulated and designed, it has been realized, and measured in an anechoic chamber. It has been seen that with this antenna, gain and front-to-back ratio of the classical Vivaldi antenna is increased. Also, comparison of the CBVA with a classical Vivaldi antenna is demonstrated through breast and tumor tissue mimicking phantom measurements. In chapter 4, another novel type Vivaldi antenna is presented for microwave imaging applications. In this antenna corrugations are introduced to a classical Vivaldi antenna. This antenna also simulated, designed, and realized on a Taconic RF-35 substrate. Radiation pattern measurements of the antennas are attained in anechoic chamber. It has been seen that without changing total size of the Vivaldi antenna, and just introducing corrugations impedance bandwidth and gain of the antenna is increased. Besides the development in the antenna characteristics, to evaluate the antennas in the microwave imaging system, antennas are compared to each other by reconstructed images that is obtained by measuring the same objects. Inverse scattering reconstruction algorithm is based on linear sampling method (LSM). It has been detected that with corrugated Vivaldi antenna more accurate images are obtained. Thesis is concluded in chapter 5, and main contributions are summarized and future research ideas are presented.

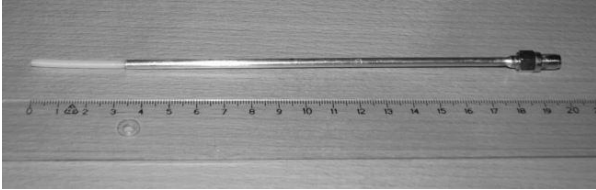
2. MICROWAVE IMAGING ANTENNAS

Antennas are one of the main part of a microwave imaging systems. Performance of the antennas have direct impact on capacity of the system principally on the resolution. Up to now, extensive literature has been formed about designing microwave imaging antennas. For ground penetrating radar (GPR) applications many antenna designs has been proposed. These include, TEM horn antennas [36], [37], wire bow-tie antenna [38], ridged horn antenna [39], cone antenna [40], log periodic antenna [41], spiral antenna [42], and etc. GPR antennas are typically suggested former than the medical imaging antennas in the literature. However, these antennas cannot be directly used in the medical applications. One of the reason is that in the medical applications antenna size is a critical parameter which can directly affect the spatial resolution, and the total number of the antenna that the system can handle. Also, medical imaging is differs from GPR by the very tiny size of the concerned objects, like as tumor. But, in the GPR case antenna size generally not a critical parameter while designing antennas. For this reason, different types of antennas are needed to be designed for later microwave imaging applications. To summarize this wide research topic, main antenna types used for microwave imaging is with these sub-titles.

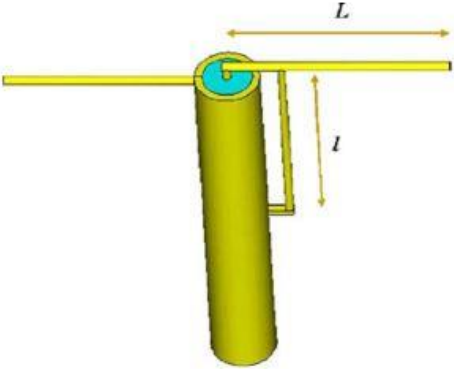
2.1 Biomedical Microwave Imaging Antennas

One of the most extensively used radiating antenna element in microwave breast cancer detection systems are dipole and monopole antennas because of their direct ready defined expression can be used in the forward solution of the electromagnetic numerical modelling regarding to the inverse problem [1], [46], [47], [48], [49]. In terms of agreement of the data and model, between the numerical model and the physics of the microwave, monopole antennas are one of the most accurate and simple radiating element generate premium quality images [50], [51]. Besides, they are easy to design, manufacture and cost low.

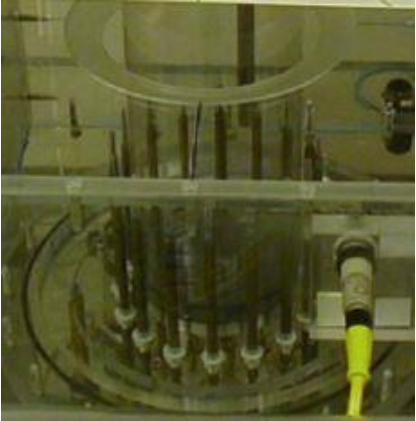
Some examples of these kinds of antennas are given in Figure 2.1. In addition, in some applications these antennas are used in coupling medium to deliver broadband bandwidth while radiation efficiency is reduced where system signal level is also weakened [52], [53], [56]. Lastly but not least, these antennas have typically omnidirectional radiation patterns which increases the multi scattering effects through with surrounding measurement devices, increase the dependence of the measurements to the nearby environment, and performance of the overall system is more dependent on the quality of the feeding cables.



(a)



(b)



(c)

Figure 2.1: Most widely preferred antenna elements in microwave imaging. (a) Monopole antenna formed from coaxial cable in which outer conductor is stripped 3.5cm from the top [29](b) Dipole antenna using with a balun reducing the additional radiation caused by undesirable currents on the outer shield of the cable [46](c) Antenna array consisting of 32 monopole antennas [49].

Another proposed antenna to be used in biomedical microwave applications is a ridged pyramidal horn antenna has been released to be used in the microwave imaging applications by Li et al [43]. In this design to decrease the size of the classical ridged horn antenna, resistive loading technique has been used, which result in low efficiency.

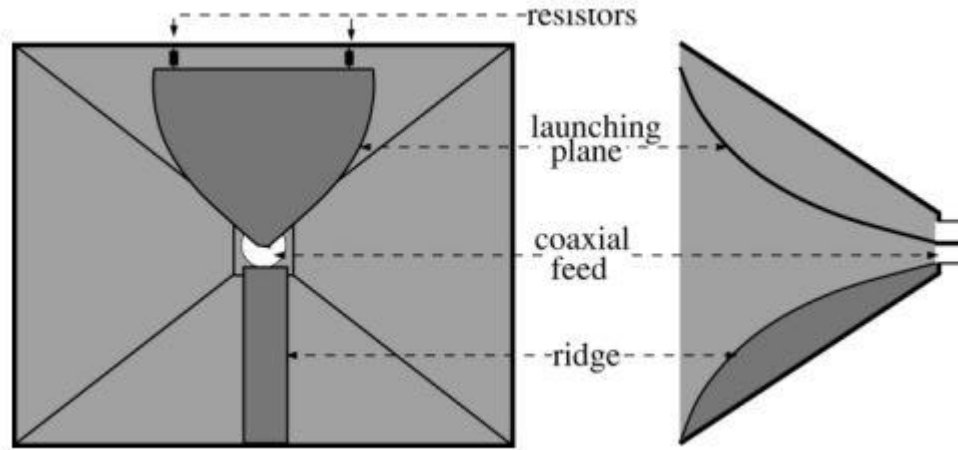


Figure 2.2 : Pyramidal ridged horn [43].

2.2 Wideband Imaging Antennas

With the improvement of the high quality microwave substrate materials has permit planar antenna designs. Properties of the planar antennas realized on high performance substrates do not alter achievements of the three dimensional (3D) initial antenna designs. Above mentioned microwave imaging antennas which are used in GPR applications are all 3D antennas, where size of the antenna is not essential.

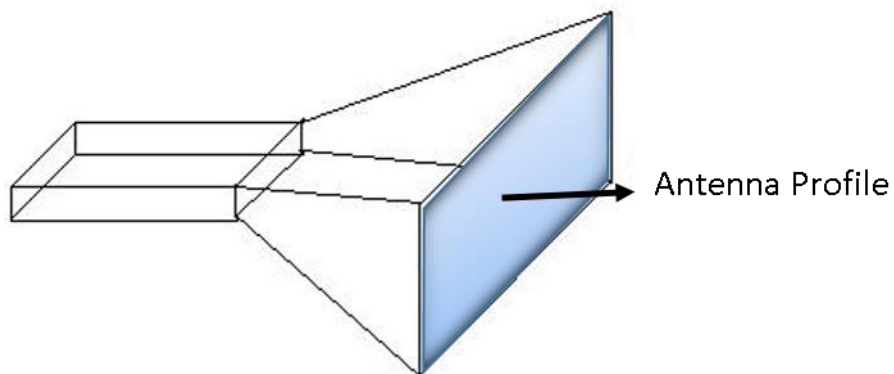


Figure 2.3: Horn antenna profile.

Antenna profile is an important parameter in the medical microwave imaging. Antenna profile can be defined as the total area of the antenna covers in the direction of the main beam of the antenna, as shown in Figure 2.3 for the horn antenna case. For example in the breast tumor detection system, total area of the breast is limited. So that, to increase the spatial resolution antenna profile must be minimized. For this

reason planar type of the antennas using high performance dielectric substrates are much more preferred in medical microwave imaging systems.

2.3 Antennas Design criteria's specifically for LSM and Contrast Source

Algorithms

The most promising advancements in the microwave imaging has been occurred in the nonlinear algorithms to solve the reconstruction problems, in recent times. With these powerful algorithms nonlinear problems, to which linear algorithm approach had been applied previously, is now easily solvable. Recently, in our research group (ITU – Electromagnetic Research Group) two methods has been proposed and published for microwave breast cancer imaging. The first one is a nonlinear microwave tomography approach based on the Contrast Source Inversion (CSI) method, and this nonlinear inversion method can perform imaging of tumors with size of 4mm, where the operating frequency is 1 GHz [54]. Furthermore, this method can easily reconstruct the breast tumor with a resolution of $\lambda / 75$, which shows the super-resolution of the method. As it is explicitly shown that with this nonlinear algorithms, half-wavelength diffraction limit can be overcome, and where the spatial resolution of the image was limited by the signal-to-noise ratio (SNR) [54]. For this reason antenna design for increasing the signal-to-noise ratio of the microwave imaging system is essential to expand the spatial resolution of the system. Second one is qualitative inverse scattering methods for microwave imaging applications, which are Linear Sampling Method (LSM) and Factorization Method (FM) [55], [98]. These are very promising methods which requires lesser computational power, and not so demanding to implement. In a recent work these methods are extended to their S-parameter based versions, which are more suitable for real world applications [98]. With these methods it is shown that by means of multi frequency measurements, the resolution of the image can be improved dramatically since the information related with the scatterer increases with increasing frequency diversity [98]. Hence, the bandwidth of the measurement system is going to be another critical parameter in the design process of the antenna, where the main purpose is increasing the spatial resolution of the system. Finally, both of the above mentioned algorithms are formulated for the cases where the incident electric field has single polarization. This is mainly due to the fact that the calibration of

measurement system is more reliable if the incident electric field is polarized in a single direction. Therefore, another specification for the antenna design is to achieve polarization purities as high as possible.

3. MICROWAVE BREAST PHANTOM MEASUREMENTS with a CAVITY-BACKED VIVALDI ANTENNA

3.1 Introduction

Microwave tomography is a broad term covering various biomedical imaging modalities mostly concentrated on breast cancer diagnosis. Such concentration on breast cancer is motivated by both technical aspects such as non-ionizing nature of microwaves as well as humanitarian impacts of prevalence of breast cancer worldwide [57]. The basic imaging mechanism among all microwave tomography methods is based on the observation that different tissues possess different electrical properties specifically in terms of dielectric permittivity. This contrast among various tissues can be exploited to detect malignant tumours in breast which are measured to have higher dielectric permittivity as compared to normal tissues [58]. Great variety of methodologies ranging from Ultrawide-band radar based approaches to nonlinear inverse scattering methods which aims to reconstruct breasts' dielectric profile have been attempted for imaging purposes [59], [60], [61], [62], [63], [64], [65], [66], [67], [68], [69]. Consequently several microwave imaging systems for breast cancer diagnosis have matured enough to reach clinical trials [70], [71], [72], [73], [74]. For a recent review of microwave imaging modalities, we refer to [75].

3.2 Microwave Breast Measurement Systems

To our knowledge most of the microwave measurement systems for breast cancer diagnosis consists of multiple antennas with fixed positions. These antenna systems are mostly immersed into lossy coupling medium. Later S_{21} measurements are performed with a vector network analyser (VNA) that is connected to a microwave switching matrix. Such configuration has several advantages like miniaturized antenna dimensions due to higher dielectric permittivity of the coupling medium and relatively short scanning duration because of electronic switching. On the other hand, the lossy

coupling medium which is in fact used for attenuating the multiple scattering effects, dramatically reduces the scattered field levels as well. Another issue with this approach is that the number of measurements for a certain frequency is limited with the number of fixed antenna positions which in turn depends on the switch's number of ports and its performance characteristics.

In this paper, we consider an alternative measurement approach where two rotating antennas are employed. In this case, the receiving and the transmitting antennas are mounted on a mechanical scanner and the antennas are directly connected to the VNA without any switching matrix. We intentionally avoided lossy immersion medium which is not feasible with mechanical scanner and concentrated on free-space measurements. This measurement configuration is not appropriate for radar based imaging methods where the primary reflection from the skin poses a challenge on the other hand, nonlinear inversion methods such as the contrast source inversion (CSI) method can benefit greatly due to increased number of measurements [76]. The major drawback of free-space measurements configuration is multiple scattering from mechanical parts. In order to reduce multiple scattering effects, such systems are needed to be covered with microwave absorbing materials like pyramid absorbers and the antennas mounted on the system are needed to be highly directional since side lobes creates unwanted reflections from mechanical parts.

Within this context, we designed a novel cavity-backed Vivaldi antenna (CBVA) specifically for two rotating antenna configuration. The foremost novelty of the antenna lies on the use of reflector structure which results in reasonable increase in gain compared to conventional Vivaldi antennas. In the design of the antenna, we prioritize miniaturized overall dimensions that are appropriate to be mounted on rotating mechanical parts. Furthermore, broadband radiation characteristics and linear polarization are other requirements of the design specifications. Later, we have performed various microwave breast phantom measurements with the realized antennas for validating the design criteria as well as gaining insights about possible outcomes before human experimentation. The main objective of these measurements is to reveal if the realized antennas allow us to measure scattered field contributions of the small dielectric inclusions inside the breast phantom structure. The ability to sense such small changes in scattered field is a crucial issue for the microwave breast

scanners and the antenna characteristics are integral part of the mechanism. Thus we organize the measurement scenario to emphasize the measurement of the scattered field due to a tumour.

3.3 Antenna Design and Performance

The basic premise in microwave tomography is to exploit variation of complex dielectric permittivity among different tissues to reconstruct an image. It is generally regarded that to achieve a better resolution for reconstructed images microwave excitations with higher frequency components are necessary but this contradicts to well-known skin depth effects which restricts penetration of higher frequency components into biological tissues a result of high conductivity associated with water content of those tissues. Thus usage of multi-frequency measurements is quite important to take advantage of both better resolution as well as better microwave penetration which in particular may enable to diagnose deeper tumors for breast cancer screening. Furthermore, complex dielectric permittivities of biological tissues are frequency dependent quantities and their frequency dependencies may be exploited to characterize tissues for diagnosing malignancies. Accordingly, the antennas employed in the measurement system are needed be broadband to take advantage of such information. As noted earlier, practical microwave tomography systems extensively employ VNAs to measure scattering parameters instead of directly measuring electric field. The measured S-parameters are later converted to scattered electric field under several assumptions one of which is linear polarization of antennas. Under linear polarization assumption, vector nature of electromagnetic scattering mechanism can be reduced to scalar case which simplifies imaging algorithms such as CSI [76]. After converted to associated scattered electric field, various imaging methods can be applied to measured quantities. The antenna specifications that are outlined earlier lead us to design of a CBVA. The design process is realized using commercial 3D finite element solver (HFSS) and the dimensions of the antenna is finalized as $63 \times 51 \times 1 \text{ mm}^3$ and the realized prototype on FR4 substrate with $\epsilon_r = 4.4$ is shown in 0. The feed section is designed such that the antenna can be fed at the centre of substrate which is more convenient for the rotating scanner. At the bottom side of the antenna radiation flares are placed, which is exponentially tapered slotline given with $1.416 \times e^{0.081}$, and

slotline is terminated by rectangular slot cavity at back with dimension of $5.67 \times 21 \text{ mm}^2$. Top of the antenna consists of microstrip feed line, with a width of $W_{stub} = 0.976 \text{ mm}$, ended with radial open stub with a radius of $R_{stub} = 9 \text{ mm}$, and angle of $\theta_{stub} = 90^\circ$.

After the standalone antenna design, to further enhance the antenna radiation characteristics, reflector structure has been affixed. The dimensions of the trapezoidal reflector are carefully determined as $49 \times 83 \text{ mm}^2$ on the front and $25 \times 83 \text{ mm}^2$ on the backside with 94 mm width to avoid the impedance mismatch. The prototype which is realized with a thin copper as covering material and stabilized with foam is shown in Figure 3.2.

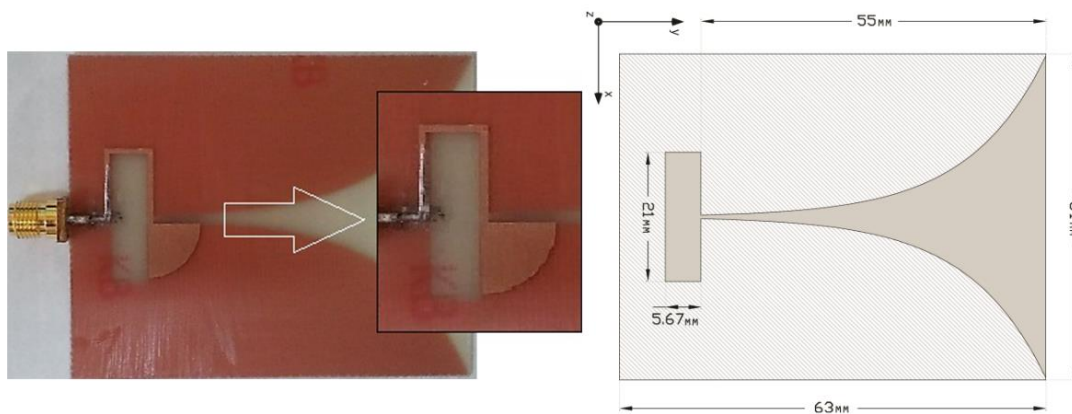


Figure 3.1: Front view of the designed Vivaldi antenna: Feed section is detailed.

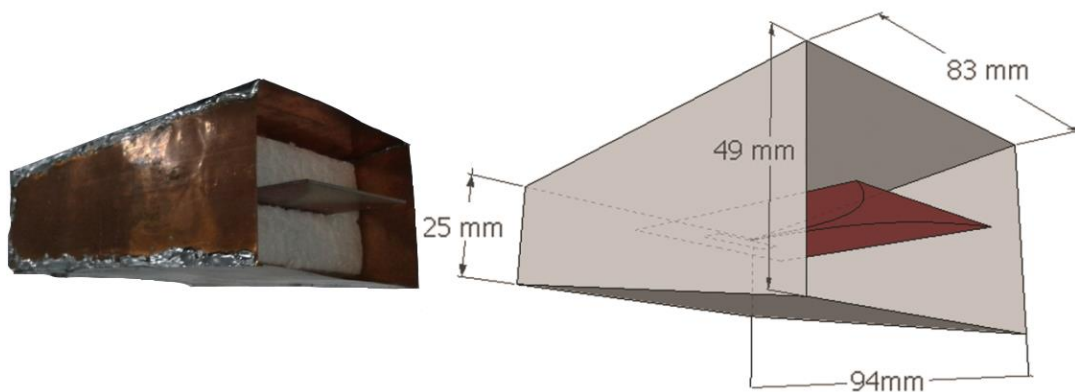


Figure 3.2: Cavity-backed Vivaldi type antenna (CBVA).

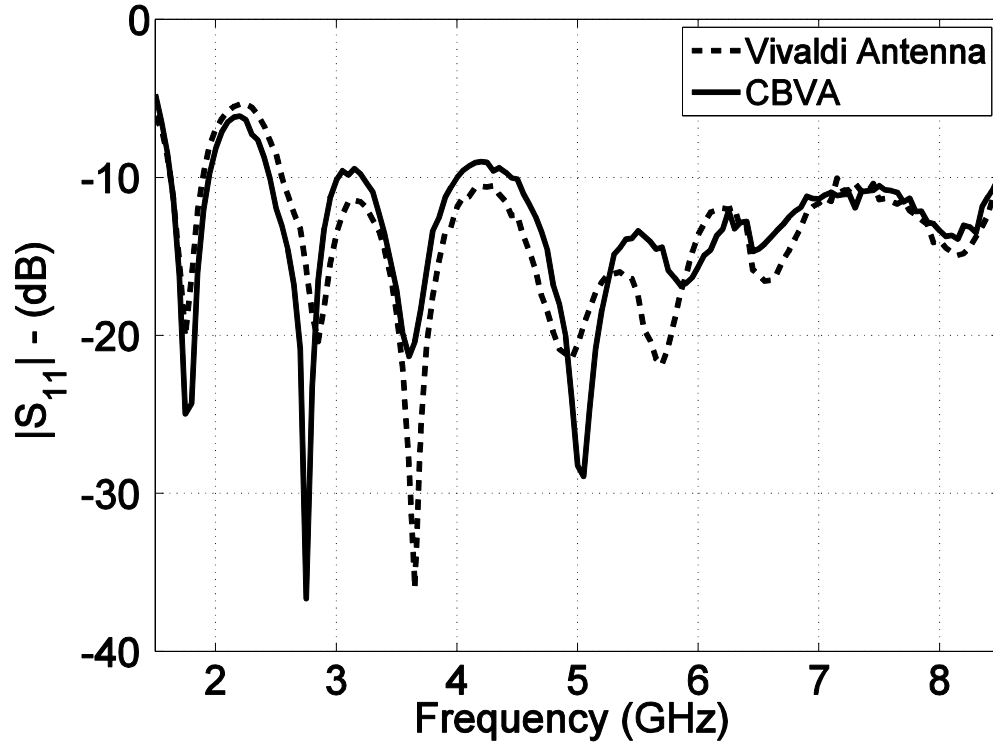


Figure 3.3: The reflection coefficient of the antennas (S_{11}).

The prototypes of the antennas are measured with a planar near field antenna measurement inside an anechoic chamber using Agilent N5242A VNA. Measured reflection coefficients up to 8.5 GHz for the standalone antenna and cavity-backed antenna is shown in 0. The -10 dB bandwidth of 6 GHz starting from 2.5 GHz to 8.5 GHz is obtained. The measured radiation patterns at several frequencies of 4 GHz, 6 GHz, and 8 GHz are plotted and shown in 0. The measured maximum gain of the antennas on the broadside direction is shown in 0. While overall characteristics of CVBA resembles ridged horn antennas, CVBAs offer lightweight structure and compact dimensions as compared to horn antennas, which makes them convenient for rotating systems. We observe that CBVA compared to standalone antenna, the maximum gain is increased 2.1 dB at the boresight of the antenna and the front to back ratio is decreased by 8.5 dB on average across the operating bandwidth. These improvements on the antenna characteristics are important to able to sense and measure small differences in the field. Furthermore, improved front to back ratio warrants reduced multiple scattering effects from the mechanical parts.

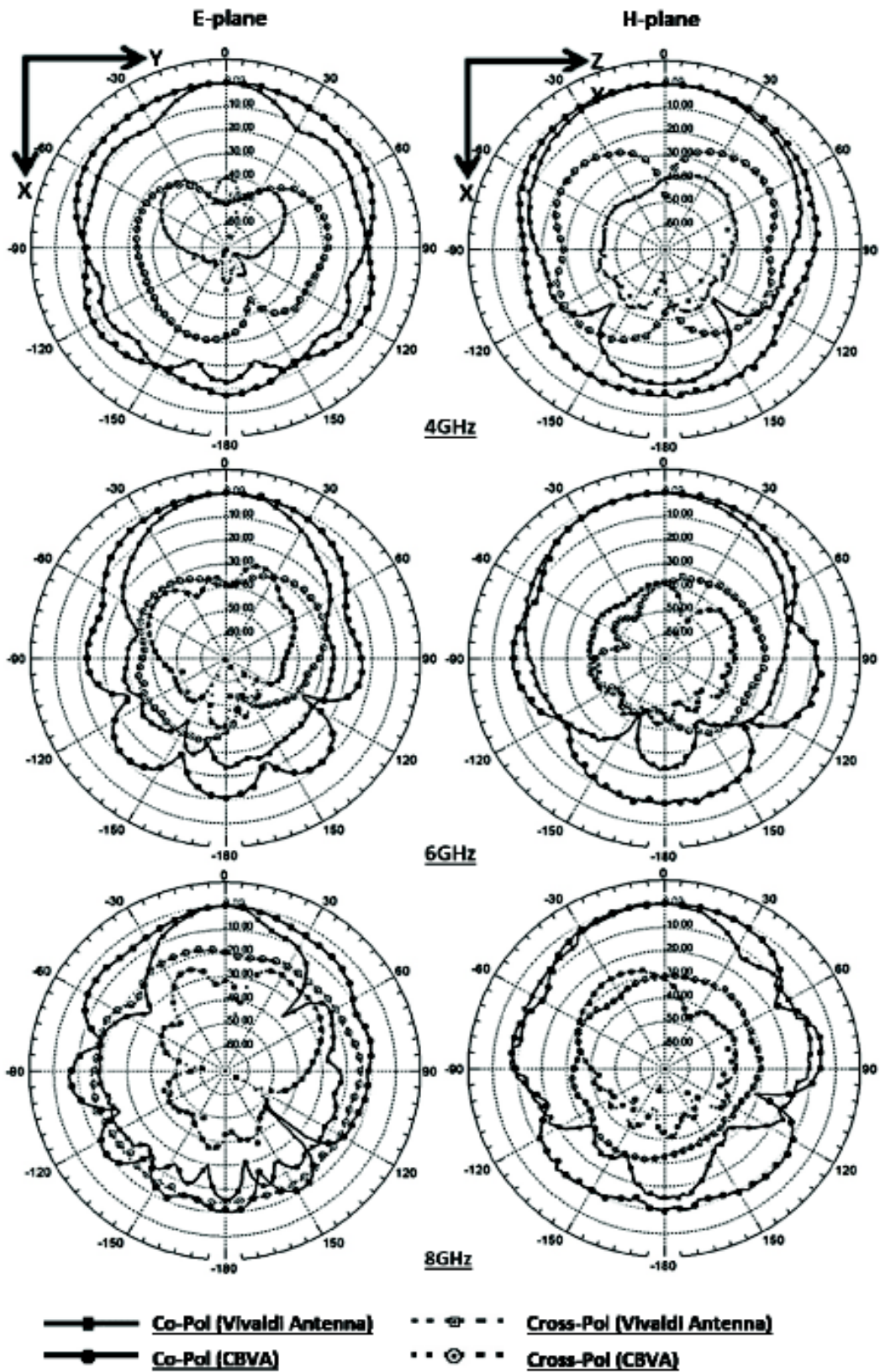


Figure 3.4: Measured radiation patterns at 4GHz, 6GHz, and 8GHz.

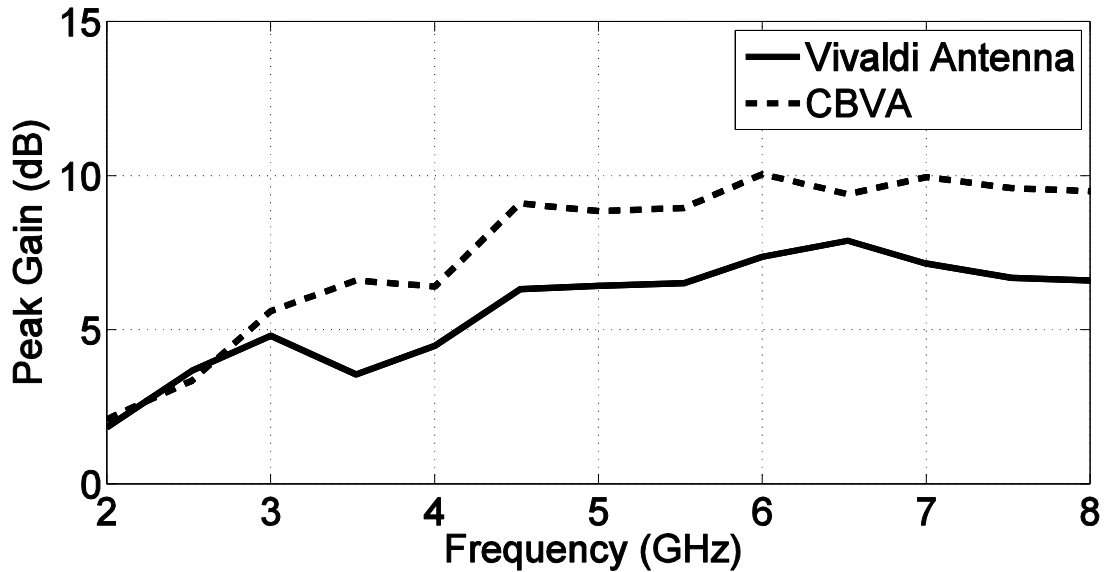


Figure 3.5: Maximum gain on broadside direction.

3.4 Breast Phantom Measurements

Our motivation with the breast phantom measurements is to understand what to expect in terms of field strength when a small high contrast dielectric inclusion like a malignant tumour is present inside a homogeneous breast phantom. This is an important, initial step because the ultimate goal in microwave breast imaging is to detect such small tumours inside a female breast. In terms of electrical properties, the female breast is highly inhomogeneous and lossy, furthermore contains fibro glandular tissues which is known to possess comparable electrical properties with malignant tumours [77]. While the field strength cannot be directly related to the ability of detecting tumours, it is evident that microwave scattering is a volumetric interaction, thus to be able to sense a small tumour, any microwave breast scanning system is required to be able to measure corresponding small field changes. Besides the performance of other system blocks such as dynamic range of the VNAs or isolation of microwave switches, the antenna characteristics are significant factors that determine the overall sensitivity of the system. Hence to test the designed prototype antenna in microwave breast phantom measurements, we used a custom built mechanical scanner which can rotate antennas in polar coordinates $\varphi \in [0, 2\pi)$. The antennas are placed such that their front edge is 11.5 cm away from the centre which is a moderate distance if we consider semi-spherical scanning when patient is lying in

a prone position. All field measurements are performed at total 72 equiangular points with 5° separations. Since we use only two antennas, nonlinear multiple scattering effects are less effective than in the case of scanners with multiple fixed antennas. Moreover, number of measurement points is not limited with number of fixed antennas or number of ports in microwave switches. The scanner is placed inside a full anechoic chamber together with additional absorbers covering the scanner. The field measurements are performed with a VNA (Agilent N5242A) and VNA parameters are set as follows: IF bandwidth is 10 Hz, output power is 10 dBm and frequency range is from 2GHz to 8GHz with 250MHz separations. Before further advancing, it should be noted that IF bandwidth of VNA is a critical parameter for overall performance of measurement system. While reducing IF bandwidth greatly enhances the dynamic range of VNA, it is the leading factor that determines total data acquisition time of measurement system even when latencies due to mechanical movements of rotating scanners are considered. In fact, mechanical movements can be highly accelerated by optimizing motor controllers. On the other hand, there is no way to decrease total measurement duration other than increasing IF bandwidth which is inversely proportional to sweep time of VNA.

A semi spherical breast phantom with radius 5 cm which is shown in 0 is modelled after breast fatty tissue and a cylindrical tumour phantom with radius 2.5 mm and height 20 mm is produced as explained in [77]. Later, the breast phantom is placed inside a very thin ceramic carrier as seen in 0. The relative dielectric permittivities and conductivities of phantoms and ceramic carrier, which are plotted in 0, are measured with Agilent 85070 dielectric measurement kit.



(a)



(b)

Figure 3.6: Homogenous breast and tumour phantoms (a) Semi-spherical breast phantom (b) The tumour phantom is inserted inside breast phantom.

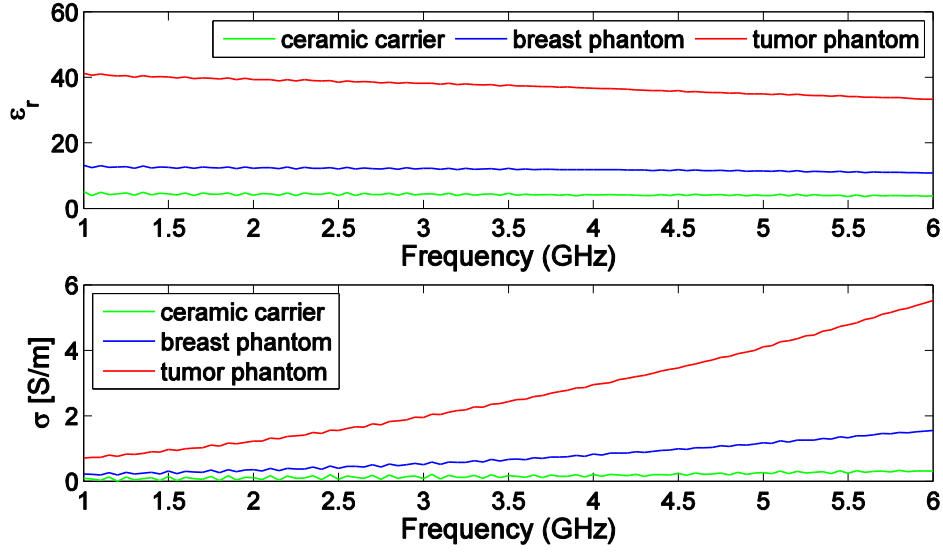
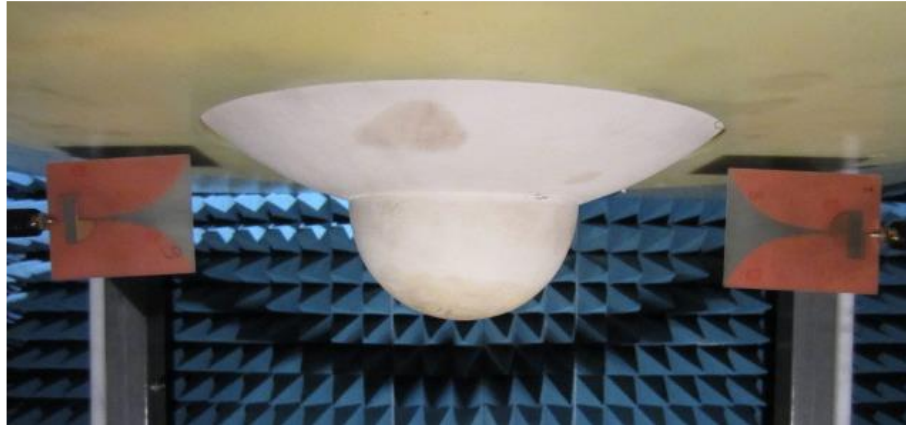


Figure 3.7: Relative dielectric permittivities ϵ_r and conductivities σ of breast and tumour phantoms.

Most of the inversion methods which aim to reconstruct complex dielectric permittivity distribution ϵ_r' of the breast from the measured scattered field are formulated in terms of electric field vector. Thus, it is required to measure the scattered electric field vector with an appropriate microwave measurement system. On the other hand, the electric field vector can be related with the S_{21} parameter of the measurement system containing breast phantom. Our measurement procedure is implemented as follows: First the microwave system which contains cables and VNA is electronically calibrated with Agilent N4691 E-Cal module. Then the realized antennas are mounted to the system and the scattering parameter S_{21}^{brs} of the breast phantom without tumour phantom inclusion is measured. Later a tumour phantom is inserted inside the breast phantom (See 0) and the scattering parameter S_{21}^{tot} of this new configuration is repeated. Finally, the scattered field parameter S_{21}^{sct} due to the existence of the tumour phantom is obtained as:

$$S_{21}^{sct}(\varphi) = S_{21}^{tot}(\varphi) - S_{21}^{brs}(\varphi) \quad (3)$$



(a)



(b)

Figure 3.8 : Measurement configurations (a) Two antennas are positioned opposite to each other and the breast phantom is in between (b) Antennas positioned side by side and directed towards the breast phantom.

It is obvious that multiple scattering effects due to antennas and other reflections from scanner parts should be minimized for the validity of Eq. 3. We consider two different measurement configurations:

- I) The receiving and the transmitting antennas are positioned opposite to each other as shown in Figure 8(a) which is similar to the Computed Tomography (CT)
- II) The receiving and the transmitting antennas are located side by side as shown in 0(b) which is similar to bi-static radar configurations.

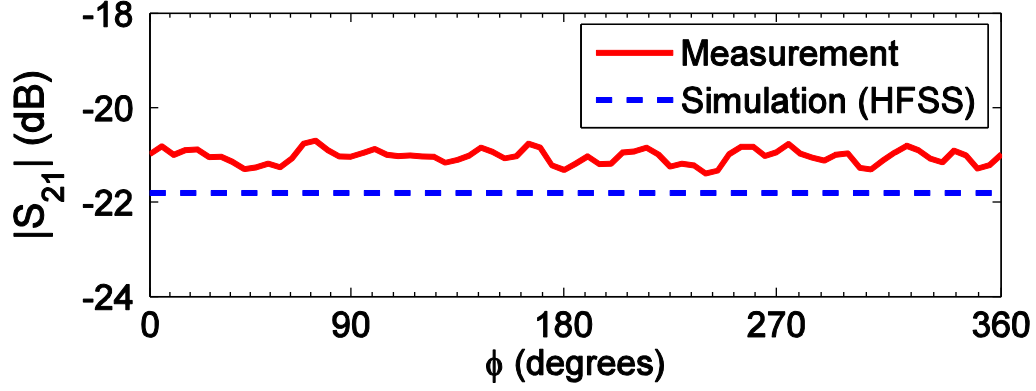


Figure 3.9: Comparison of S_{21} between the measured and the simulation.

Before advancing, to attest the validity of the measurement system, we have compared the magnitude of S_{21} measurements in free space for the configuration (II) against simulation results. As it can be seen in 0, the measured and simulated values of S_{21} are very close. The flatness of the measurement result is actually an indicator of the accuracy of the measurement system. We note that while it is possible to make measured data smoother with filtering, all the measurement results in the paper are presented in their raw form without any post-processing.

As noted earlier, our aim with these measurements is to sense field changes due to small inclusions inside the breast phantom, thus to understand the upper level of scattered field strength, we have repeated same measurements for a metallic inclusion with same dimensions with tumour phantom.

In Figure 3.10 we first present the total field measurement results from the breast phantom in the absence of tumour at 4 GHz, for both measurement configurations. Since the breast phantom is almost homogeneous and the measurement system is symmetrical, the field variation is almost flat for all angular positions. Note that the field level in the measurement configuration (II) is much stronger than that of configuration (I).

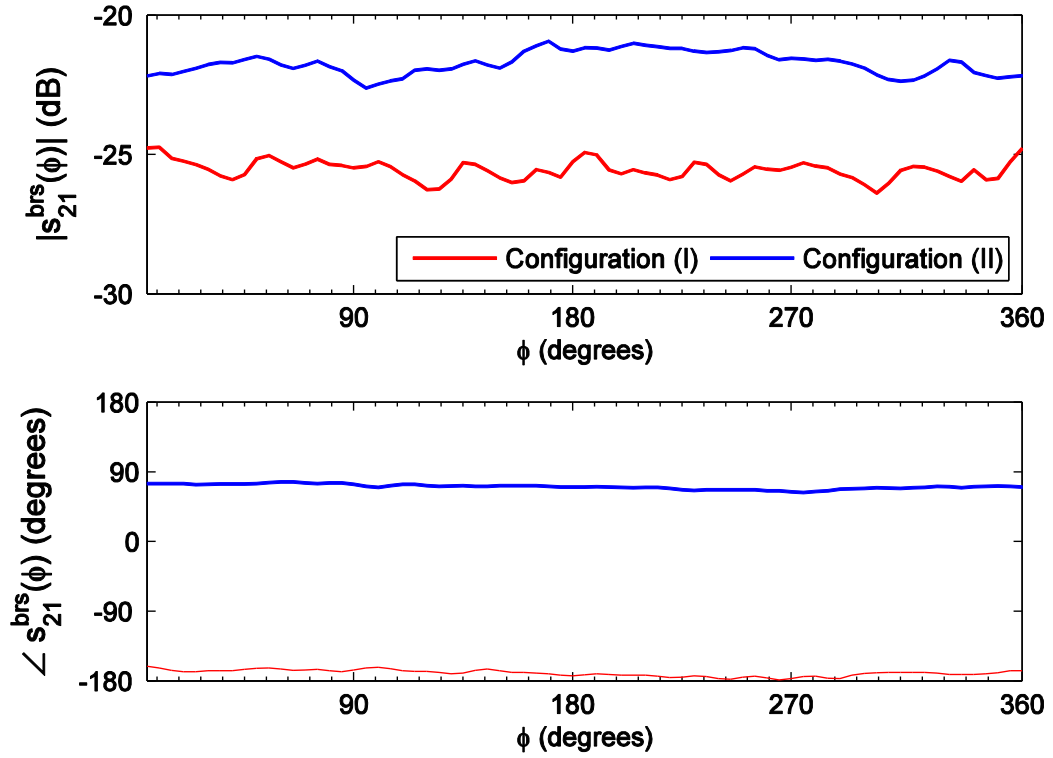


Figure 3.10: Amplitude and phase of measured $S_{21}^{brs}(\varphi)$ values for the configurations (I) and (II) at 4 GHz.

The scattered field values due to the tumor phantom and the metallic object obtained in measurement configuration (II) at 4 GHz are shown in 0. The measured field levels of both inclusions are comparable while the field variation due to the metallic object has sharper pattern. As mentioned earlier, broadband operation of the antenna is in our design criteria, to demonstrate the performance of the antenna at 8 GHz, we performed same measurement in configuration (I) which is shown in 0. It is evident from both measurements that the scattered field due to the tumour is a quite weak signal. While the overall sensitivity of the scanning system is limited with the VNA's dynamic range which is typically higher than 100 dB, increasing output power can improve the sensitivity for free-space measurement systems. From the practical perspective, this requires to use power amplifiers at transmitters and LNAs at the receivers because the output power level for most VNA's are around 10 dBm. On the other hand such configurations complicates the calibration procedure, thus it is quite important to increase sensitivity passively with antenna characteristics. In this context, to see the effect of the reflector structure, we have repeated measurements for the horizontal

polarization in configuration (I). The comparison of the measured $S_{21}^{sct}(\varphi)$ with the standalone antenna and the antenna with reflector cases for the tumour and the metallic object is shown in Figure 13. It is clear that the reflector improved the measured signal level approximately 5 dB at average. Such improvements are crucial for increasing the overall sensitivity of the measurement system. Consequently, the dielectric contrast among tissues is the very basis of microwave tomographic approaches for breast cancer screening. It is evident that when the dielectric contrasts among tissues get closer or the dimensions of the tumor get smaller, it is unlikely to diagnose the tumor with microwaves since the level of scattered field may easily fall below the noise floor. To overcome such cases, it is hypothesized that contrast agents which can enhance the dielectric permittivity of tumours may be developed.

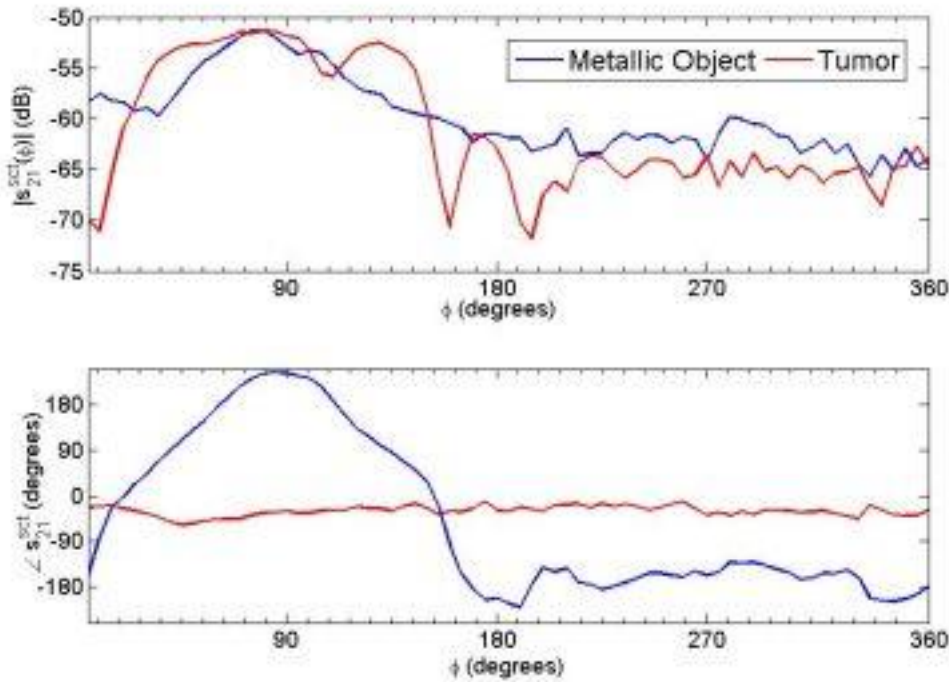


Figure 3.11: Amplitude and phase of $S_{21}^{sct}(\varphi)$ for the tumour and the metallic object at 4 GHz in configuration (II).

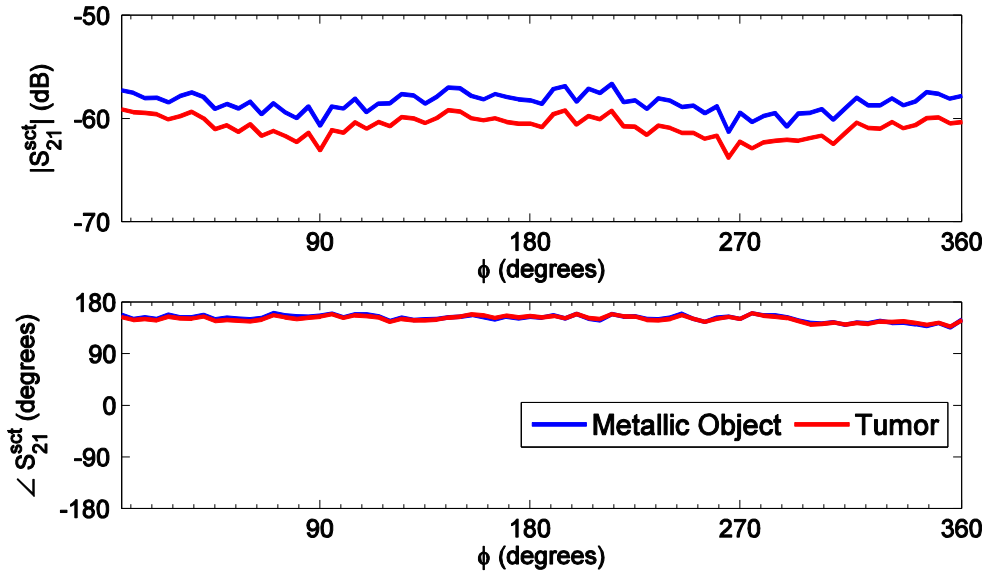


Figure 3.12: Amplitude and phase of $S_{21}^{sct}(\varphi)$ for the tumour and the metallic object at 8 GHz in configuration (I).

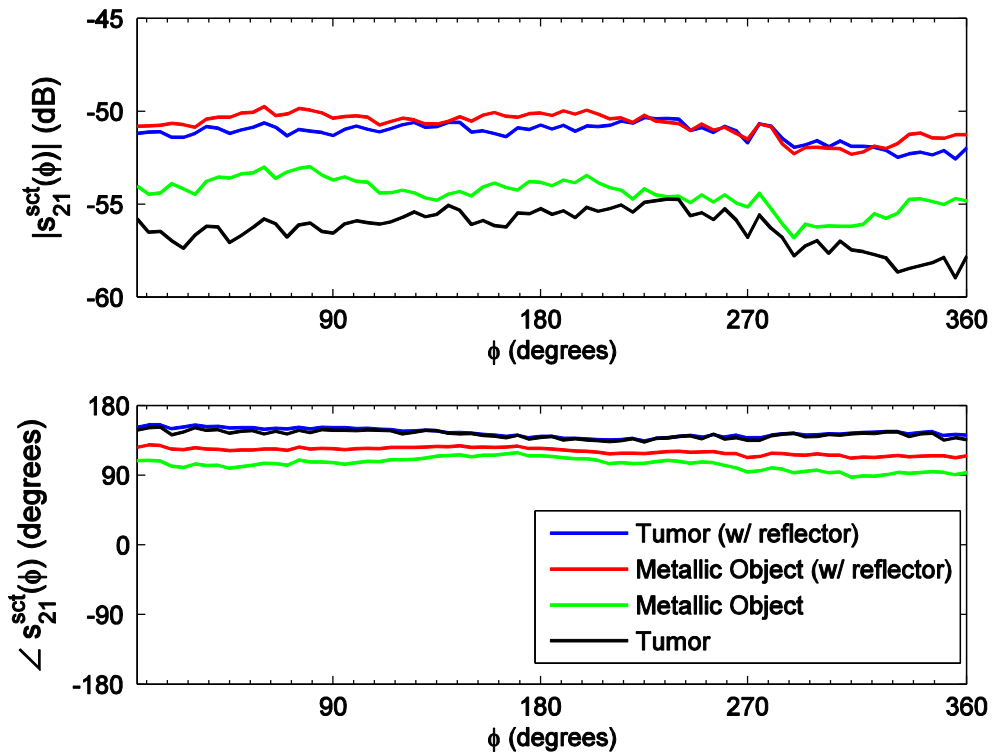


Figure 3.13: The comparison of measured $S_{21}^{sct}(\varphi)$ for the standalone antenna and CVBA in configuration (I). The measurements are performed for horizontal polarization at 8 GHz.

3.5 Conclusion

We design a new CBVA which is appropriate to be mounted on rotating microwave breast scanners that performs free-space measurements. By affixing a carefully designed reflector structure, antenna gain is increased at least 2.1 dB compared with the conventional Vivaldi antennas. This increase in gain is advantageous because the output power levels for microwave breast scanners are generally limited the output powers of vector network analysers. Furthermore, the effects of multiple scattering from mechanical parts are reduced with the increased directivity. The evaluation of the antennas for microwave breast phantom measurements reveals that the designed antennas are suitable to measure small changes in field distribution which is the basis for detecting early stage tumours inside the female breast.

4. CORRUGATED VIVALDI ANTENNA for MICROWAVE IMAGING

4.1 Introduction

Antennas are important parts of microwave imaging (MWI) systems and antenna radiation characteristics significantly affects the imaging capabilities. Regardless of the imaging method, the common basis of MWI is to exploit the scattered electric field to retrieve physical properties of inaccessible objects remotely. Such procedures are quite challenging due to the ill-posed nature of the inverse problems [78]. One effective solution to combat with the ill-posedness is to increase the amount of information in the scattered field by designing antennas with better characteristics.

Vivaldi antennas are one of the member of the travelling wave antennas with endfire radiation characteristics. First stripline-fed exponentially tapered slot antenna is introduced 1970's [79] . Later, a variant antenna with antipodal feed structure is presented [80]. After, a balanced antipodal design with three layers of tapered slots is suggested in [81]. However, the offset between exponentially tapered slots causes substantial cross-polarization [82]. Another fundamental variation of the Vivaldi antenna has double exponentially tapered slots where outer edge is also tapered [83]. Vivaldi antennas have been a good candidate for many real life applications, extending from radar systems to ultra-wideband imaging systems due to their radiation patterns and impedance matching performance [84][85]. Although being theoretically infinite, their operating bandwidth is practically limited due to the transition between the slotline and the feedline. Also, these antennas have other attractive features like compact size, low cost and easy fabrication with the printed circuit technology. They deliver medium gain depending on the length of the taper and exponential shape. However, at the lower end of the operating bandwidth a dipole like radiation is observed and the gain becomes lower. This is due to fact that the length of the slot becomes electrically small in this frequency band. Several studies give detailed design criteria's and performance analyses of Vivaldi antennas [86][87]. Other than that,

some compact Vivaldi antenna design techniques have been proposed also, but they have limited gain especially at the low frequency band [88][89][90].

Main goal of this work is to design a Vivaldi type antenna to achieve a higher maximum gain at the boresight throughout the operating bandwidth, especially for the problematic low frequencies. The reason to select such a specification is that the improvement of the radiation characteristics at low frequency band increases the overall imaging performance. This is especially true for the medical imaging, since microwave illumination at low frequencies enables high penetration into human body and allows a multiple frequency imaging, which is shown to be significant in [91]. Moreover, as the directivity increases, the beamwidth of the antenna decreases and a smaller spot with limited volume is illuminated by a more focused beam. It is shown that more energy can penetrate into the tissue and the signal-to-noise (SNR) of the system can be increased, by decreasing the beamwidth of the antenna [84]. Apart from the high gain requirement, a low level back to front ratio is desired for the microwave imaging purposes. This is also an important measure for the antennas employed in MWI, since the higher back radiation levels turns into the increasing measurement deficiencies caused by the multiple scattering through the interaction with the environment. Another objective in the design of the Vivaldi type antenna is to obtain a relatively small size compared to the anatomy of the scatterer. This is important from the aspect that as the size of the antenna gets smaller the sampling density of the field distribution can be increased, which gives rise an increase in the resolution of the reconstructed image. Furthermore, having low cross polarization levels in the operating bandwidth is another target, since the high cross polarization levels increase the measurement imperfections for the situations where the polarization purity becomes critical. Lastly, operating frequency band of the antenna is desired as 2 to 8 GHz, since this frequency band is shown to be useful for different microwave imaging modalities such as medical imaging [18].

In this work, we introduce a novel Corrugated Vivaldi antenna (CVA), which utilizes the idea of creating corrugations to attain the above mentioned properties by decreasing the induced currents on the edge of the Vivaldi antenna, which can degrade the performance [92]. The notion of using corrugations to obtain better characteristics is used for different antennas, such as Horn antennas [93][94]. However, this concept

is not yet applied to the Vivaldi antennas except the antipodal Vivaldi antennas, which have relatively high cross polarization levels [95][96][97]. We make a detailed analysis of the characteristic parameters of the designed CVA both by means of the measurements. Going beyond to giving characteristics of the designed CVA, we experimentally show the performance of the CVA compared to a generic Vivaldi antenna (VA) of the same size. For this purpose, we set several experimental configurations and data acquisition is made by both VA and CVA for the same configurations. Then, obtained scattering parameter (S-parameter) data is directly used in a newly proposed a MWI method, the S-parameter based Linear Sampling Method [98], which originates from a well-known qualitative inverse scattering method Linear Sampling Method (LSM) [99]. We choose S-LSM method for MWI purposes because of its simplicity and its antenna dependent nature, which makes S-LSM more suitable for real life applications. Qualities of the obtained results are assessed by two quantitative criterions. Both the visual results and the quantitative criterions show that the novel CVA design performs better than VA.

Organization of the work is as follows: In the subsequent section, a detailed analysis of CVA is made, measured characteristics of the CVA are given. Then in the next section, S-LSM is briefly explained. After, a comparative performance analysis of the VA and the CVA for S-LSM is made by means of several experimental datum retrieved in an anechoic environment. Throughout this study, the time factor is assumed as $\exp(-i\omega t)$ and suppressed.

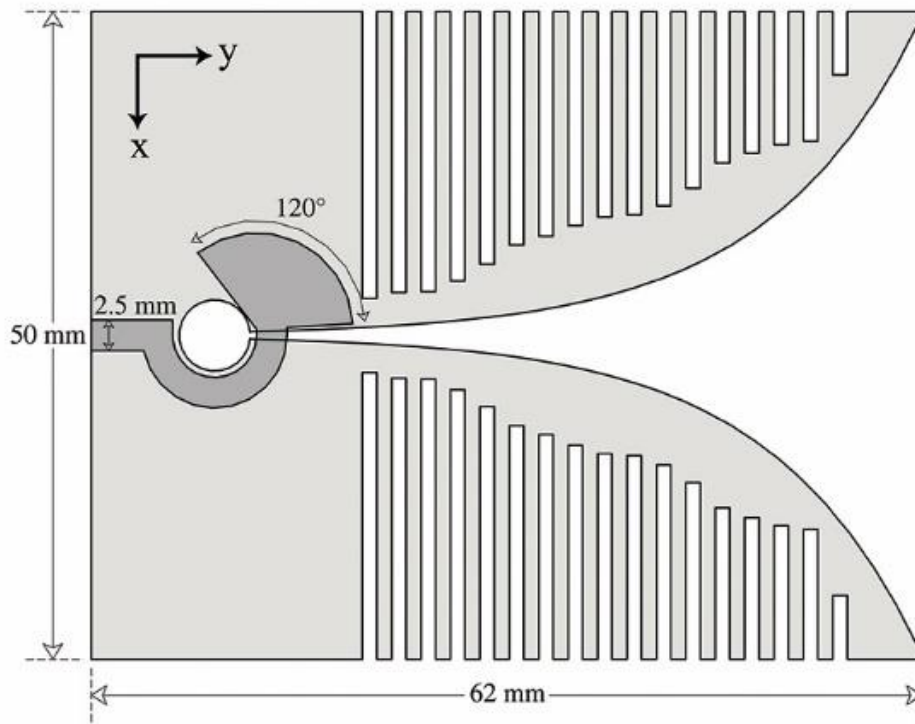


Figure 4.1: Top view of the proposed CVA. (Darker gray part is the back view.)

4.2 Corrugated Vivaldi Antenna

The initial design of the proposed corrugated Vivaldi antenna (CVA) originates from a conventional Vivaldi antenna. As an initial work the generic Vivaldi antenna (VA) is designed, realized and measured. The top view of the VA including the feed, which is at the back of the substrate, is shown in Figure 4.1. The dimensions of the VA are 50 mm x 62 mm. To validate the proposed design, it is simulated and realized on a Taconic RF-35 substrate with relative dielectric constant ϵ_r of = 3.5, the lost tangent of $\tan \delta = 0.0018$ and substrate height of $h = 1.52$ mm. The feed of the VA is a microstrip to slotline transition, which is at the back side of the substrate. Exponentially tapered radiation flares are at the top side of the antenna as shown in Figure 4.1. In Figure 4.1, the antenna lies in the xy-plane and its normal direction is directed along z-axis. In such a configuration, E- and H-planes of the antenna is xy- and yz-planes, respectively. For ease of physical connection with the coaxial input, microstrip line feed is centred with respect to the x-axis. Having a width of 2.5 mm,

this feed constitutes a broadband stripline to slotline transition by a radial open stub, which has a radius of $R_{stub} = 6.5$ mm and angle of $\theta_{stub} = 120^\circ$. The exponential tapers are defined with the equation of $x = 1.528 \times \exp(0.079y)$, which is backed by a circle with a radius of 2.92 mm. The proposed structure is designed and optimized using the commercial electromagnetic simulation tool HFSS by ANSYS.

Table 4.1: Lengths of the slots.

Slot # 1	22.4 mm
Slot # 2	21.96 mm
Slot # 3	21.88 mm
Slot # 4	21.20 mm
Slot # 5	19.75 mm
Slot # 6	18.20 mm
Slot # 7	17.57 mm
Slot # 8	16.70 mm
Slot # 8	16.60 mm
Slot # 10	15.90 mm
Slot # 11	15.30 mm
Slot # 12	13.80 mm
Slot # 13	12.10 mm
Slot # 14	11.90 mm
Slot # 15	10.50 mm
Slot # 16	10.20 mm
Slot # 17	5.20 mm

After finalizing the design of the VA, both edges are symmetrically corrugated by the slots parallel to x-axis. 17 slots on each side, which are separated by 1.2 mm, constitute the total corrugation of the antenna. The width of the corrugations are 1.15 mm and their lengths range from 5 mm to 22.4 mm as listed in Table 4.1. The distance between the y-coordinate of the first slot and the connector is 20.20 mm. During the addition of the corrugations no change is made on the primary design. Geometrical parameters of all slots (i.e. the position of the first slot, the distance between the slots, the length and the width of the slots) are optimized with the HFSS. The targets of this optimization are to achieve the maximum gain and the maximum front-to-back ratio as well as a -10 dB frequency bandwidth as large as possible.

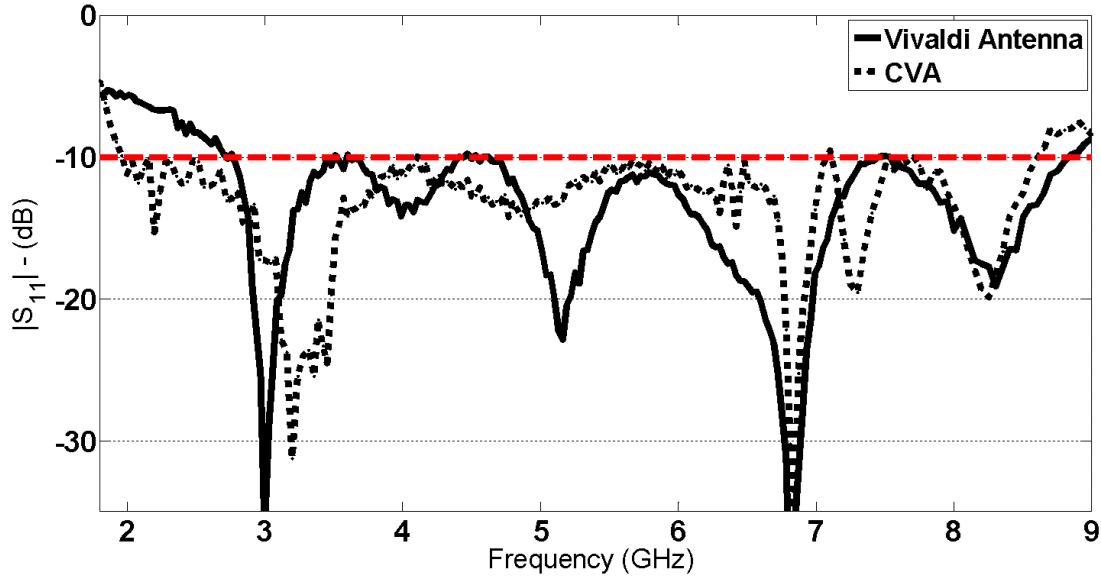


Figure 4.2: Measured reflection coefficient ($|S_{11}|$) response for both antennas.

To verify the developed designs both antennas are fed by 50Ω SMA connectors. Measurements to evaluate the performance of the antennas are carried out between 1.8 GHz to 9 GHz, which covers the desired frequency band for microwave imaging operations. Throughout the antenna measurements Agilent 5242A vector network analyser is used for scattering parameter (S-parameter) measurements. Figure 4.2 shows the measured reflection coefficients ($|S_{11}|$) for both antennas. $|S_{11}|$ measurements show that the measured reflection coefficient is better than -10 dB from 2.72 GHz to 8.84 GHz for VA and 1.96 GHz to 8.61 GHz for CVA. This means that the input impedance operating bandwidth of 125% is achieved for the proposed CVA. By comparing these results, it can be told that the CVA successfully decreases $|S_{11}|$ at the lower edge of the operating frequency band. However, the upper edge of the -10 dB operation band also decreases slightly. In conclusion, this improvement corresponds to an antenna miniaturization of 28%.

Radiation characteristics of the antennas are measured inside an anechoic chamber. Obtained patterns for the xz-plane and the yz-plane for the frequencies of 2, 4, 6, and 8 GHz are shown in Figure 4.3. In all cases, the main lobe is directed towards the y-axis. As can be seen from the Figure 4.3 cross-polarization levels of the CVA are at least 25 dB lower than the co-polarization values in the direction of maximum radiation for both principal planes. Furthermore, both antennas can said to exhibit a good end-fire radiation characteristic. The maximum gain of the antennas are

measured by using a double ridged standard horn reference antenna. As can be observed from Figure 4.4, maximum gain of the both antennas increases as the frequency gets larger. This is due to the fact that the antennas become electrically larger with decreasing wavelength. The increase in the gain values continues up to 7.5 GHz and after that frequency the gain levels start to decrease due to the losses. Lastly, front-to-back (F/B) ratios of the measured radiation patterns also indicate the superiority of the CVA design. In particular, the VA exhibits an F/B ratio of 10.85 dB while F/B ratio of the CVA is 14.95 dB. (The F/B ratio values given here are the values averaged over the main operating frequency band of 2 - 8 GHz.)

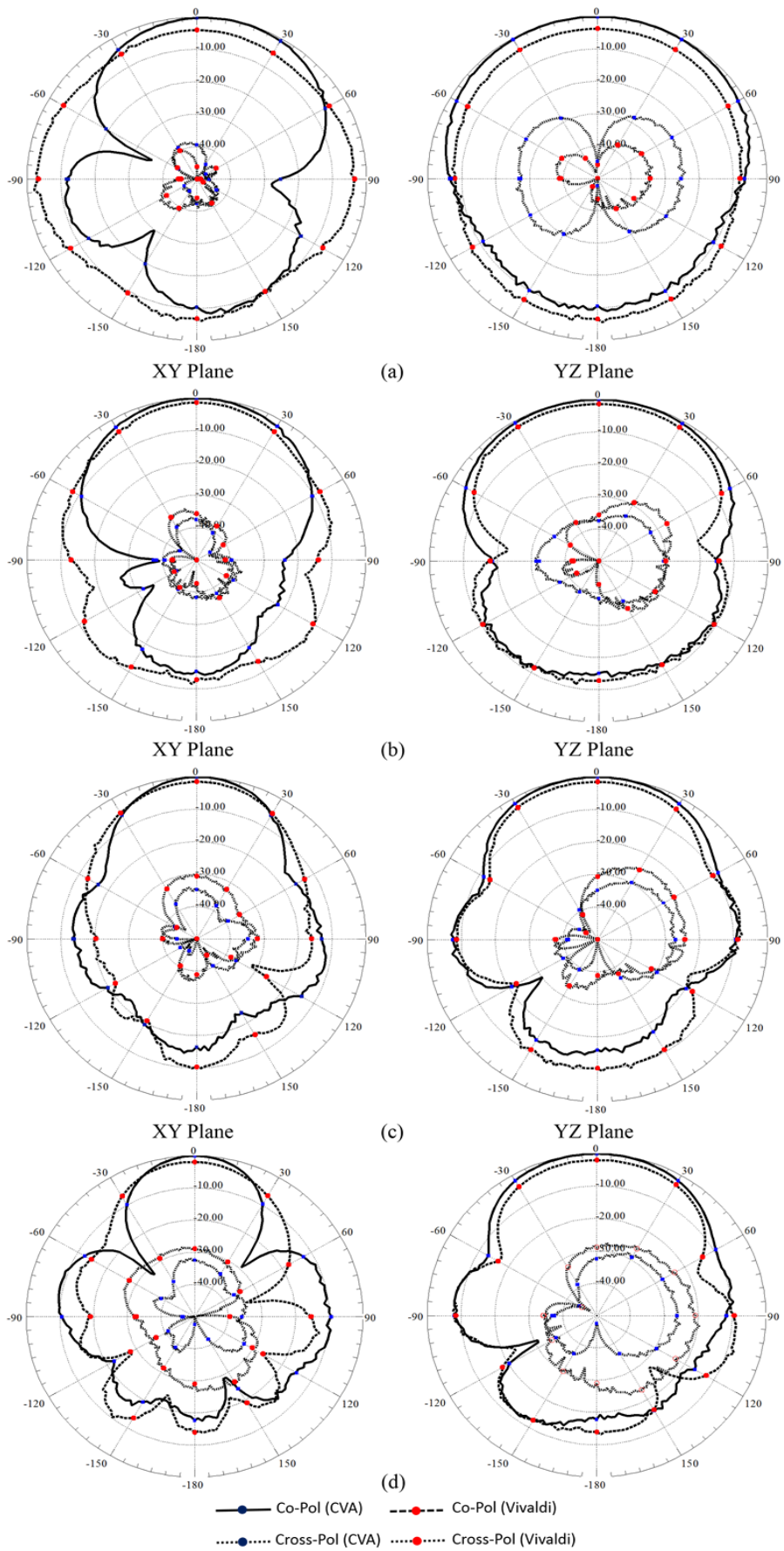


Figure 4.3: Measured principal plane radiation patterns of the VA and the CVA.

Consequently, while keeping the same dimensions of the VA, the CVA shows improved impedance characteristics in the lower frequency band. Additionally, compared to the VA, the CVA exhibits improved radiation characteristics overall operating frequencies. In particular, the frequency averaged boresight gain of the CVA is 2.2 dB greater than that of VA. Besides, F/B ratio of the CVA becomes much better than the F/B ratio of the VA. In fact, such improvements can be ascribed to two main factors: first, the slots effectively limits the induced currents on the edge of the antenna, which reduces the general radiation performance of the Vivaldi antennas [92]. Second, the corrugations, especially the longer ones that are closer to the feed, induce extra resonances and broadens the antenna impedance bandwidth [90]. Finally, the designed CVA has a good polarization purity, which can partially lessen the errors that occurred during the calibration when using the antenna for the imaging applications.

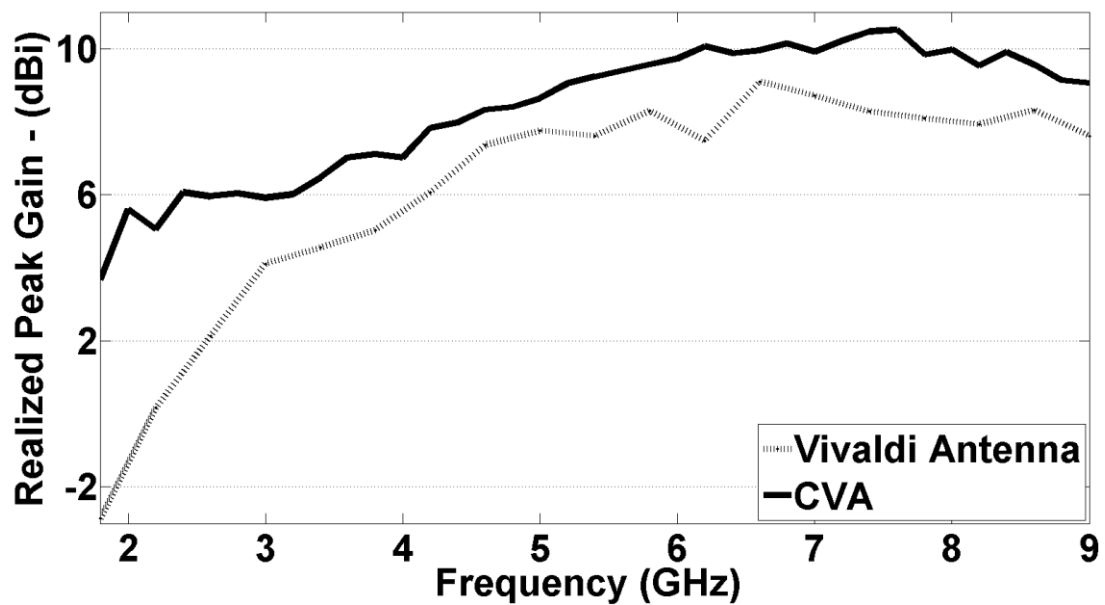


Figure 4.4: Measured gain characteristics of the proposed antenna and the VA.

4.3 Microwave Tomography System and Experimental Verification

After measuring certain characteristics of the proposed CVA, it must be tested with a microwave tomography system to better understand the imaging performance. To this end, this section provides an analysis of the presented CVA, when a qualitative inverse scattering method, scattering parameter based Linear Sampling Method (S-LSM) [98], is employed for microwave imaging purposes. We choose a qualitative method for experimental verification since such methods have quite attractive features as low computational complexity and ease of implementation. Besides, they are shown to be useful in different imaging problems such as non-destructive testing (NDT) [100][101], subsurface sensing [102][103], medical imaging [104][105] and etc. In this paper, instead of the canonical LSM formulation the S-LSM is employed, due to its being more suitable for real world applications [98].

4.3.1 Brief Introduction to S-LSM

As shown through Figure 4.5(a) - Figure 4.5(c), we prepare an experimental setup in which all antennas are vertically polarized and collecting data around a circle having radius of R . The measurement system employs a vector network analyser (Agilent N5230A) to collect bistatic measurements at uniformly distributed points, which are located on the aforementioned circle. Scattering parameters (S-parameters) are sampled at M discrete frequencies f_1, f_2, \dots, f_M for multi-frequency operation. The vertical component of the scattered vector S-parameters $S_{ver}^{s,k}$ at frequency f_k , can be obtained as [98]:

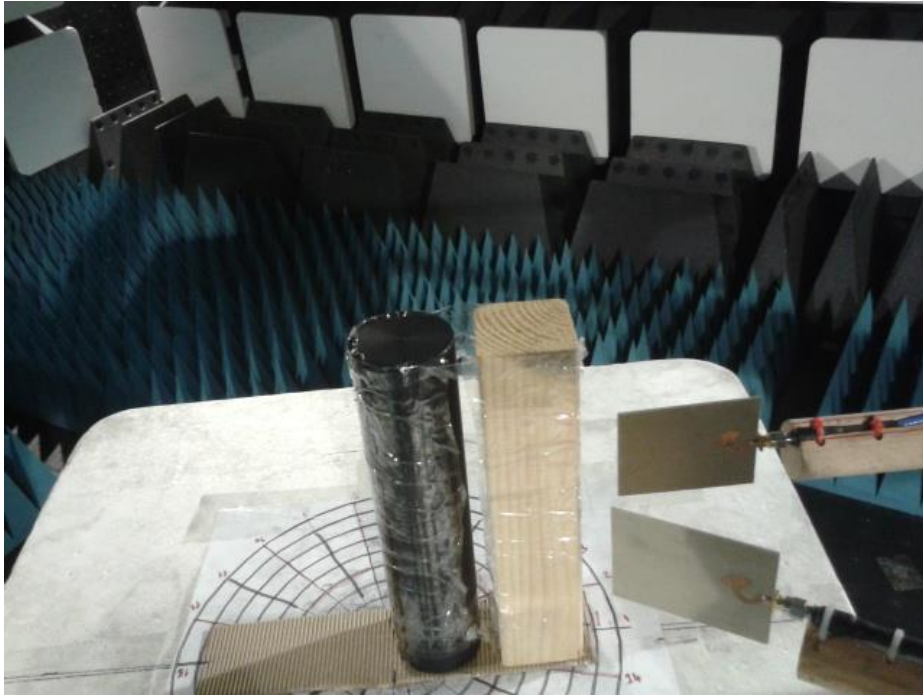
$$\mathbf{S}_{ver}^{s,k} = \mathbf{S}_{ver}^{t,k} - \mathbf{S}_{ver}^{i,k} \quad (4)$$

where $S_{ver}^{s,k}$ is the measured S-parameters when the objects are present and $S_{ver}^{i,k}$ stands for the background field measured when there is no object illuminated by the antennas. Then the S-LSM states that the equation of:

$$(\mathbf{F}^k \mathbf{g}_p^k)(\boldsymbol{\theta}_r) = \mathbf{U}_p^k(\boldsymbol{\theta}_r); \mathbf{p} \in \mathbf{D}, \boldsymbol{\theta}_r \in \Gamma \quad (5)$$

has no finite solution if a sampling point p , which belongs to sampling domain D , does not fall into an object Ω [98]. Here F^k is the near field scattering operator for frequency f_k , which is defined by [98]:

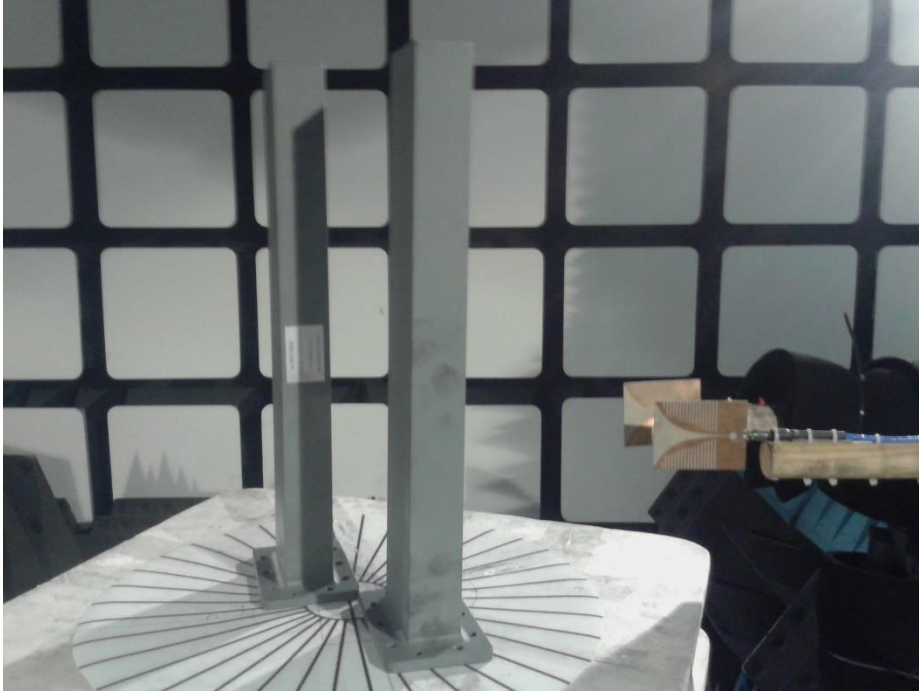
$$(F^k g_p^k)(\theta_r) = \int_{\Gamma} S_{ver}^{s,k}(\theta_i, \theta_r) g^k(\theta_i) d\Gamma(\theta_i); \quad \theta_r \in \Gamma \quad (6)$$



(a)



(b)



(c)

Figure 4.5: Experimental setups for (a) dielectric scatterer (b) single metallic scatterer (c) double metallic scatterer

In (5), (6) U_p^k is the vertical component of the normalized incident field at point p , which is generated by the receiver antenna located at θ_r [98], and θ_i denotes the source position on arc Γ . As stated above, the Euclidian norm of the solution in the Hilbert space of $L^2(\Gamma)$, $\|g_p^k\|_{L^2(\Gamma)}$, is infinite when p does not belong to a scatterer. Hence an indicator function can be defined as [98]:

$$W^k(p) := \|g_p^k\|_{L^2(\Gamma)}^{-1} = \left(\int_{\Gamma} |g_p^k(\theta_i)|^2 d\Gamma(\theta_i) \right)^{-1}; \quad p \in D \quad (7)$$

Finally, a multi-frequency approach can be exploited to enhance the quality of the reconstructions. For this aim, the indicator functions are integrated over all frequencies and the resultant multi-frequency indicator function becomes [98][106]:

$$W(p) := \sum_{k=1}^M W^k(p) \quad (8)$$

Therefore, the indicator functions W (or a post-processed version of W) must be plotted on entire sampling domain D , to obtain a reconstruction of the shape of the scatterers [98].

4.3.2 Experimental Results and Performance Assessment of Vivaldi Antennas

This subsection aims to compare the imaging performance of the two designed antennas, i.e. Corrugated Vivaldi antenna (CVA) and the generic Vivaldi antenna (VA), through the experimental results, which are obtained with S-LSM. As previously stated, S-LSM produces an image of the supports of the all scatterers by plotting the indicator function W over the entire sampling domain D . Therefore, before advancing into imaging results, a few points about the visualization of the obtained indicator function must be stressed. First of all, the scattered field operator F does not contain sufficient information to correctly reconstruct the dimensions along vertical axis, since the measurement configuration supplies only single polarization samples of the scattered vector scattering parameters (S-parameters) on just one circle [107]. Therefore, the reconstructions provides an image of a single horizontal slice of the sampling domain D . Furthermore, since S-LSM provides a qualitative image for the scatterers, all images must be taken in the same scale to be able compare the reconstructions. Additionally, instead of qualitatively commenting on the images, a quantitative measure of quality must be employed for comparative purposes. Although there exists a few other approaches as in [108] [109], a normalized gradient based threshold selection method is utilized when forcing all figures in the same scale [102]. In this way, the multi-frequency indicator $W(p)$, is normalized with its maximum to obtain the normalized indicator function $W_n(p)$. Next, the absolute value of the normalized gradient of the normalized indicator function $\nabla_n W_n(p) = \frac{|\nabla W_n(p)|}{\max_{p \in D} |\nabla W_n(p)|}$ is computed. The region I , on which $\nabla_n W_n(p)$ is greater than an arbitrarily selected threshold $0 < Q < 1$ is determined. Then, the threshold for normalized indicator function T , can be found as:

$$T := \min_{p \in I} W_n(p); I := \{q : q \in D, \nabla_n W_n(p) \geq Q\} \quad (9)$$

As the next step the binarized indicator function $W_b(p)$, is obtained by filtering the normalized indicator function $W_n(p)$:

$$W_b(p) = \begin{cases} 1, & \text{if } W_n(p) \geq T \\ 0, & \text{if } W_n(p) < T \end{cases} \quad (10)$$

Finally, the pixels that fall into a scatterer are determined as the points in the region where the binarized indicator function has value of 1. For comparative purposes, the quantitative errors defined in [100][101][102] is calculated for the binary reconstructions obtained with (9), (10). These errors are the *localization error*:

$$\epsilon_{loc} = \frac{N_{MP}}{N_{SP}} \quad (11)$$

and the *shape reconstruction error*:

$$\epsilon_{shape} = \frac{N_{MP}}{N_{TP}} \quad (12)$$

where N_{MP} , N_{SP} , and N_{TP} are the number of misclassified pixels, sampling points and targets pixels, respectively.

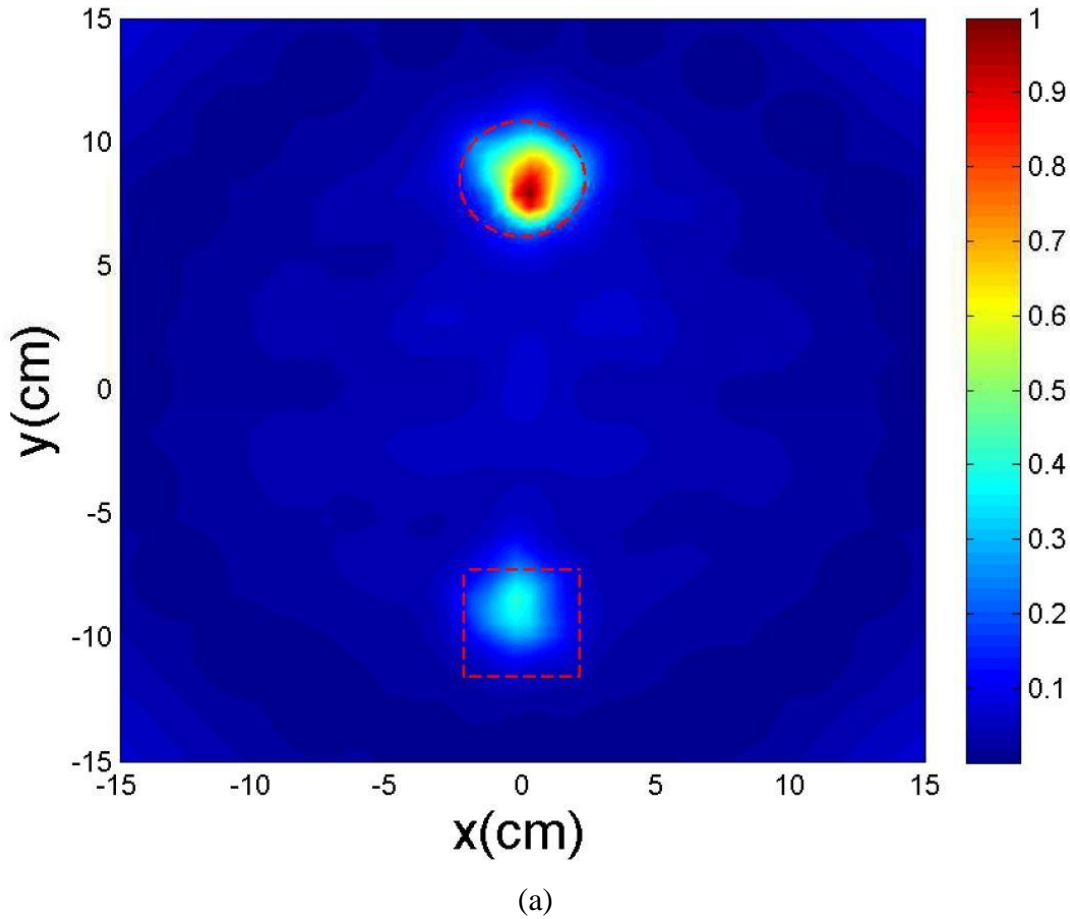
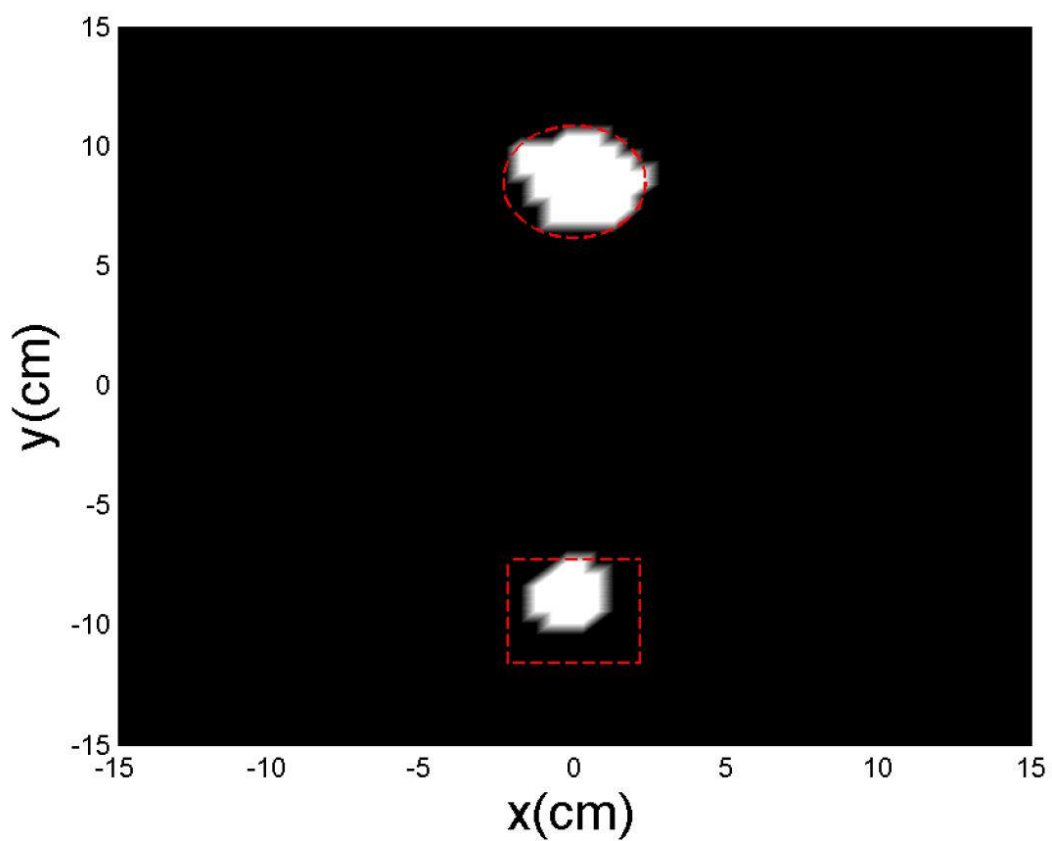
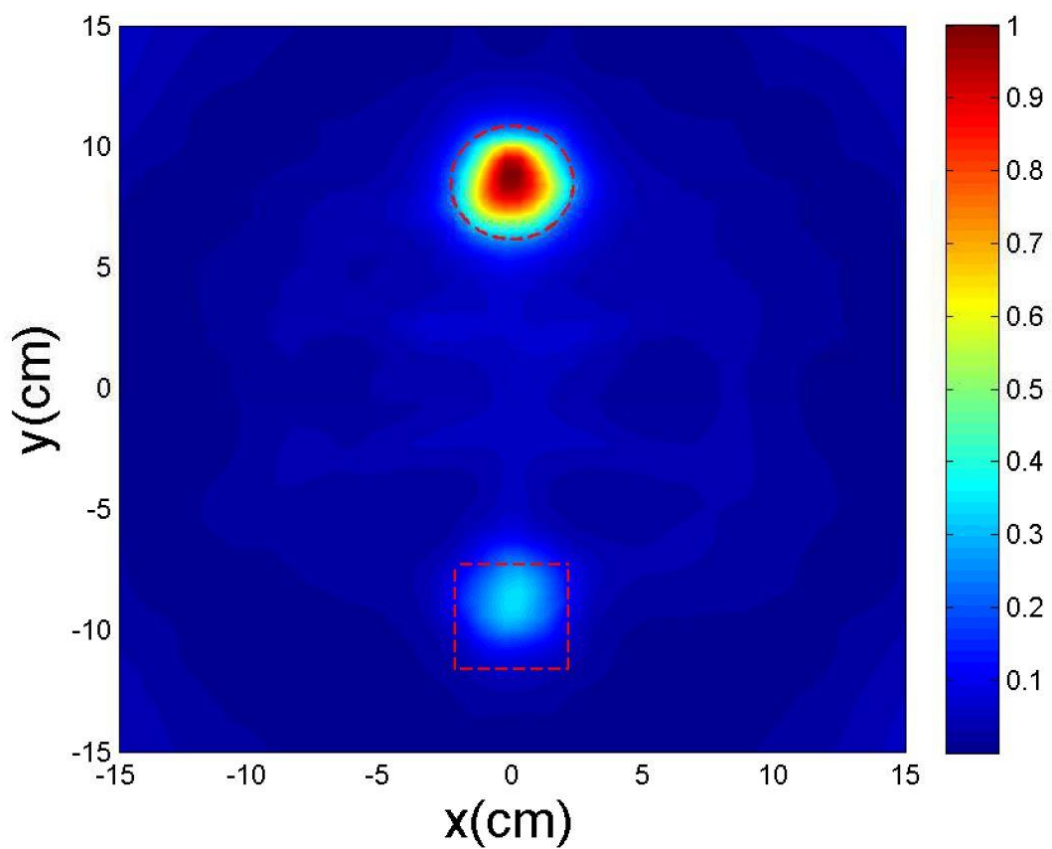
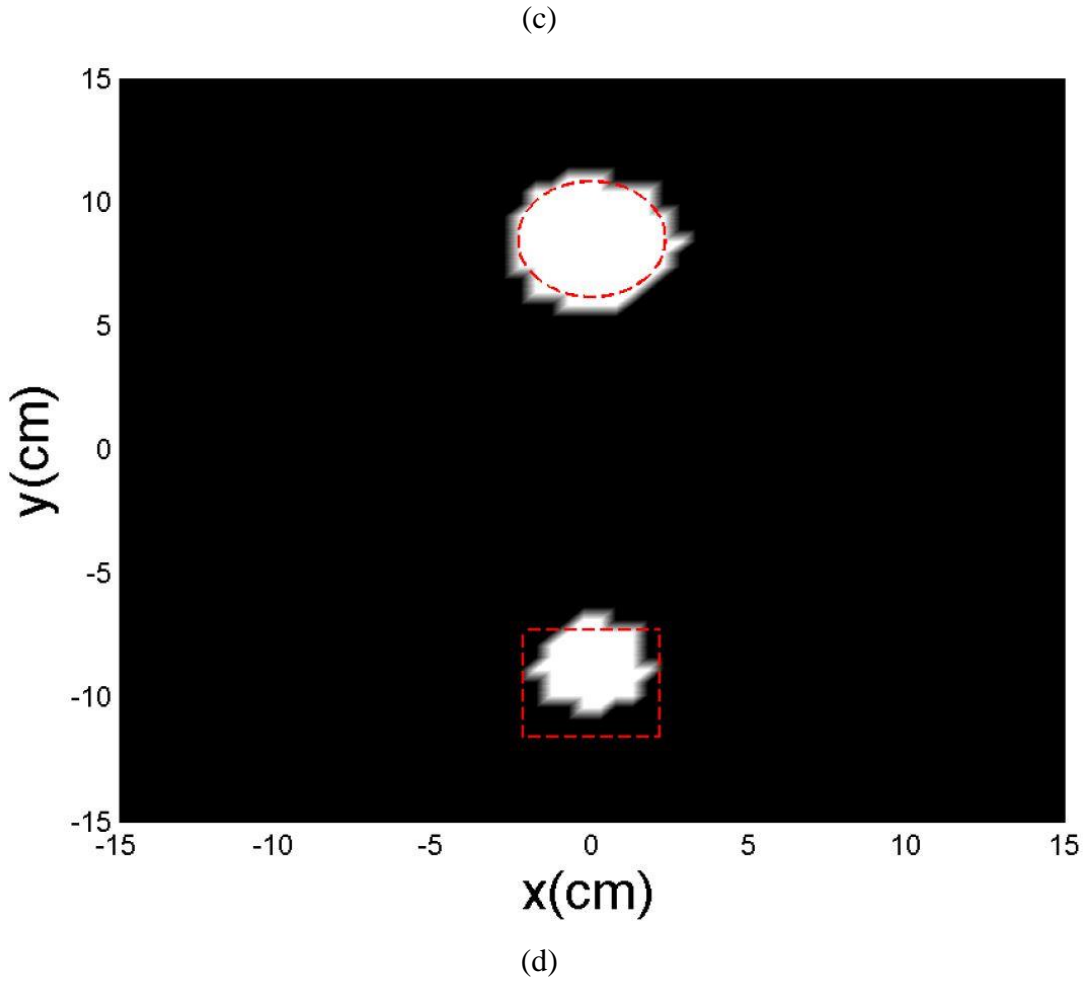


Figure 4.6: Indicator function for the dielectric scatterers obtained with following antenna: (a) W_n ; with CVA (b) W_b ; with CVA (c) W_n ; with VA (d) W_b ; with VA (Exact borders of the scatterers are marked with red dashed lines, threshold for normalized gradient is selected as $Q = 0.7$)



(b)





Firstly the dielectric scatterer case is considered, as shown in Figure 4.5(a). The targets are chosen as a wooden cylinder having a height of 21 cm, a radius of 2.4 cm and a square prism made of delrin having a height of 21 cm, an edge length of 4 cm. For these setups, the measurements are taken by the antennas, which are placed $R=15$ cm away from the center. For multi-frequency operations, S-parameters are sampled at $M = 41$ frequencies which are equilinearly distributed between $f_1 = 2$ GHz and $f_{41} = 6$ GHz. For all cases, the sampling domain D is selected as a square centered around the origin, having an edge length of 30 cm. This domain is divided into 60×60 cells for discretization purposes. For a detailed testing of the performances of the antennas S-parameter measurements are repeated for three different configurations in which the distance between the dielectrics are $d = 0$ cm, $d = 2$ cm and $d = 12$ cm. For $d = 12$ cm case S-parameters are sampled with 15° angular variations whereas for the other two cases measurements are taken with 30° angular variations. Thus, obtained scattering matrices are 24×24 for $d = 12$ cm case and 12×12 for the remaining

cases. Imaging results for $d = 12$ cm case are shown in Figure 4.6(a), Figure 4.6(b) for the CVA and Figure 4.6(c), Figure 4.6(d) for the VA.

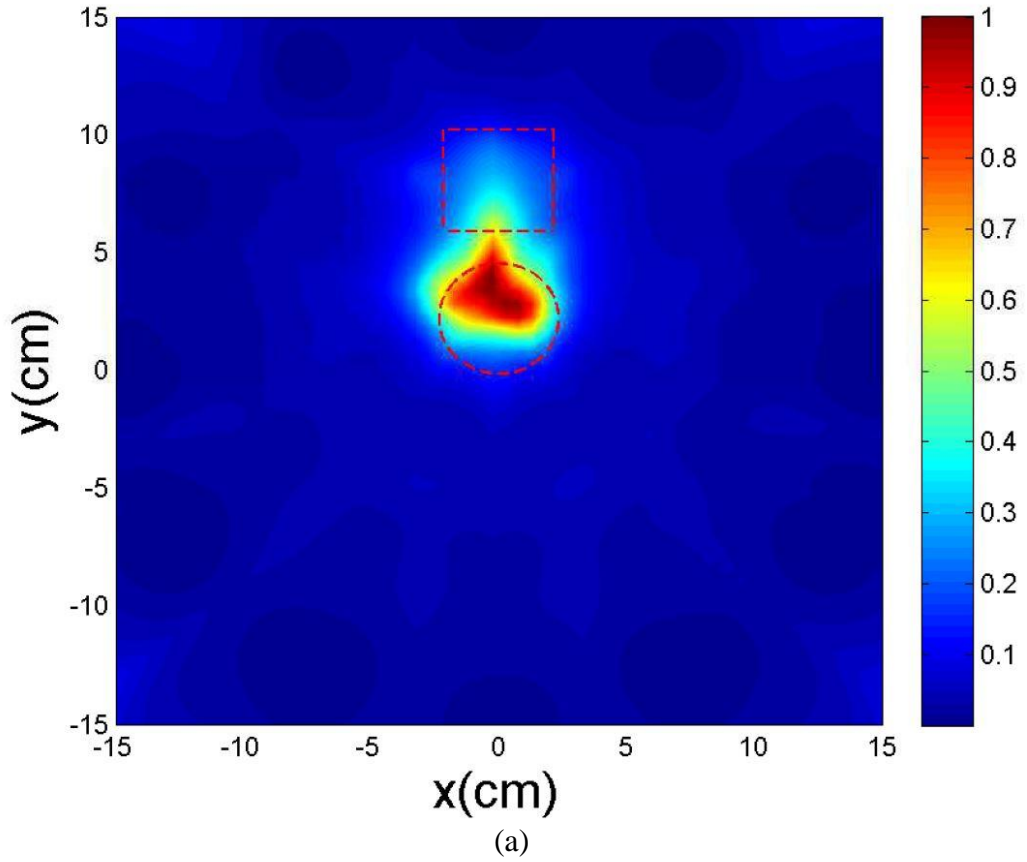
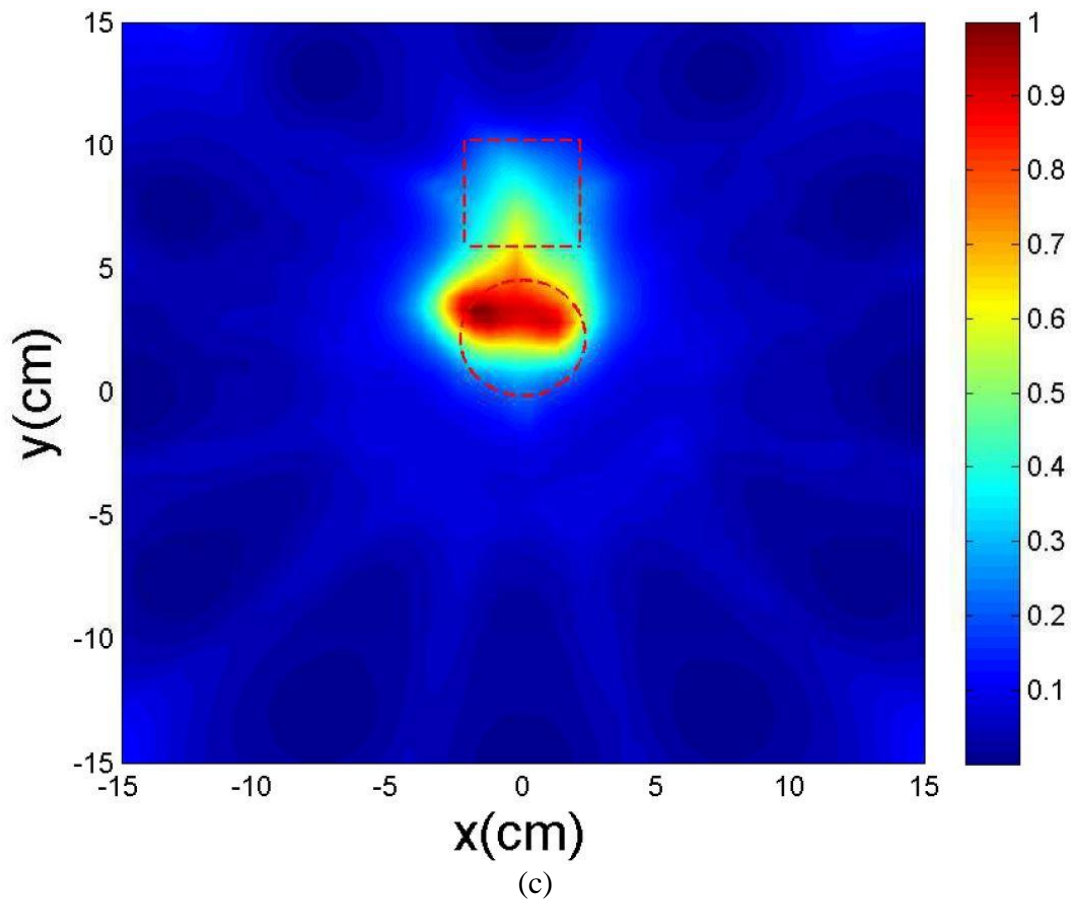
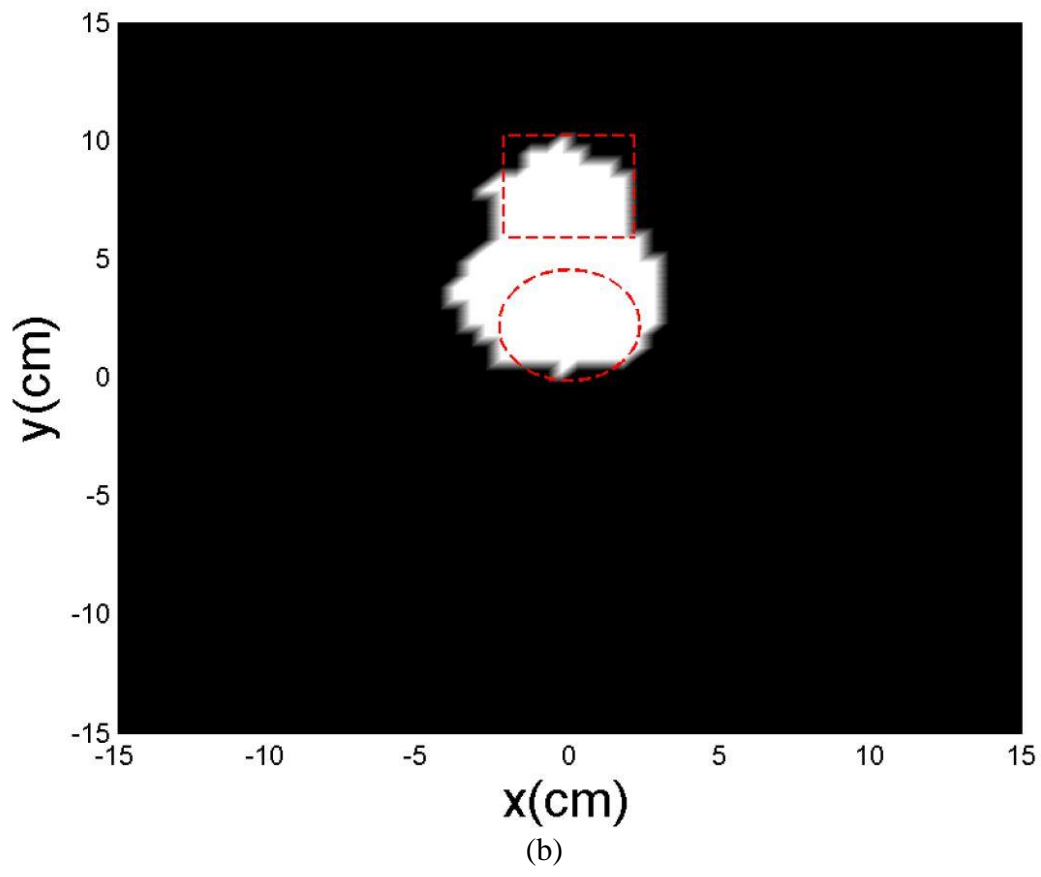
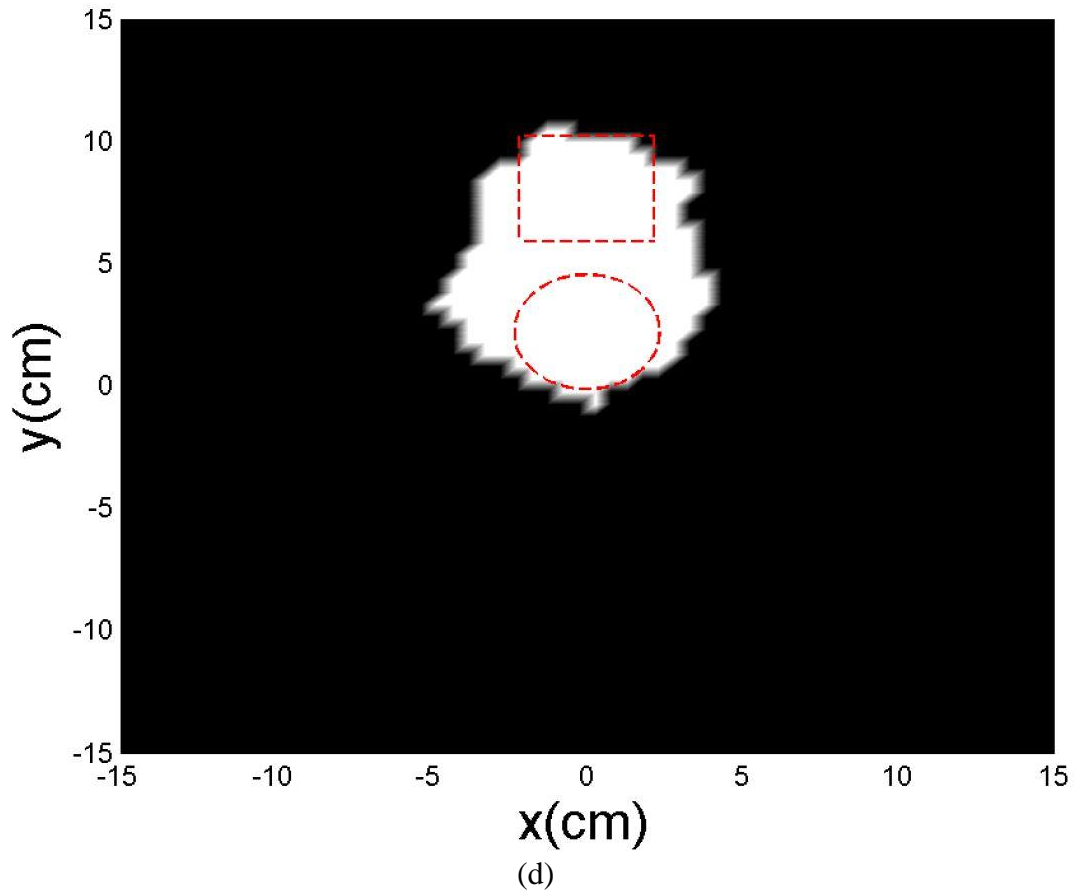


Figure 4.7: Indicator function for the dielectric scatterers obtained with following antenna: (a) W_n ; with CVA (b) W_b ; with CVA (c) W_n ; with VA (d) W_b ; with VA (Exact borders of the scatterers are marked with red dashed lines, threshold for normalized gradient is selected as $Q = 0.7$)





The localization and shape reconstruction errors for these results are given in the Table 4.2. As clearly seen from the images and the error levels, both antennas exhibit a good performance for this particular case. In fact, this result is not surprising, since the number of measurement samples are high enough to reconstruct the scatterers [110]. To further understanding of the capabilities of two antennas, one must investigate the reconstructions for $d = 2$ cm and $d = 0$ cm cases, which are given in Figure 4.7(a) - Figure 4.7(b), Figure 4.8(a) - Figure 4.8(b) for the CVA and Figure 4.7(c) - Figure 4.7(d), Figure 4.8(c) - Figure 4.8(d) for the VA. It is obvious that both imaging results and the reconstruction errors given in Table 4.2 imply that the CVA performs better than the VA. This is indeed an obvious result of the higher gain of the new design compared to the classical one, since the increase in the gain makes the scattered field stronger, which in turns a high signal-to-noise ratio (SNR) in the scattered field operator F . Thus, it is not surprising to have less artifacts in the reconstructions. Therefore, by examining through Figure 4.6 to Figure 4.8, it can be inferred that the CVA performs better than the classical design, since it enables to have better

reconstructions by increasing the immunity of the overall imaging system against noise.

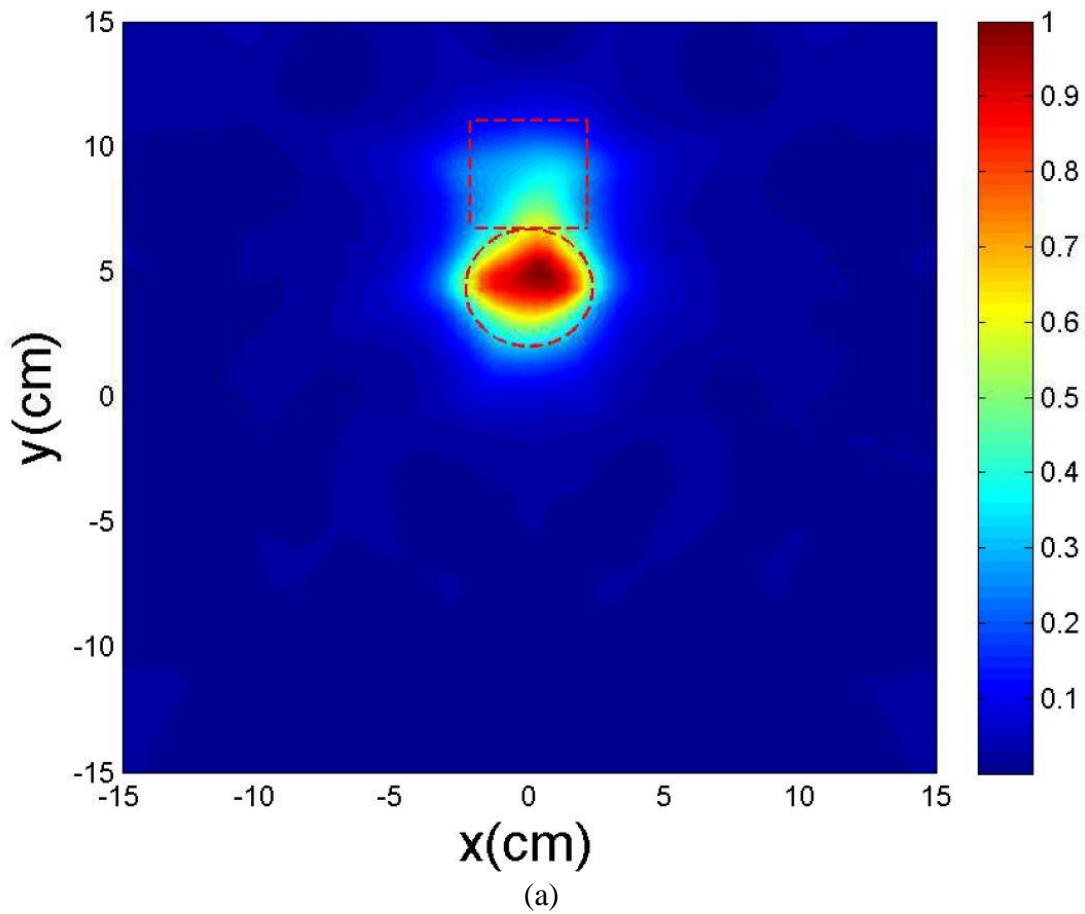
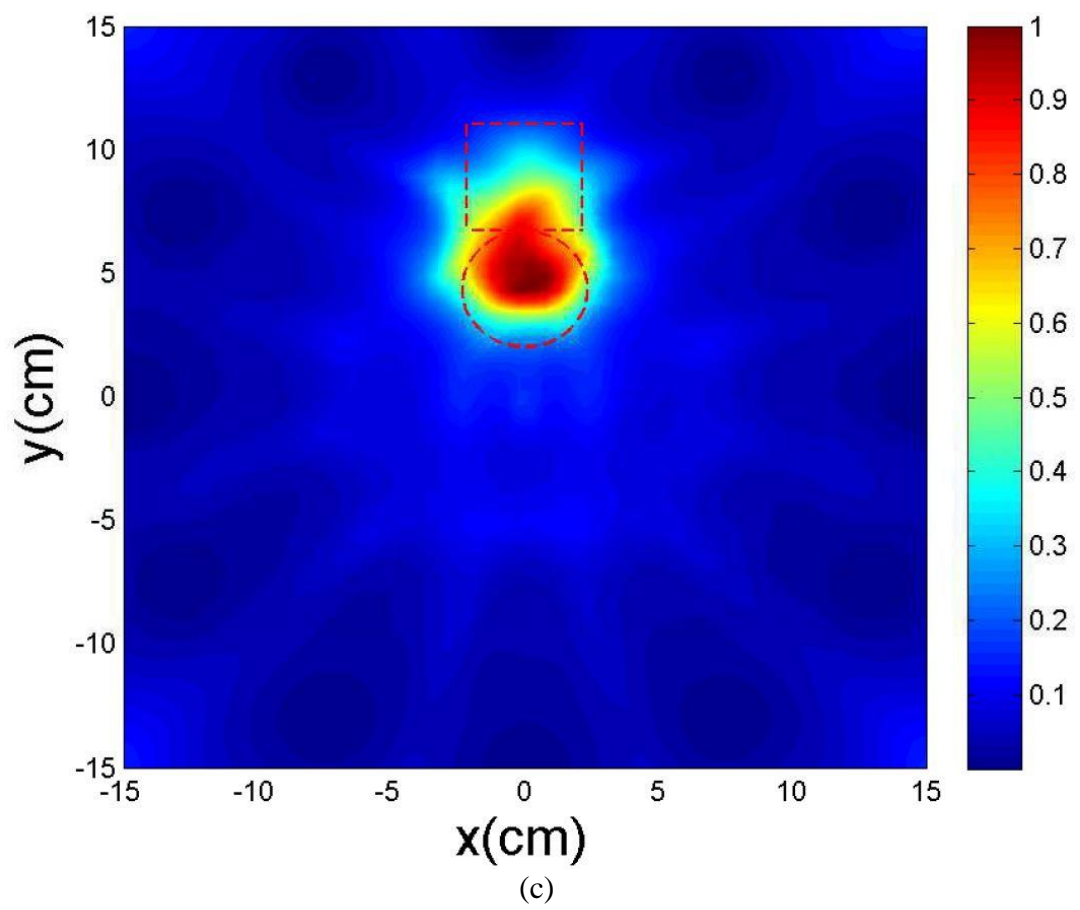
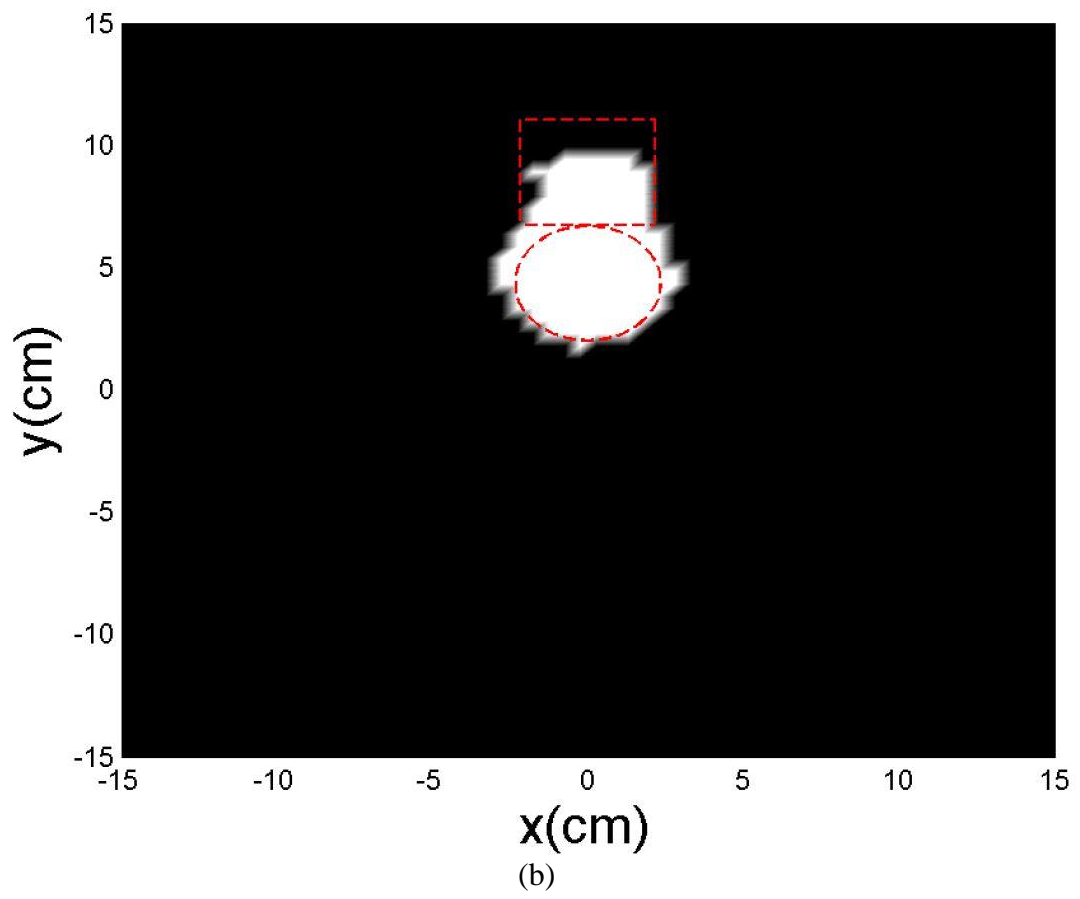
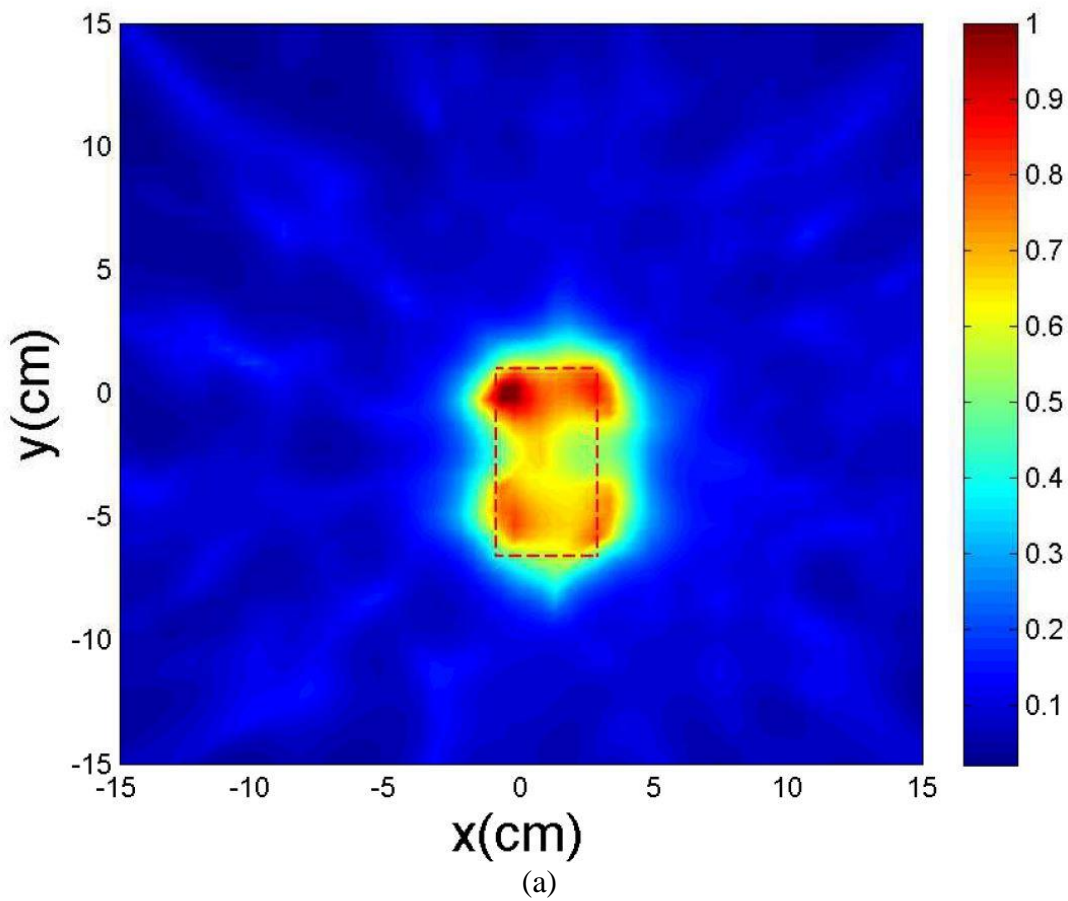
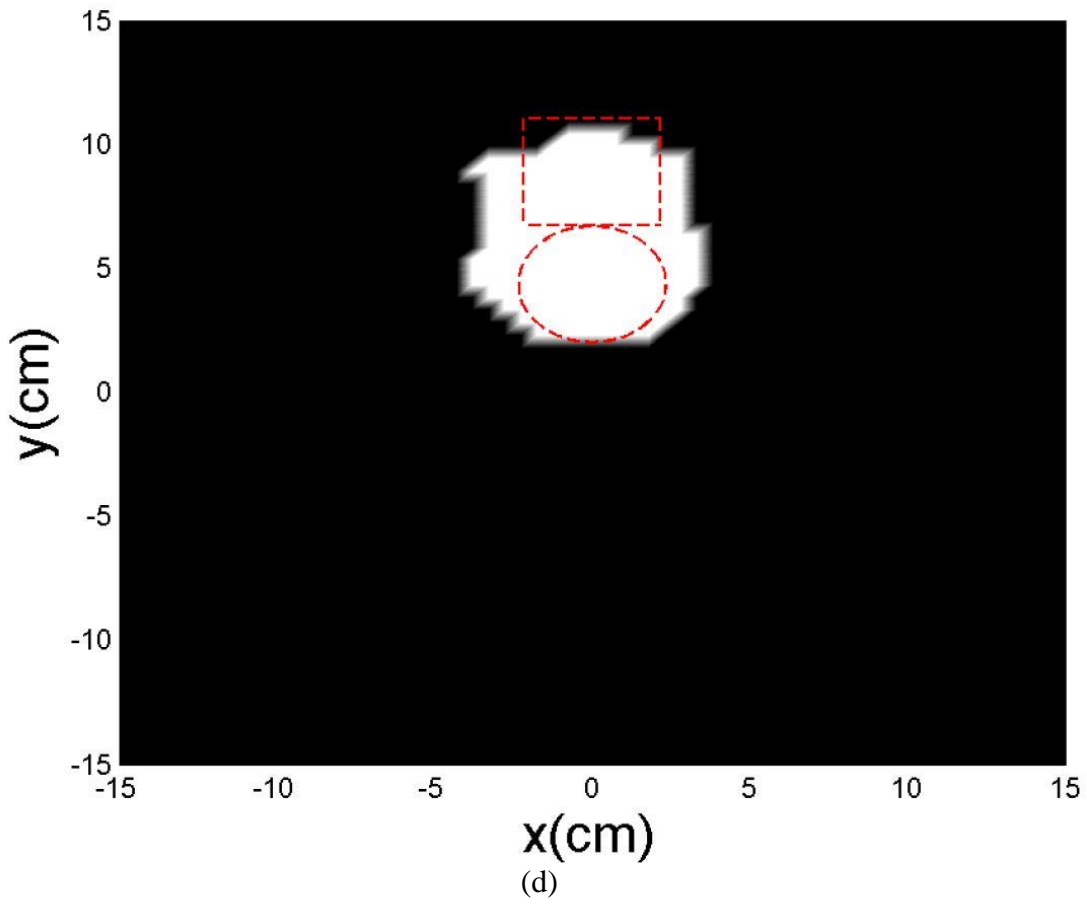
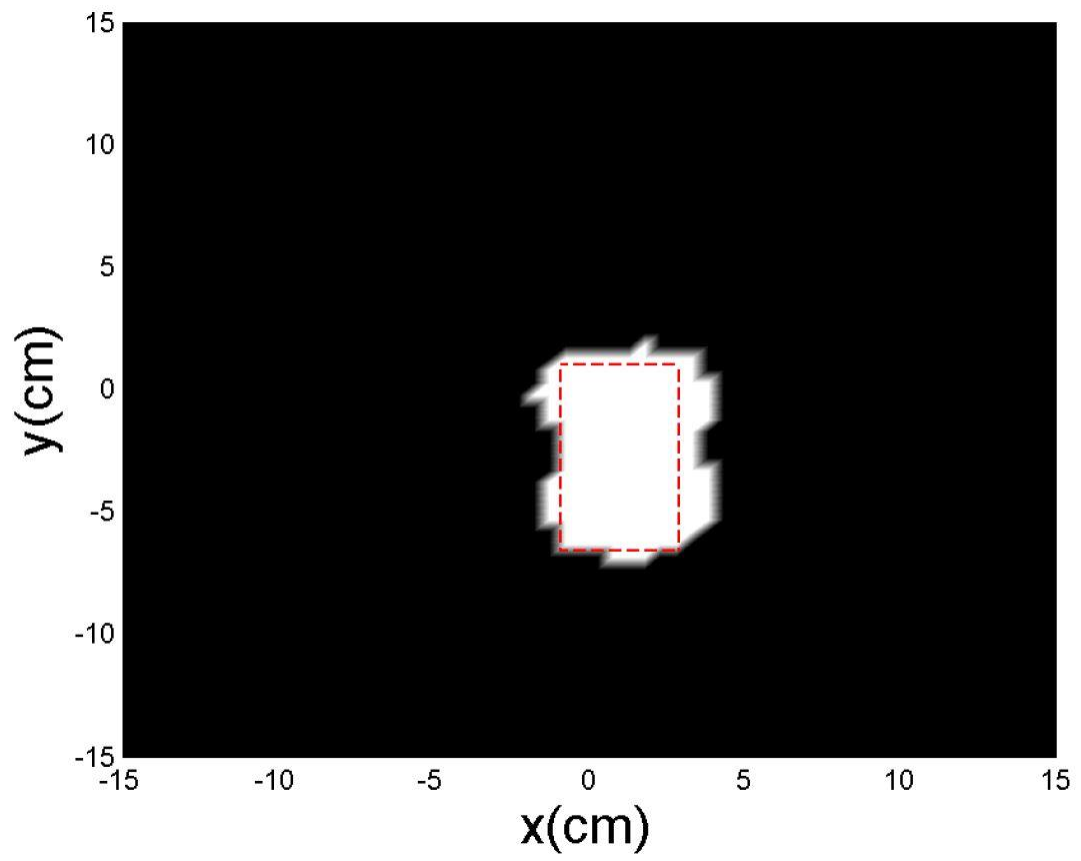


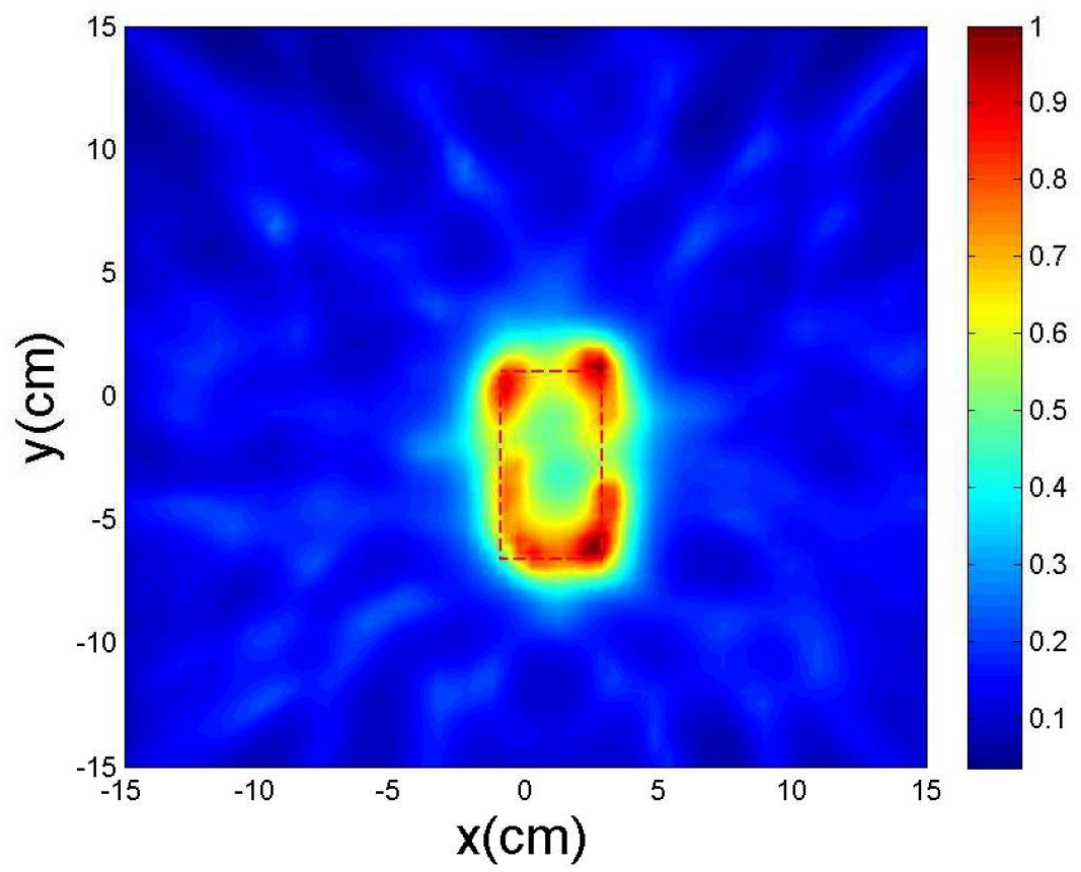
Figure 4.8: Indicator function for the dielectric scatterers obtained with following antenna: (a) W_n ; with CVA (b) W_b ; with CVA (c) W_n ; with VA (d) W_b ; with VA (Exact borders of the scatterers are marked with red dashed lines, threshold for normalized gradient is selected as $Q = 0.7$)







(b)



(c)

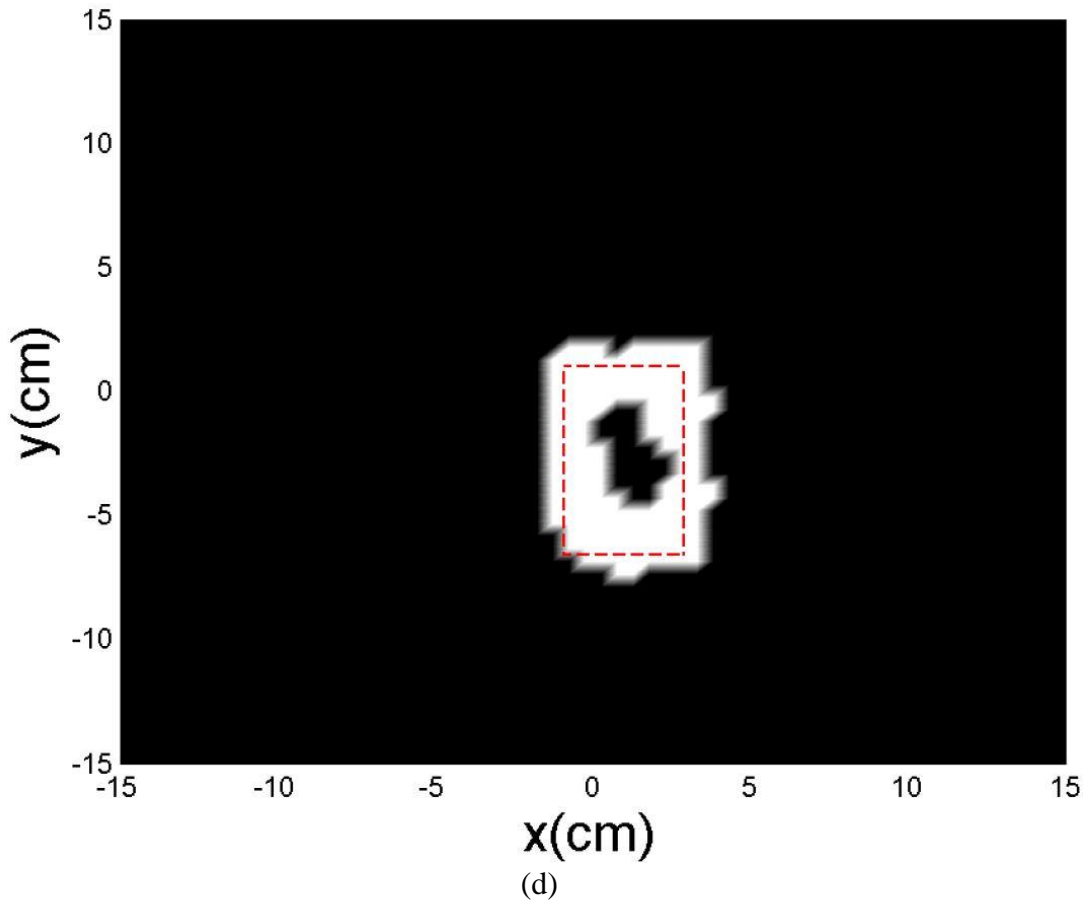


Figure 4.9: Indicator function for the single conductor scatterer obtained with following antenna: (a) \mathbf{W}_n ; with CVA (b) \mathbf{W}_b ; with CVA (c) \mathbf{W}_n ; with VA (d) \mathbf{W}_b ; with VA (Exact borders of the scatterers are marked with red dashed lines, threshold for normalized gradient is selected as $Q = 0.9$)

To further show the effectiveness of the introduced design, two more experimental setups are prepared with metallic scatterers. In the first configuration, a rectangular prism shaped conductor, which has a height of 41 cm and edge lengths of 7.5 cm, 3.7 cm, is placed in the sampling domain as shown in Figure 4.5(b). Here the antennas are placed $R = 24$ cm away from the center and S-parameters are sampled at the same frequencies of the dielectric case with 30° angular variations. Reconstructions produced by S-LSM are given in Figure 4.9(a), Figure 4.9(b) for the CVA and Figure 4.9(c), Figure 4.9(d) for the VA. Different from the dielectric scatterer case, the threshold for the normalized gradient is chosen as $Q = 0.9$ for the conductor targets. The reconstruction errors are given in Table 4.2, which clearly show that the performance of the presented design exceeds that of the VA. Similar to the dielectric

case, the performance difference between two designs arises from the higher gain of the CVA, which results in a higher SNR level in the measurement data.

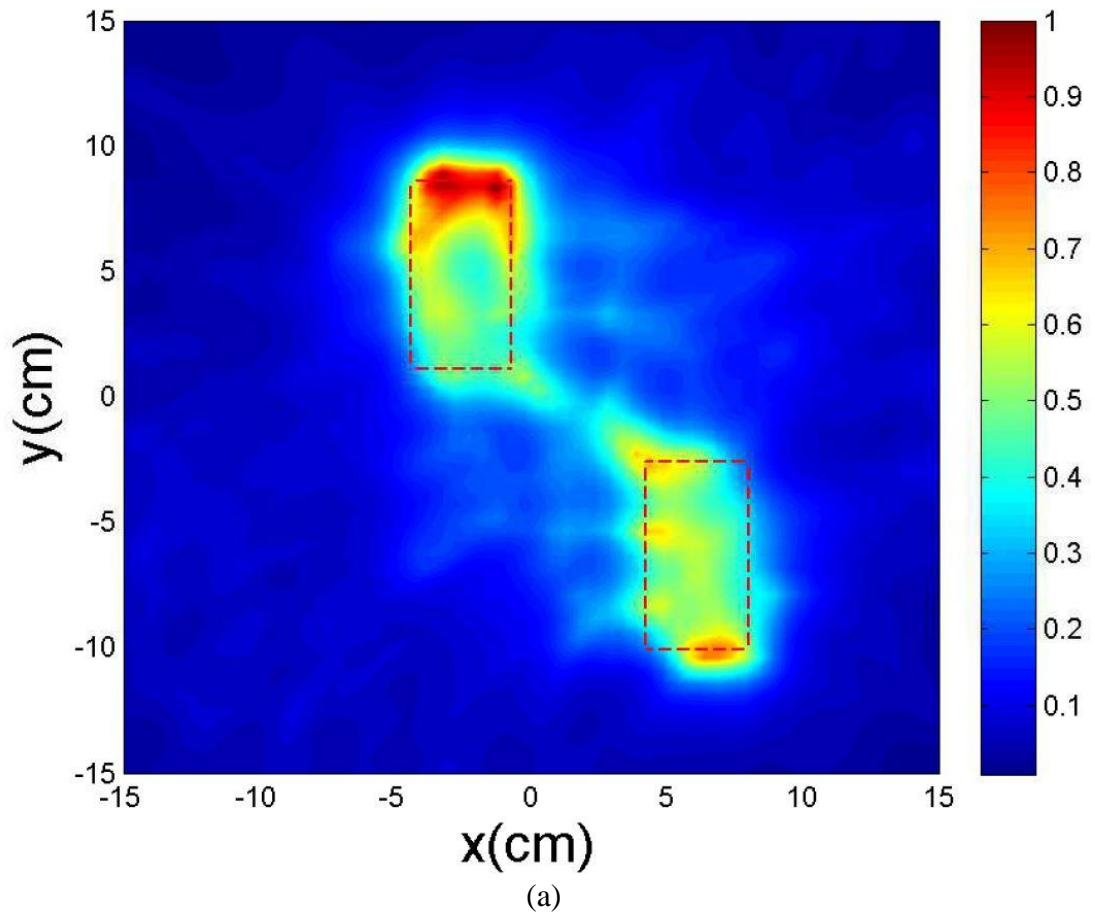
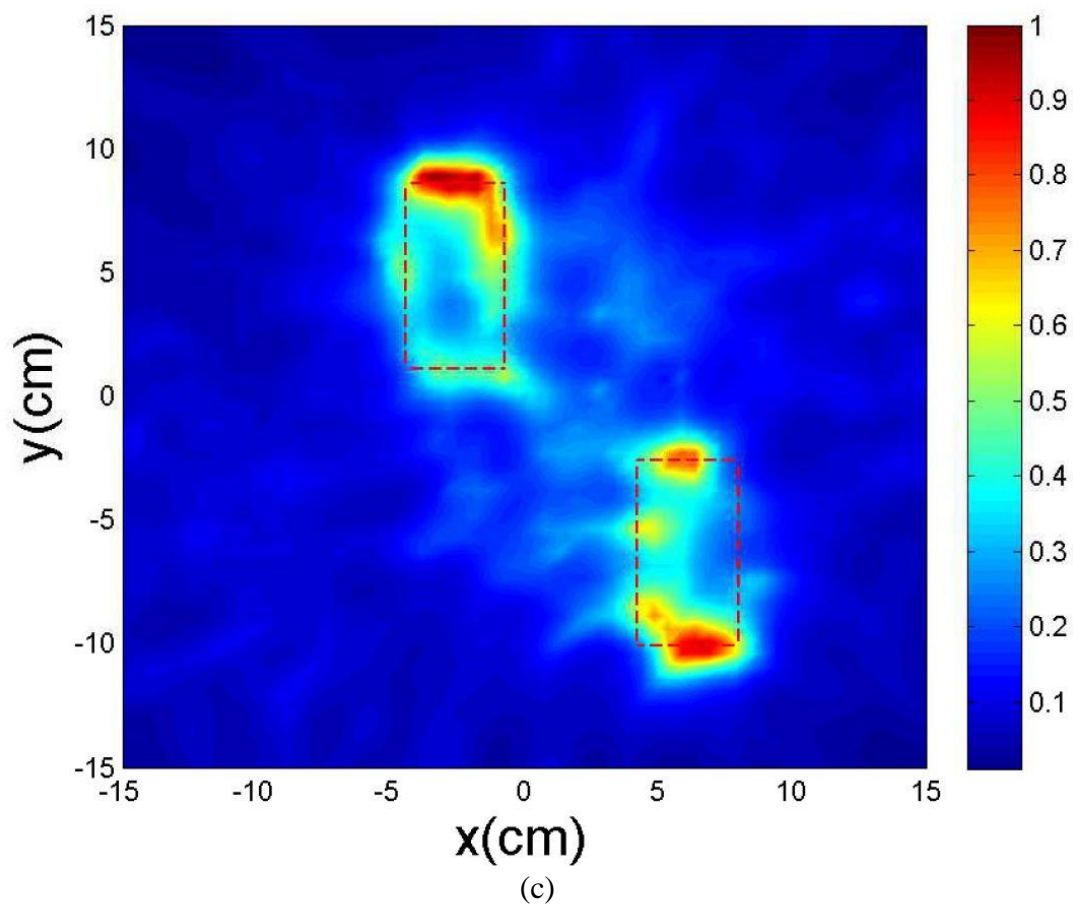
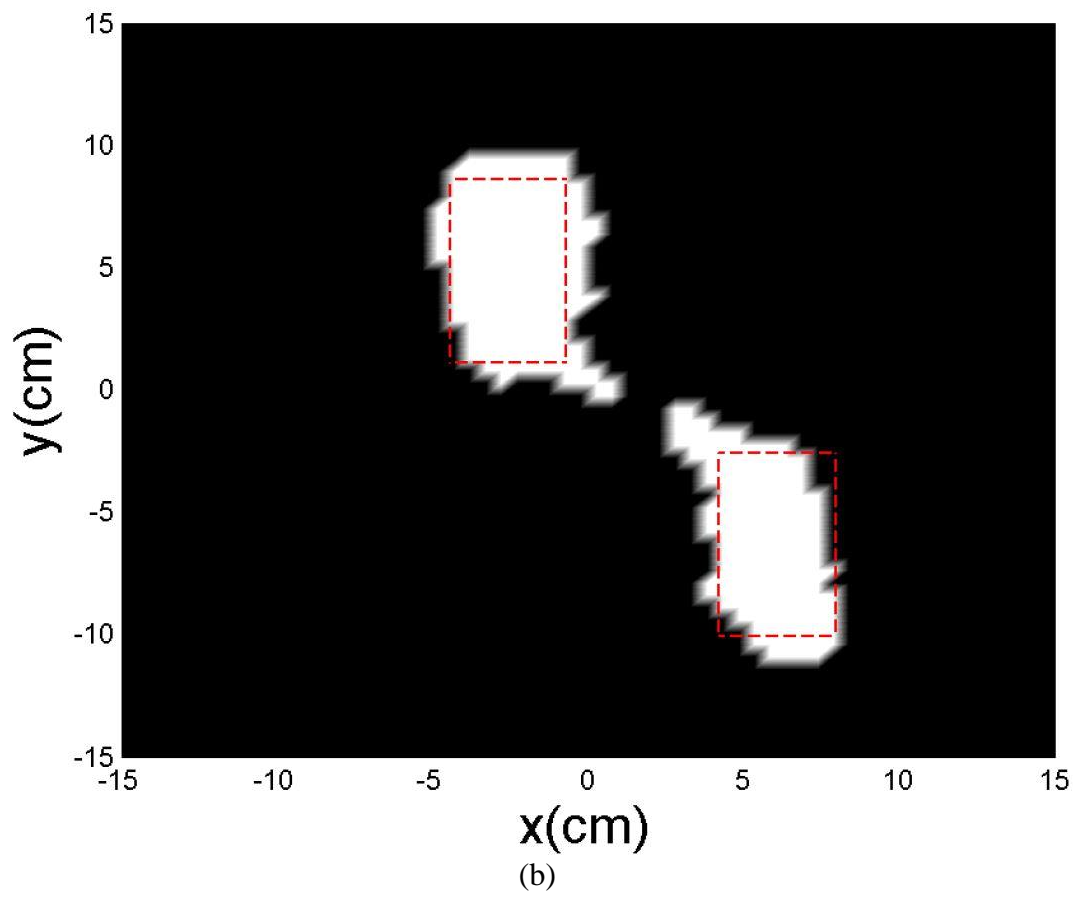


Figure 4.10: Indicator function for the double conductor scatterers obtained with following antenna: (a) W_n ; with CVA (b) W_b ; with CVA (c) W_n ; with VA (d) W_b ; with VA (Exact borders of the scatterers are marked with red dashed lines, threshold for normalized gradient is selected as $Q = 0.9$)



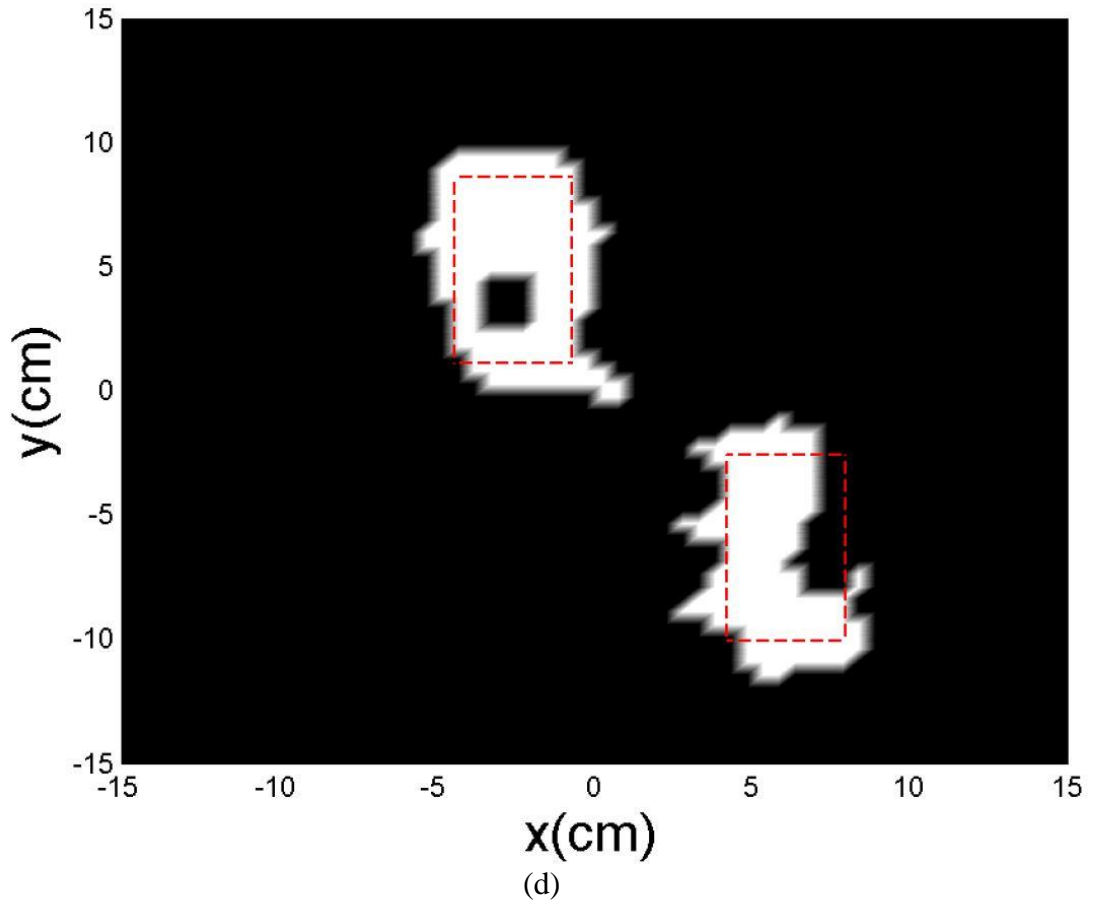


Table 4.2: Localization and shape errors.

Configuration	Antenna Type	ϵ_{loc}	ϵ_{shape}	Q
Two dielectric scatteres with distance $d = 12\text{ cm}$	CVA	1.75	45.00	0.7
	VA	1.56	40.00	
Two dielectric scatteres with distance $d = 2\text{ cm}$	CVA	2.58	70.45	0.7
	VA	3.94	107.58	
Two dielectric scatteres with distance $d = 0\text{ cm}$	CVA	1.47	38.41	0.7
	VA	2.61	68.12	
Single Metallic Scatterer	CVA	1.28	38.33	0.9
	VA	2.33	70.00	
Double Metallic Scatterers	CVA	2.97	44.58	0.9
	VA	4.25	63.75	

As a final example, an experimental configuration, which consists of two metallic scatterers, is prepared as shown in Figure 4.5(c). The dimensions of the both targets are the same of the metallic structure, which is used in the single conducting scatterer case. The illumination of the setup is also exactly the same of the single metallic scatter

case, except that the antennas are rotated with 15° angular variations for this case. Imaging results are given in Figure 4.10(a), Figure 4.10(b) for the CVA and Figure 4.10(c), Figure 4.10(d) for the VA. The reconstruction errors for both cases are as given in Table 4.2. Similar to the single conductor target case, both imaging results and the error levels indicate that performance the CVA is better than the generic VA. Consequently, by observing through Figure 4.6 - Figure 4.10, one can conclude that the improved characteristics of the CVA (i.e. the higher gain, the higher front-to-back ratio) leads to more clear results regardless of the type of the obstacle.

4.4 Conclusion

In this work have presented a novel Corrugated Vivaldi antenna (CVA), which is designed for MWI purposes. The idea behind the design was to lessen the edge currents, which limit the performance of Vivaldi antennas, by means of the corrugations on the patch. The characteristic parameters of the CVA was measured and compared with the Vivaldi antenna (VA) of the same model except the corrugations. Results showed that the CVA is more suitable for MWI purposes with its higher gain, lower beamwidth and higher front-to-back ratio.

In addition to measuring fundamental parameters of both antennas, we also tested them in a MWI procedure. For this purpose, several experimental configurations were prepared. The required data for inversions was collected by each antenna, for the same experimental setups. Retrieved scattering parameters were then employed in a qualitative MWI procedure, the scattering parameter based Linear Sampling Method. Obtained results were qualified with respect to a quantitative measure. Reconstructions showed that the presented CVA performs better than the VA without any corrugations. Lastly, we want to emphasize that the main point of this paper was to show that the effectiveness of the Vivaldi antennas can be improved by etching proper corrugations on the metallic patch. The importance of the work can be expressed from several aspects. Firstly, the Vivaldi antennas are already compact, low cost antennas. Opening corrugations on the patch makes those antennas more compact while maintaining the same cost. Secondly, the characteristics of these antennas are enhanced with respect to a generic design. Note that, designing compact antennas with improved characteristics is very important in many MWI problems, such as medical imaging or subsurface

sensing. For instance, the aim of obtaining an high gain is to retrieve a high signal-to-noise(SNR) for the medical imaging problems, since the suspect that is to be imaged can be quite small in dimension; while one of the main challenges of the subsurface imaging techniques is to obtain compact, lightweight (hand-held if possible) imaging systems. Consequently, our future research will be devoted extend the proposed CVA structure to more specific real world problems as well as developing novel, more effective and more efficient design principles for the Vivaldi antennas.

5. CONCLUSION

The aim of this thesis is to develop antennas, which are specifically optimized with respect to the requirements of the microwave imaging of breast cancer. In this direction, we have designed a cavity-backed Vivaldi antenna (CBVA) for microwave breast measurements. The design requirements is adjusted with respect to a free-space measurement scenario. We have also performed various breast phantom measurements with the designed CBVA. Obtained results show the effectivity of the designed antenna for a free space breast measurement scenario.

Additionally, we have proposed a novel Corrugated Vivaldi antenna (CVA), which is designed by opening corrugations on the edge of the antenna. These corrugations are known to decrease the induced currents on the edge of the antenna, which can degrade the radiation performance. We have shown that, the designed CVA has better properties such as higher gain, smaller beam width, lower back-to-front ratio when compared with a generic Vivaldi antenna of the same dimensions. The characteristics of the obtained CVA is measured in a detailed manner. Furthermore, we have also compared the imaging performance of the introduced design with the same generic Vivaldi antenna. For this aim, we have prepared several experimental configurations in the anechoic chamber of Istanbul Technical University. Then, scattering parameter (S-parameter) measurements are performed by means of the both the designed CVA and the classical Vivaldi antenna. Next, measured S-parameters are employed in a recently proposed qualitative imaging method, which is the S-parameter based Linear Sampling Method (S-LSM). Results show that the performance of the designed antenna exceeds the performance of the classical Vivaldi antenna in such real world microwave imaging problems. Future work will be devoted to extend the presented designs for more realistic measurement models. Also, metamaterials and dielectric loading techniques can be analysed for proposed antennas to miniaturize.

REFERENCES

- [1] **P. Gould**, (2003). The rise and rise of medical imaging, *Physics World*, pp. 29-31
- [2] **Anonymous**, (2000). Looking back on the millennium in medicine, *New England Journal of Medicine*, vol. 342, no. 1, pp. 42–49.
- [3] **Larsen E.L, Jacobi J.H** (1985). Medical Applications of Microwave Imaging, *IEEE Press, The institute of Electrical and Electronic Engineers, Inc.*
- [4] **England T. S.; and N. A. Sharples** (1949). Dielectric properties of the human body in the microwave region of the spectrum, *Nature*, vol. 163, pp. 487–488.
- [5] **Pethig R.** (1984). Dielectric properties of biological materials: Biophysical and medical applications, *IEEE Trans. Elect. Insulation*, vol. 5, pp. 453–474.
- [6] **Foster K. R.; and H. P. Schwan.** (1989). Dielectric properties of the human body in the microwave region of the spectrum, *Crit. Rev. Biomed. Eng.*, vol. 17, pp. 25–104.
- [7] **Gabriel G.; S. Gabriel; and E. Corthout** (1996). The dielectric properties of biological tissues: I. Literature survey, *Phys. Med. Biol.*, vol. 41, pp. 2231–2249.
- [8] **Gabriel S.; R. W. Lau; and C. Gabriel** (1996). The dielectric properties of biological tissues: II. Measurements in the frequency range 10 Hz to 20 GHz, *Phys. Med. Biol.*, vol. 41, pp. 2251–2269.
- [9] **Semenov S.Y.; R.H. Svenson; V.G. Posukh; A.G. Nazarov; Y.E. Sizov, A.E. Bulyshev, A.E. Souvorov, W. Chen, J.Kasell, G.P. Tatsis** (2002). Dielectrical spectroscopy of canine myocardium during acute ischemia and hypoxia at frequency Spectrum From 100 kHz to 6 GHz, *IEEE Transactions on Medical Imaging*, vol. 21, no. 6, 703-707.
- [10] **Golnabi, A.H.; Meaney, P.M.; Geimer, S.; Tian Zhou; Paulsen, K.D.** (2011). Microwave tomography for bone imaging, *Biomedical Imaging: From Nano to Macro, IEEE International Symposium*, pp.956,959
- [11] **Pichot C., L. Jofre, G. Peronnet, and J.-C. Bolomey** (1985). Active microwave imaging of inhomogeneous bodies, *IEEE Transactions on Antennas and Propagation*, vol. 33, pp. 416-425.

- [12] **Meaney P. M.; K. D. Paulsen, A. Hartov, and R. C. Crane** (1996). Microwave imaging for tissue assessment: Initial evaluation in multitarget tissue-equivalent phantoms, *IEEE Transactions on Biomed. Eng.*, vol. 43, pp. 878–890.
- [13] **Moghaddam M.; W. C. Chew, and M. Oristaglio** (1991). Comparison of the Born iterative method and Tarantola's method for an electromagnetic time-domain inverse problem, *Int. J. Imaging Syst. Tech.*, 3:318–333.
- [14] **Moghaddam M.; and W. C. Chew** (1992). Nonlinear two-dimensional velocity profile inversion using time domain data, *IEEE Transactions on Geoscience and Remote Sensing*, vol. 30, pp. 147 – 156.
- [15] **Gilmore C.; P. Mojabi, A. Zakaria, S. Pistorius, and J. LoVetri** (2010). On super-resolution with an experimental microwave tomography system, *IEEE Antennas and Wireless Propagation Letters*, vol. 9, pp. 393–396.
- [16] **Chen F. C.; and W. C. Chew** (1998). Experimental verification of super resolution in nonlinear inverse scattering, *Appl. Phys. Lett.*, vol. 72, no. 23, pp. 3080–3082.
- [17] **Vorst V.; Rosen A.; and Y. Kotsuka** (2006). RF/Microwave Interaction with Biological Tissues, *Hoboken, NJ: Wiley*.
- [18] **Lin J. C.** (1985). Frequency optimization for microwave imaging of biological tissues, *Proc. IEEE*, vol. 73, no. 2, pp. 374–375.
- [19] **Azaro R.; Caorsi S.; and M. Pastorino** (1998). A 3-GHz microwave imaging system based on a modulated scattering technique and on a modified Born approximation. *Int. J. Imag. Syst. Technol.*, vol. 9, pp.395 – 403
- [20] **Pastorino, M.; Massa, A.; Caorsi, S.** (2000) A microwave inverse scattering technique for image reconstruction based on a genetic algorithm, *Instrumentation and Measurement, IEEE Transactions on*, vol.49, no.3, pp.573 – 578
- [21] **Otto, G.P.; Weng Cho Chew** (1994). Microwave inverse scattering - local shape function imaging for improved resolution of strong scatterers. *Microwave Theory and Techniques, IEEE Transactions on*, vol.42, no.1, pp.137 – 141
- [22] **Miyakawa M.** (1993). Tomographic measurement of temperature change in phantoms of the human body by chirp radar-type microwave computed tomography. *Med. Biol. Eng. Computat.*, vol. 31, pp.531 – 536
- [23] **Goldsmith, P.F.; Hsieh, C.T.; Huguenin, G.R.; Kapitzky, J.; Moore, E.L.** (1993). Focal plane imaging systems for millimeter wavelengths. *Microwave Theory and Techniques, IEEE Transactions on*, vol.41, no.10, pp.1664 – 1675
- [24] **Preece, A.W.; Johnson, R.H.; Green, J.L.; Robinson, M.P.** (1993). Dielectric imaging for localization and detection of breast tumours. Microwave Symposium Digest, *IEEE MTT-S International*, vol. 2, pp.1145 – 1146
- [25] **Preece, A.W.; Green, J.L.; Potheary, N.; Johnson, R.H.** (1994). Microwave imaging for tumour detection, *Radar and Microwave Imaging, IEE Colloquium on*, vol. 9, pp.1 – 4

- [26] **Hsia, R.P.; Cheng, S.; Geck, W.R.; Domier, C.W.; Luhmann, N.C., Jr.** (1993). Millimeter-wave Schottky diode imaging array development, *Microwave Conference Proceedings*. APMC '93., Asia-Pacific , vol.1, no., pp.1 – 6
- [27] **Semenov S. Y.; and Corfield D. R.** (2008). Microwave tomography for brain imaging: Feasibility assessment for stroke detection. *Int. J. Antennas Propag.*, vol. 2008
- [28] **Fhager, A.; Persson, M.** (2012). Stroke detection and diagnosis with a microwave helmet. *Antennas and Propagation (EUCAP)*, 6th European Conference on , vol., no., pp.1796 - 1798
- [29] **T. Rubaek, O. Kim, and P. Meincke,** (2009). Computational validation of a 3-D microwave imaging system for breast-cancer screening, *IEEE Transactions on Antennas and Propagation*, vol. 57, pp. 2105–2115.
- [30] **J. G. Elmore, M. B. Barton, V. M. Mocerri, S. Polk, P. J. Arena, and S. W. Fletcher** (1998). Ten-year risk of false positive screening mammograms and clinical breast examinations, *The New England J.of Med*, vol. 338, pp. 1089–1096.
- [31] **American Cancer Society,** (2003). Cancer facts and figures, www.cancer.org
- [32] **Cancer Research UK,** (2011), <http://info.cancerresearchuk.org>
- [33] **M. Malvezzi, P. Bertuccio, F. Levi, C. La Vecchia, and E. Negri** (2012). European cancer mortality predictions for the year 2012, *Annals of Oncology*, vol. 23, no. 4, pp. 1044–1052.
- [34] **Fear, E.C.; Hagness, S.C.; Meaney, P.M.; Okoniewski, M.; Stuchly, M.A.** (2002). Enhancing breast tumor detection with near-field imaging. *Microwave Magazine, IEEE*, vol.3, no.1, pp.48 - 56
- [35] **J. G. Elmore, M. B. Barton, V. M. Mocerri, S. Polk, P. J. Arena, and S. W. Fletcher** (1998). Ten-year risk of false positive screening mammograms and clinical breast examinations, *The New England J.of Med*, vol. 338, pp. 1089 – 1096
- [36] **Lee, R.T.; Smith, G.S.** (2004). A design study for the basic TEM horn antenna. *Antennas and Propagation Magazine, IEEE*, vol.46, no.1, pp. 86 – 92
- [37] **Chung, B. & Lee, T.** (2008). UWB antenna assists ground-penetrating radar. *Microwave & RF Magazine*, pp. 59 – 65
- [38] **Lestari, A.A.; Yarovoy, A.G.; Lighthart, L.P.** (2005). Adaptive wire bow-tie antenna for GPR applications. *Antennas and Propagation, IEEE Transactions on*, vol.53, no.5, pp. 1745 – 1754
- [39] **Teggatz A.; Jostingmeier A.; Omar A.** (2006). A new TEM double-ridged horn antenna foreground penetrating radar applications. *Proc. GeMic*
- [40] **Taniguchi, T.; Kobayashi, T.** (2003). An omnidirectional and low-VSWR antenna for the FCC-approved UWB frequency band. *Antennas and Propagation Society International Symposium. IEEE*, vol.3, pp. 460 - 463

- [41] **Excell, P.S.; Tinniswood, A.D.; Clarke, R.W.** (1999). An independently fed log-periodic antenna for directed pulsed radiation. *Electromagnetic Compatibility, IEEE Transactions on*, vol.41, no.4, pp. 344 – 349
- [42] **Penney, C.; Luebbers, R.J.** (1994). Input impedance, radiation pattern, and radar cross section of spiral antennas using FDTD. *Antennas and Propagation, IEEE Transactions on*, vol.42, no.9, pp.1328 – 1332
- [43] **Li, Xu; Hagness, S.C.; Choi, M.K.; Van Der Weide, D.W.** (2003). Numerical and experimental investigation of an ultrawideband ridged pyramidal horn antenna with curved launching plane for pulse radiation, *Antennas and Wireless Propagation Letters, IEEE* , vol.2, no.1, pp.259 - 262
- [44] **S. Y. Semenov and D. R. CorVeld** (2008). Microwave tomography for brain imaging: Feasibility assessment for stroke detection, *International Journal of Antennas and Propagation*, vol. 2008
- [45] **T. Rubaek, O. Kim, and P. Meincke,** (2009). Computational validation of a 3-D microwave imaging system for breast-cancer screening, *IEEE Transactions on Antennas and Propagation*, vol. 57, pp. 2105–2115.
- [46] **D C. Yu, M. Yuan, J. Stang, E. Bresslour, R. George, G. Ybarra, W. Joines, and Q. Liu** (2008). Active microwave imaging II: 3-D system prototype and image reconstruction from experimental data, *IEEE Transactions on Microwave Theory and Techniques*, vol. 56, pp. 991–1000.
- [47] **P. Meaney, K. Paulsen, A. Hartov, and R. Crane** (1995). An active microwave imaging system for reconstruction of 2-D electrical property distributions, *IEEE Transactions on Biomedical Engineering*, vol. 42, pp. 1017–1026.
- [48] **D. Li, P. Meaney, T. Raynolds, S. Pendergrass, M. Fanning, and K. Paulsen** (2004). Parallel-detection microwave spectroscopy system for breast imaging, *Review of Scientific Instruments*, vol. 75, no. 7, pp. 2305–2313.
- [49] **P. M. Meaney, M. Fanning, T. Raynolds, C. Fox, Q. Fang, C. Kogel, S. Poplack, and K. Paulsen** (2007). Initial clinical experience with microwave breast imaging in women with normal mammography, *Academic Radiology*, vol. 14, pp. 207–218.
- [50] **P. M. Meaney, K. D. Paulsen, and J. Chang** (1998). Near-field microwave imaging of biologically-based materials using a monopole system, *IEEE Transactions Microwave Theory Tech.*, vol. 46, pp. 31–45.
- [51] **P. M. Meaney, K. D. Paulson, A. Hartov, and R. K. Crane** (1996). Multi-target microwave imaging for tissue assessment: Initial evaluation in tissue-equivalent phantoms, *IEEE Transactions Biomedical Engineering*, vol. 43, pp. 878–890.
- [52] **J.M. Sill, E.C. Fear** (2005). Tissue sensing adaptive radar for breast cancer detection - experimental investigation of simple tumor models, *IEEE Transactions Microwave Theory Tech.*, vol. 53, no. 11, 3312-3319.
- [53] **J. H. Jacobi, L. E. Larsen, and C. T. Hast** (1979). Water-immersed microwave antennas and their application to microwave interrogation of biological

- targets, *IEEE Transactions Microwave Theory Tech.*, vol. 27, no. 1, 70-78.
- [54] **Gürbüz, T.U.; Aslanyürek, B.; Yapar, A.; Şahintürk, H.; Akduman, I.** (2014) A Nonlinear Microwave Breast Cancer Imaging Approach Through Realistic Body–Breast Modeling. *Antennas and Propagation, IEEE Transactions on*, vol.62, no.5, pp.2596 – 2605
- [55] **Akinci, M.N.; Abbak, M.; Ozgur, S.; Cayoren, M.; Akduman, I.** (2014) Experimental comparison of qualitative inverse scattering methods. *Antenna Measurements & Applications (CAMA)*, 2014 IEEE Conference on, vol. 1, no. 4, pp. 16 - 19
- [56] **Broquetas, A; Romeu, J.; Rius, J.M.; Elias-Fuste, AR.; Cardama, A; Jofre, L.** (1991). Electromagnetic imaging of underground targets using constrained optimization, *IEEE Transactions Microwave Theory Tech.*, vol. 39, no. 5, 836-844.
- [57] **R. Siegel, D. Naishadham, and A. Jemal**, Cancer statistics, 2012, CA: *A Cancer Journal for Clinicians*, vol. 62, no. 1, pp. 10–29, 2012.
- [58] **Lazebnik M, Popovic D, McCartney L, Watkins CB, Lindstrom MJ, Harter J, et-al.** “A large-scale study of the ultrawideband microwave dielectric properties of normal, benign and malignant breast tissues obtained from cancer surgeries. *Physics in Medicine and Biology*. 2007; 52(20):6093.
- [59] **Nilavalan R, Gbedemah A, Craddock I, Li X, Hagness SC.** Numerical investigation of breast tumour detection using multi-static radar. *Electronics Letters*. 2003; 39(25):1787--1789.
- [60] **Jafari HM, Deen JM, Hranilovic S, Nikolova NK.** Co-polarised and cross-polarised antenna arrays for breast, cancer detection. *IET Microwaves, Antennas & Propagation*. 2007; 1(5):1055.
- [61] **Nilavalan R, Craddock IJ, Preece A, Leendertz J, Benjamin R.** Wideband microstrip patch antenna design for breast cancer tumour detection. *IET Microwaves, Antennas & Propagation*. 2007; 1(2):277.
- [62] **Kurrant DJ, Fear EC, Westwick DT.** Tumor response estimation in radar-based microwave breast cancer detection. *IEEE Trans Biomed Eng*. 2008 Dec; 55(12):2801-2811.
- [63] **Woten DA, El-Shenawee M.** Broadband Dual Linear Polarized Antenna for Statistical Detection of Breast Cancer. *IEEE Trans Antennas Propag*. 2008; 56(11):3576--3580.
- [64] **Cheeseman B, Huang Y.** Use of an adaptive filter for shape detection in microwave imaging with a focus on breast cancer detection. *IET Microwaves, Antennas & Propagation*. 2010; 4(4):553.
- [65] **Klemm M, Leendertz JA, Gibbins D, Craddock IJ, Preece A, Benjamin R.** Microwave Radar-Based Differential Breast Cancer Imaging: Imaging in Homogeneous Breast Phantoms and Low Contrast Scenarios. *IEEE Trans Antennas Propag*. 2010; 58(7):2337--2344.
- [66] **Zhurbenko V, Rubaek T, Krozer V, Meincke P.** Design and realization of a microwave three-dimensional imaging system with application to

- breast-cancer detection. *IET microwaves, antennas & propagation*. 2010; 4(12):2200--2211.
- [67] **Kumar R, Chaubey PN.** Design of coplanar waveguide-feed pentagonal-cut ultra-wide bandwidth fractal antenna and its backscattering. *IET Microwaves, Antennas & Propagation*. 2012 Oct; 6(13):1407-1414.
- [68] **Mohammed BJ, Ireland D, Abbosh AM.** Experimental investigations into detection of breast tumour using microwave system with planar array. *IET Microwaves, Antennas & Propagation*. 2012; 6(12):1311.
- [69] **Firoozy N, Tavakoli A.** Breast tumour identification based on inverse scattering approach. *IET Microwaves, Antennas & Propagation*. 2013
- [70] **Meaney PM, Fanning MW, Li D, Poplack SP, Paulsen KD.** A clinical prototype for active microwave imaging of the breast. *IEEE Trans Microw Theory Tech*. 2000; 48(11):1841-1853.
- [71] **Klemm M, Craddock IJ, Leendertz JA, Preece A, Benjamin R.** Radar-Based Breast Cancer Detection Using a Hemispherical Antenna Array- Experimental Results. *IEEE Trans Antennas Propag*. 2009; 57(6):1692-1704.
- [72] **Klemm M, Craddock IJ, Leendertz JA, Preece A, Gibbins DR, Shere M, et-al.** Clinical trials of a UWB imaging radar for breast cancer. *Antennas and Propagation (EuCAP)*, 2010 Proceedings of the Fourth European Conference on; 2010. p. 1-4.
- [73] **Grzegorzczuk TM, Meaney PM, Kaufman PA, di Florio-Alexander RM, Paulsen KD.** Fast 3-D Tomographic Microwave Imaging for Breast Cancer Detection. *IEEE Trans Med Imag*. 2012; 31(8):1584-1592.
- [74] **Fear EC, Bourqui J, Curtis C, Mew D, Docktor B, Romano C.** Microwave Breast Imaging With a Monostatic Radar-Based System: A Study of Application to Patients. *Microwave Theory and Techniques, IEEE Transactions on*. 2013; 61(5):2119-2128.
- [75] **Hassan AM, El-Shenawee M.** Review of Electromagnetic Techniques for Breast Cancer Detection. *IEEE Trans Biomed Eng*. 2011; 4:103--118.
- [76] **Abubakar A, Vanden Berg PM, Mallorqui JJ.** Imaging of biomedical data using a multiplicative regularized contrast source inversion method. *IEEE Trans Microw Theory Tech*. 2002; 50(7): 1761-1771.
- [77] **M. Lazebnik, E. L. Madsen, G. R. Frank, and S. C. Hagness,** Tissue-mimicking phantom materials for narrowband and ultrawideband microwave applications. *Phys Med Biol*, vol. 50, no. 18, pp. 4245–4258, Sep 2005.
- [78] **A. Kirsch,** (1996) An Introduction to the Mathematical Theory of Inverse Problems, vol. 120, :Springer-Verlag
- [79] **Gibson, P. J.** (1979). The Vivaldi Aerial. Microwave Conference, 9th European, pp.101-105.
- [80] **Gazit, E.,** (1988). Improved design of the Vivaldi antenna. *Microwaves, Antennas and Propag. IEEE Proc. H* , vol.135, no.2, pp.89-92

- [81] **Langley, J.D.S.; Hall, P.S.; Newham, P.** (1993). Novel Ultrawide-bandwidth Vivaldi antenna with low cross-polarization. *Electron. Lett.*, vol.29, no.23, pp.2004-2005
- [82] **Milligan T.** (2005). *Modern Antenna Design*, 2nd ed. Piscataway, NJ: *IEEE Press*.
- [83] **Lee, J. J. and Livingston, S.** (1993). Wide band bunny-ear radiating element. *IEEE AP-S Symposium*, pp. 1604–1607.
- [84] **Bourqui, J.; Okoniewski, M.; Fear, E.C.** (2010). Balanced Antipodal Vivaldi Antenna With Dielectric Director for Near-Field Microwave Imaging. *IEEE Trans. Antennas and Propag.*, vol.58, no.7, pp.2318-2326
- [85] **Yunqiang Yang; Fathy, A.E.** (2009). Development and Implementation of a Real-Time See-Through-Wall Radar System Based on FPGA. *IEEE Trans. Geosci. Remote Sens.*, vol.47, no.5, pp.1270-1280
- [86] **Yngvesson, K.S.; Korzeniowski, T.L.; Young-Sik Kim; Kollberg, E.L.; Johansson, J.F.** (1989). The tapered slot antenna—a new integrated element for millimeter-wave applications. *IEEE Trans. Microw. Theory Tech.*, vol.37, no.2, pp.365-374
- [87] **Janaswamy, R.; Schaubert, D.H.** (1987) Analysis of the tapered slot antenna, *IEEE Trans. Antennas and Propag.*, vol.35, no.9, pp.1058-1065.
- [88] **Hood A.Z.; Karacolak, T.; Topsakal, E.** (2008). A Small Antipodal Vivaldi Antenna for Ultrawide-Band Applications. *IEEE Antennas and Wireless Propag. Letters*, vol.7, pp.656-660.
- [89] **Greenberg M. C.; Virga K. L. and Hammond C. L.** (2003). Performance characteristics of the dual exponentially tapered slot antenna (DE TSA) for wireless communications applications. *IEEE Trans. Veh. Technol.*, vol. 52, no. 2, pp. 305–312.
- [90] **Bai J.; Shi S. and Prather D. W.** (2011). Modified compact antipodal Vivaldi antenna for 4–50-GHz UWB application. *IEEE Trans. Microw. Theory Tech.*, vol. 59, no. 4, pp. 1051–1057.
- [91] **Fang, Q.; Meaney, P.M.; Paulsen, K.D.** (2004). Microwave image reconstruction of tissue property dispersion characteristics utilizing multiple-frequency information. *IEEE Trans. Microw. Theory Tech.*, vol.52, no.8, pp.1866-1875
- [92] **Rizk, Jad B.; Rebeiz, G.M.** (2002). Millimeter-wave Fermi tapered slot antennas on micromachined silicon substrates. *IEEE Trans. Antennas and Propag.*, vol.50, no.3, pp.379-383
- [93] **Lawrie, R. E.; Peters, L., Jr.** (1966). Modifications of horn antennas for low sidelobe levels. *IEEE Trans. Antennas and Propag.*, vol.14, no.5, pp.605-610
- [94] **Sugawara, S.; Maita, Y.; Adachi, K.; Mori, K.; Mizuno, K.** (1998). Characteristics of a MM-wave tapered slot antenna with corrugated edges. *Microw. Symp. IEEE MTT-S International*. vol.2, pp.533-536

- [95] **Abbosh, A.** (2009). Miniaturized Microstrip-Fed Tapered-Slot Antenna with Ultrawideband Performance. *IEEE Antennas and Wireless Propag. Letters*, vol.8, pp.690-692
- [96] **Peng F.; Yong-Chang J.; Wei H.; Fu-Shun Z.** (2011). A Miniaturized Antipodal Vivaldi Antenna with Improved Radiation Characteristics. *IEEE Antennas and Wireless Propag. Letters*, vol.10, no., pp.127-130
- [97] **Teni, G.; Ning Z.; Jinghui Q.; Pengyu Z.** (2013). Research on a Novel Miniaturized Antipodal Vivaldi Antenna with Improved Radiation, *IEEE Antennas and Wireless Propag. Letters*, vol.12, pp.417-420
- [98] **Akinci M. N.; Ozgur S.; Alkasi U.; Ahmadzay H.; Abbak M.; M. Cayoren, and I. Akduman** (2015). Qualitative microwave imaging with scattering parameters measurements. *IEEE Trans. Microw. Theory Tech.*
- [99] **Cakoni F.; Colton D. and Monk P.** (2011). The Linear Sampling Method in Inverse Electromagnetic Scattering. *SIAM*
- [100] **Catapano, I.; Crocco, L.** (2009). An Imaging Method for Concealed Targets. *Geoscience and Remote Sensing, IEEE Transactions on*, vol.47, no.5, pp.1301-1309
- [101] **Catapano, I.; Crocco, L.** (2010). A Qualitative Inverse Scattering Method for Through-the-Wall Imaging. *Geoscience and Remote Sensing Letters, IEEE*, vol.7, no.4, pp.685-689
- [102] **Catapano, I.; Crocco, L.; Isernia, T.** (2008) Improved Sampling Methods for Shape Reconstruction of 3-D Buried Targets. *Geoscience and Remote Sensing, IEEE Transactions on*, vol.46, no.10, pp.3265-3273
- [103] **Akinci, M. N. and Çayören M.** (2014). Microwave subsurface imaging of buried objects under a rough air–soil interface. *Remote Sensing Letters*, vol. 5, no. 8, pp. 703–712
- [104] **Colton, D. and Monk P.** (1998). A linear sampling method for the detection of leukemia using microwaves. *SIAM Journal on Applied Mathematics*, vol. 58, no. 3, pp. 926–941
- [105] **Bozza, G.; Brignone, M.; Pastorino, M.** (2010). Application of the No-Sampling Linear Sampling Method to Breast Cancer Detection, *Biomedical Engineering, IEEE Transactions on*, vol.57, no.10, pp.2525-2534
- [106] **Guzina, B. B.; Cakoni, F.; and Bellis C.** (2010). On the multi-frequency obstacle reconstruction via the linear sampling method. *Inverse Problems*, vol. 26, no. 12, p.125005
- [107] **Catapano, I.; Crocco, L.; Urso, M. D.; and Isernia, T.** (2009). 3D microwave imaging via preliminary support reconstruction: Testing on the Fresnel 2008 database. *Inverse Problems*, vol. 25, no. 2, pp.024002
- [108] **Cheney, M.** (2001). The linear sampling method and the MUSIC algorithm. *Inverse Problems*, vol. 17, pp.591 – 595

- [109] **Colton, D.; Haddar, H.; and Piana, M.** (2003). The linear sampling method in inverse electromagnetic scattering theory. *Inverse Problems*, vol. 19, pp.105 – 137
- [110] **Bucci, O. M.; and Isernia, T.** (1997). Electromagnetic inverse scattering: Retrievable information and measurement strategies. *Radio Science*, vol. 32, no. 6, pp.2123 – 2137

CIRRICULUM VITAE



Name Surname: Mehmet ABBAK

Place and Date of Birth: Aydın – 1983

E-Mail: mehmetabbak@gmail.com

B.Sc: Telecommunications Engineering, Sabanci University (June 2006)

M.Sc: Electronics Engineering, Sabanci University (August 2008)

Publications / Presentations on the Thesis

Journal:

- **Abbak, M.;** Çayören, M.; Akduman, I. (2014) Microwave breast phantom measurements with a cavity-backed Vivaldi antenna," *Microwaves, Antennas & Propagation, IET* , Volume 8, Issue 13, Pages: 1127-1133
- J. J. Golezani, **M. Abbak**, and I. Akduman (2012) Modified directional wide band printed monopole antenna for use in radar and microwave imaging applications," *Progress In Electromagnetics Research Letters*, Vol. 33, 119 - 129

Conference:

- Akinci, M.N.; **Abbak, M.;** Ozgur, S.; Cayoren, M.; Akduman, I. (2014) Experimental comparison of qualitative inverse scattering methods," *Antenna Measurements & Applications (CAMA), 2014 IEEE Conference on* , vol., no., pp.1 - 4
- **Abbak, M.;** J. Janghi, I. Akduman (2012) A novel compact wideband directional monopole antenna for use in radar applications" *Antenna Technology and Applied Electromagnetics (ANTEM), Toulouse*
- **Abbak, M.;** I. Akduman (2012) Miniaturized tapered slot antenna for microwave breast imaging", *Telecommunications Forum (TELFOR), Belgrade*

